A Tropical Survey of Mid-Tropospheric Cyclones, their Classification and Genesis over the Arabian Sea

A THESIS

SUBMITTED FOR THE DEGREE OF

Doctor of Philosophy

IN THE CENTRE FOR ATMOSPHERIC AND OCEANIC SCIENCES

by

Pradeep Kushwaha

Centre for Atmospheric and Oceanic Sciences

Indian Institute of Science

BANGALORE – 560 012

JUNE 2022

Acknowledgements

If you are not having fun, you are not learning; there is pleasure in finding things out.

During such an unpredictable time of the COVID-19 pandemic, it is difficult to believe that I am writing a Ph.D. dissertation and in the final stages of my Ph.D. Degree. These difficult times show us how important it is to support an individual to grow at various levels. A few years back, pursuing a Ph.D. and writing a document as significant as a Ph.D. dissertation was not even a dream for me. However, the saying, "A good mentor can change a game, but a great mentor can change your life," by John Wooden, sums up my journey toward pursuing a Ph.D.

My love for rain and thirst to know monsoons found its place during my undergraduate days when I came to know about the Center for Atmosphere and Oceanic Science (CAOS) department at IISc, and the journey began. In retrospect, I realized that what we achieve in life is not entirely determined by our competence but by whom we surround ourselves. I was fortunate that I have been in the company of great mentors, friends, teachers, and well-wishers from the very beginning who not only stood by my side in the ups and downs of life but also nurtured me emotionally, intellectually, socially, and professionally and helped me grow as a sensible human being. Therefore the successful completion of this Ph.D. thesis speaks not so much about my competence but more about the great human beings and mentors who supported and guided me at various levels during my life. I bow down and dedicate this Dissertation to all who made this dream a reality.

It has been a fascinating, adventurous, and incredible journey. I was privileged and blessed to spend my intellectually formative years under the care of a great supervisor like Prof. Jai Sukhatme and a constant wonderful mentor like Prof. Ravi S. Nanjundiah. Both made this Ph.D. journey effortless and enriching.

I am deeply grateful to Prof. Jai Sukhatme for choosing me as a Ph.D. student. Your unwavering trust always lifted me, helped me focus on my strengths, gave me the courage to overcome challenges, and allowed me to work at my best during the critical years of my Ph.D. Your incredible understanding of atmospheric fluid dynamics and quick insights into new topics were exceptional. Several discussions with you gave me a different, broader perspective and understanding of atmospheric sciences. I was so fortunate to attend the Atmosphere Dynamics and GFD classes of Prof. Jai, which were always exciting and so in-depth, which ignited a whole new love for atmosphere

sciences and allowed me to observe weather events completely different way. Every discussion and interaction with you was enlightening, opened up a new dimension of knowledge, and taught me something exciting and new. Apart from being a wonderful mentor, great teacher, and scientist, Prof. Jai Sukhatme is one of the kindest, most patient, and very compassionate human beings. The freedom and great working environment you have given allowed me to do what I love joyfully and effortlessly. I was often slow, but your infinite patient guidance allowed me to work with ease. I was often shortsighted, but you envisioned me on a beautiful and successful academic journey. I am thankful for your enthusiastic encouragement, valuable research work reviews, editing, and assistance in keeping my progress on schedule. I am blessed to work with a great mentor like Prof. Jai and would like to express my deep gratitude for your support and the opportunities I was given to further my research.

I also extend my sincere thanks to my M-Tech supervisor and constant Ph.D. mentor, Prof. Ravi S. Nanjundiah, for his care and support throughout. A few years back, it was just a dream to write literature as significant as a Ph.D. dissertation. However, I took the courage to peruse a Ph.D. mainly because of the foundation Prof. Ravi nurtured and kept the constant trust in my abilities which ignited my belief in myself and shaped my inner and outer self, which helped me to grow personally and professionally. Your constant encouragement, support, and valuable feedback in IISc, even when you were in IITM, kept me on track and inspired me a lot. You introduced me to the world of academia during M-Tech at CAOS from the root level, where I was able to build a solid foundation where the heights of a Ph.D. could have been possible. Apart from being a great mentor, your compassionate and friendly nature was constantly elevating and relaxing. I remember when I had just started diving into atmosphere science and struggled to write programs, you gently introduced me to the book ”Computer Programming in Fortran 90 and 95 by V Rajaraman. That was the turning point of my computational skills.

Completing this study could not have been possible without my beloved mentors’ expertise; your insightful feedback encouraged me to sharpen my thinking and brought my work to a higher level.

At CAOS, I also extend my deepest gratitude to Prof. Prof. J. Srinivasan, Prof. V. Venugopal, Prof. Debasis Sengupta, Prof G.S. Bhat, Prof Govindsamy Bala, Prof. S.K. Satheesh, Prof P.N. Vinayachandran, Prof. Arindam Chakraborty, and Prof Ashwin K Seshadri for introducing me to various fundamentals of atmosphere and ocean

sciences, without which it would have been much more challenging to execute, understand and interpret the results. I am grateful to Prof. J. Srinivasan for valuable discussions about monsoon dynamics during the monsoon cafes. I express my special gratitude to Prof. Debasis Sengupta, Prof. V. Venugopal, and Prof. Ashwin K Seshadri for their valuable discussions and, time-to-time, interacting and encouraging me. I also thank the various staff at CAOS and DCCC- Mrs. Radha, Mrs. Divya, Mr. Raju, Mrs. Mamta, Mr. Nagraj, Mr. Pradeep, and Mr. Mahesh for their support and help. Thank Mr. Ajay, for taking care of the system and resolving remote connectivity issues during the lockdown.

Thank Prof. Richard Johnson (Colorado State University) and James Ruppert (Oklahoma University) for providing me with insightful feedback during the 102nd AMS meeting. I am grateful to Prof. Morgan E O'Neill (Stanford University) for encouraging comments and valuable directions during the "34th Conference on Hurricane and Tropical Meteorology."

I want to express my gratitude to Dr. Chetan Kumar for being a great friend and mentor; he always helped me write complex algorithms and advised me on various levels of Ph.D.

My gratitude to Dr. Suhas D L for always showing me the positive side of every event and guiding me through and discussing progress during difficult times.

I am grateful to have such great lab members, Nihar, Abu, and Ghatak. Who always remained so supportive and encouraging that I never felt alone in this great adventure.

I also would like to thank my seniors: Joy, Depesh, Gaurav Srivastava, Gaurav Goverdhan, Subhi, Kapil, Jayesh, Surajit, Nirupam, Ram, Harshwardhan, Arun, Vishal, who supported and guided me at various levels.

I have significantly benefited from the genuinely professional support from the technical, academic & other supporting staff for making my journey much more accessible and pleasant. I want to express my gratitude to all mass workers for arranging nursing food during a difficult time like COVID-19. I am thankful to the medical team of IISc for proving us with health facilities, without which it could have been much more challenging to overcome diseases and live a healthy life. I also express my deepest gratitude to all security staff for keeping our campus safe, because of which we could have worked any time fearlessly.

To my friends, this would have been a much more difficult feat without you. Thank you all for your unwavering support and for reminding me to take breaks and have fun when I have been stressed and low. Special thanks to my friend Anoop who always helped me whenever I was in difficulty and for enriching discussions on several aspects of life. I am also thankful to Sheo, Arijit, Subham, Sourabh, Akshaya, and Pritam for being great friends and companions on this journey. I am also thankful to Kushal, Mahesh, Ashutosh, Suneel, Tejal, Harsh, Prakash, Tanmay, Rishve, Sharavan, and Lokesh, who always fellow travelers who kept positive vibes alive. Discussing the difficulties in life with friends was itself the solution. I am also grateful to have great and vibrant current joiners friends: Aditya, Priyansi, Rajat, Harpreet, Abu, Kaushik, Pooja, Sujata, Ritesh, Mahendra, Sumit, Thanangka, Mayur, Bijit, Shikhar, Devang, Sanchit, Jerry whose friendliness and inclusive nature always made the department a significant and vibrant family.

Finally, I want to acknowledge and be grateful for the support of my parents, sister, brother, and relatives; they all kept me going through all the ups and downs of life, and this research would not have been possible without them. I am incredibly grateful to my parents, who always stood behind my dreams and decisions and never troubled me in pursuing my goals despite the social pressure of a middle-class family.

Publications from this thesis

Journal Articles:

1. P. Kushwaha, J. Sukhatme & R.S. Nanjundiah, "A Global Tropical Survey of Midtropospheric Cyclones", Monthly Weather Review, doi:10.1175/MWR-D-20-0222.1, 2021. [**Chapter 3**]

2. P. Kushwaha, J. Sukhatme & R.S. Nanjundiah, "Classification and Mechanisms of Formation of Synoptic Systems over Western India", Quarterly Journal of the Royal Meteorological Society (in press). [**Chapter 4**]

3. P. Kushwaha, J. Sukhatme & R.S. Nanjundiah, "Role of Bay of Bengal low pressure systems in the formation of Arabian Sea Middle Tropopsheric Cyclones", (submitted to QJRMS) [**Chapter 5**]

Conferences:

1. P. Kushwaha, J. Sukhatme & R.S. Nanjundiah, A Global Survey of Middle Tropospheric Cyclones, AGU Fall Meeting, doi:10.1002/essoar.10505597.1, 2020.

2. P. Kushwaha, J. Sukhatme & R.S. Nanjundiah, Climatology of Mid-Troposphere Cyclones Over South East Asia, 34^th Conference on Hurricanes and Tropical Meteorology, AMS, 2021.

3. P. Kushwaha, J. Sukhatme & R.S. Nanjundiah, Quasi-Stationary Nature of Arabian Sea Mid-Tropospheric Cyclones, 34^{th} Conference on Hurricanes and Tropical Meteorology, AMS, 2021.

4. P. Kushwaha, J. Sukhatme & R.S. Nanjundiah, Synoptic Weather Regimes over Western India and the Arabian Sea. 102^{nd} AMS Annual Meeting, January, 2022.

5. P. Kushwaha, J. Sukhatme & R.S. Nanjundiah, Role of Bay of Bengal Monsoon Lows in the Genesis of Arabian Sea Middle Tropospheric Cyclones (MTCs), 35^{th} Conference on Hurricanes and Tropical Meteorology, AMS, 2022. [**Chapter 5**]

Abstract

Middle Tropospheric Cyclones (MTCs) are moist synoptic tropical systems with vorticity maxima in the middle troposphere and weak signature in the lower troposphere. We begin with a tropical survey of MTCs; in South Asia, manual tracking reveals that MTCs change character during their life, i.e., their track is composed of MTC and LTC (lower troposphere cyclone) phases. The highest MTC-phase density and least motion is over the Arabian Sea, followed by the Bay of Bengal and the South China Sea. An MTC-phase composite shows an east-west tilted warm above deep cold-core temperature anomaly with maximum vorticity at 600 hPa. In contrast, the LTC phase shows a shallow cold-core below 800 hPa and a warm upright temperature anomaly with a lower tropospheric vorticity maximum. Further, the systems with MTC-like morphology are observed over the west and central Africa and east and west Pacific in boreal summer. In boreal winter, regions that support MTCs include northern Australia, the southern Indian Ocean, and South Africa. The MTC's kinematic and thermal structure exhibit remarkable similarity among different basins, suggesting a common underlying maintenance mechanism.

Given that the Arabian Sea is a hot spot of devastating MTCs, their classification and genesis mechanisms in this region are explored. Both k-means and cyclone tracking approaches reveal four dominant weather patterns that lead to the genesis of these systems; specifically, re-intensification of westward-moving synoptic systems from Bay of Bengal (Type 1, 51%), *in-situ* formation with a coexisting cyclonic system over the Bay of Bengal that precedes (Type 2a, 31%) or follows (Type 2b, 10%) genesis in the Arabian Sea, and finally *in-situ* genesis within a northwestward propagating cyclonic anomaly from the South Bay of Bengal (Type 2c, 8%). Thus, a significant fraction of rainy middle tropospheric synoptic systems in this region form in association with cyclonic activity

in the Bay of Bengal (BOB). While *in-situ* formation with a BOB cyclonic anomaly (Type 2a and 2b) primarily occurs in June, downstream development is more likely in the core of the monsoon season. Type 2a is associated with the highest rain rate and points towards the dynamical interaction between a low-pressure system over the BOB and the development of MTCs over western India and the northeast Arabian Sea.

The frequent coexistence BOB lows during the Type 2a formation of MTCs is not merely a coincidence. Rather the BOB system induces an off-equatorial Gill type response which deepens the middle tropospheric trough and zonal shear over the Arabian Sea. In turn, this enhances the cyclonic vorticity and intensifies the middle troposphere anomalous easterlies north of 20°N. This results in reduction of dry and warm desert air advection, depletion of low-level inversion and destabilization of the lower troposphere. Following which, the eddy-induced moisture flux convergence and advection of climatological moisture increases the saturation fraction. These favorable conditions within the middle troposphere trough region triggers the genesis of MTCs over the Arabian Sea.

The proposed role of BOB lows in MTC formation is validated by numerical experiments using the state-of-the-art Weather Research & Forecast (WRF) model. Twenty one ensemble members were generated through addition of balanced vortices to the climatological flow in the BOB. Consistent with observations, in simulations, the BOB low deepens the monsoon trough over western India, enhances the cyclonic shear, reduces the inversion, and increases the middle troposphere relative humidity; supporting the genesis of an MTC over the Arabian Sea within $2.5 - 4$ days of model integration. During the first $24 - 36$ hours of intensification, advection of absolute vorticity and tilting account for the entire vorticity tendency, while during the rapid intensification phase, vortex stretching is the dominant source of vorticity enhancement. Mechanism Denial Runs with cooling and drying of BOB were then performed to show that this hinders the intensification of the low over the Bay and consequently, the MTC did not form over the Arabian Sea. This global survey, classification, identification of precursors, connection with cyclonic activity over the Bay of Bengal, and dependence on the large-scale environment provide an avenue for better understanding and predicting rain-bearing MTCs.

Contents

Abstract **vi**

Keywords **xv**

1 Introduction **1**
1.1 Middle Tropospheric Cyclones . . . 1
1.2 Motivation . . . 3
1.3 Regions of MTC Occurrence . . . 5
1.4 Arabian Sea MTC Formation . . . 7
1.5 Arabian Sea MTCs and cyclonic activity over the Bay of Bengal . . . 9

2 Data and Methods **13**
2.1 Data . . . 14
2.1.1 MERRA-2 Data . . . 14
2.1.2 ERA5 Data . . . 14
2.1.3 ISO Index . . . 16
2.1.4 Rainfall and OLR data . . . 16
2.2 Detection of MTCs and LTCs . . . 17
2.2.1 Selection of Identification Parameters . . . 18
2.2.2 Manual Tracking of MTCs . . . 22
2.2.3 Cyclone Metrics . . . 23
2.3 Classification of western Indian weather patterns using k-means . . . 23
2.4 Automatic tracking of systems and their classification . . . 28
2.5 Numerical Modeling . . . 29
2.5.1 Weather Research and Forecast Model Setup . . . 29
2.5.2 Bogus Vortex Scheme . . . 30
2.6 Moisture and Vorticity Budget . . . 32
2.6.1 Moisture Budget . . . 32
2.6.2 Vorticity Budget . . . 34

3 A Global Tropical Survey of Middle Tropopsheric Cyclones **35**
3.1 MTCs over South Asia . . . 36
3.1.1 Track density, starting location density, and cyclone motion vector . . . 37
3.1.2 Starting location and intensity distributions . . . 41
3.2 MTC statistics over globe . . . 43
3.2.1 Boreal Summer . . . 43
3.2.2 Boreal Winter . . . 48
3.3 Robustness of Results . . . 50
3.4 Conclusions . . . 52

4 Classification of MTCs over the Arabian Sea and Western India **56**

4.1 Large Scale Conditions During Western India Rainfall 57
4.2 Rainy day composites 59
4.3 Weather Regimes over Western India 61
4.4 Tracking of Western Indian Cyclonic Systems 66
4.4.1 Evolution of four categories 69
4.4.2 Meteorological characteristics of the four categories 71
4.4.3 Modulation by Intra-Seasonal Oscillations 74
4.5 Conclusions 77

5 Genesis of MTCs over the Arabian Sea **81**
5.1 Type 2a MTC formation 82
5.1.1 Evolution of Dynamic Fields 82
5.1.2 Evolution of thermodynamic fields 86
5.2 Moisture budget during Type 2a formation 89
5.3 Bogus LPS over the Bay of Bengal 94
5.3.1 Vorticity Budget 96
5.4 Mechanism Denial Experiment 103
5.5 Conclusions 107

6 Summary and Future Research Directions **112**

A Appendix **120**

List of Tables

2.1 Model Specifications 29

A.1 Mean, variance, median and probability distributions of δP_ξ of 882 detected systems over $5°$N-$25°$N and $50°$E-$95°E$ (as shown in Figure 2.3) and corresponding number of MTCs and LTCs for various combinations of layer thickness (left portion of the table); the number of MTCs and LTCs are highlighted in bold. The sensitivity of number of MTCs and LTCs for various moisture (Q_m) and relative vorticity (ξ_m) thresholds in in the right portion of the Table. 120

List of Figures

1.1 Composite kinematic structure of July 1963 MTCs from Miller and Keshavamurty (1968). Streamlines and isotachs are shown at (a) at 600 hPa and (b) 500-900 meter near-surface layer. 3

1.2 Composite kinematic structure of July 1963 MTCs from Miller and Keshavamurty (1968). Left column divergence and right panel vorticiy. 4

2.1 Joint probability distribution of $\delta\xi_p = \xi_m - \xi_l (\times 10^{-5} s^{-1})$ and the level of maximum relative vorticity (P_ξ), in hPa for 725 strong & moist cyclonic centers detected during the dates of 35 IMD MTC events over the region 5°N–25°N, 50°E–95°E. Red and black hatching indicates bounds of MTCs and LTCs, respectively. 19

2.2 Probability distribution of differential vorticity ($\delta\xi_p$, $\times 10^{-5}$ s^{-1}) cyclonic centers as in Figure 2.1. Light blue shaded region denotes lower 20th percentile (i.e., below -0.8×10^{-5} s^{-1}) and the light pink region denotes upper 20^{th} percentile (i.e., above 1.5×10^{-5} s^{-1}). 19

2.3 Relative vorticity composite from 121 middle troposphere cyclonic centers (Left Panels: a, c, e) and 126 lower tropospheric cyclone centers (Right Panels: b, d, f) from the Indian region. (a), (b) East-West-vertical cross-section through composite center y-axis is pressure in hPa. (c), (d) Horizontal cross-sections at 975 hPa and (e), (f) at 600 hPa. Dashed lines indicate axes through the composite center. Vectors indicate the composite wind of MTC and LTCs and contours represent the composite geopotential height at respective levels in m. Units of the x-y axes of sub-figures c-f are degrees east and degrees north with respect to composite cyclone center, respectively. . . 20

2.4 Sensitivity of the distribution of differential vorticity ($\delta\xi_p$) to different choices of layers combinations. LC0: lower layer 1000–850 hPa, middle layer, 650–500 hPa; LC1: lower layer 1000-850 hPa, middle layer, 850–500 hPa; LC2: lower layer 1000–650 hPa, middle layer, 650–500 hPa and LC3: lower layer, 900 hPa, middle layer, 600 hPa. 21

2.5 Selection of value of optimal cluster from 622 days of height anomalies at 600 hPa as data vectors using Elbow and Silhouette Coefficient (SC) methods Rousseeuw (1987); Satopaa et al. (2011). (a) "nx" is the normalized number of clusters k (i.e., $\frac{k_x - k_{min}}{k_{max} - k_{min}}$). Blue curve ("$ny$"): normalized within cluster sum of square (WSS) of all data vectors; Red (ny): normalized difference curve (i.e., y-axis component of perpendicular Euclidean distances of WSS values to the diagonal from first to last data point following Satopaa et al. (2011). Dotted black line: knee point at the maximum value of normalized difference curve (i.e, $nx = 0.28$); (b) Blue is the total within cluster sum of squares (WSS $\times 10^{-6}$) with varying number of clusters (k). Red: the mean SC Rousseeuw (1987) of data vectors with varying number of clusters (k), ranging from 2 to 12. Black dotted line: value of optimal $k(= 4.27)$ corresponds to the maximum of normalized difference curve (Figure S1a, red) calculated using the kneedle program Satopaa et al. (2011). Further details can be found in Section-III and Figure-2 of Satopaa et al. (2011). 25

2.6 Schematic of tracking procedure 27

3.1 South Asian composites from 1107 MTC-phase track points (a) Relative vorticity (shaded) and PV anomaly in contours (c) Temperature anomaly (shaded) and specific humidity anomaly (contours). In both (a) and (c), positive contours are solid, and negative are dashed. Panels (e) and (g) are plan views of vorticity (shaded) and wind vectors at 600 and 975 hPa, respectively. Panels (b), (d), (f) and (h) are the same quantities as (a), (c), (e) and (g) but constructed from 401 LTC-phase track points. Units of PV is 10^{-1} PVU, and specific humidity is g/kg. Results are only shown if they are significant at 1% significance under a two-tailed t-test. 38

3.2 (a) Track density (shaded) and starting location density (contours) of 261 MTCs over South Asia. Arrows denote the cyclone motion vectors; arrow length is proportional to the propagation speed in m/s. The vectors are shown only if any wind components are significantly different from zero at 1% significance under a two-tailed t-test. (b) Same as (a), except calculation is done for each track segment if it is in the LTC-phase (c) is same as (a) except results are for the MTC-phase. (d) the mean of change in along-track differential vorticity of all tracks. (e) and (f), percent of systems at every 8 degrees with the negative and positive rate of differential vorticity change, respectively. Here, negative values denote an increase in low-level cyclonic vorticity, and positive values show an increase in mid-level cyclonic vorticity. Velocity vectors in (d,e,f) are the same as in (a) and are shown to guide the eye. 40

3.3 Monthly starting location probability (in percent) of 261 South Asian MTCs over (a) Arabian Sea (AS),(b) Bay of Bengal (BO) and (c) South China Sea (SC). Panels (d), (e), (f) follow (a), (b) and (c) but show the initial location (red, STR) and lysis (blue, LYE) probability distribution with latitude for the three regions. (g) and (h) show the joint probability distribution of $\delta\xi_p$ and ξ_m respectively with respect to latitude for all 261 tracks. 42

3.4 (a) Overall cyclone center density during boreal summer for 20 years. (b) same as (a) except for MTC centers. (c) same as (a) except for LTC centers. (d) $\frac{b-c}{b+c}$, only shown if total density exceeds 3. Note that the colorbar panel (a) is different from that in (b) and (c). 44

3.5 Composites of anomalies for MTCs (left column) and LTCs (right column) in the East Pacific region (a,b,c,d,e,f,g,h) and the Africa (i,j,k,l,m,n,o,p); (a,b and i,j) Relative vorticity (shading) and contours of potential vorticity (10^{-1} PVU); (c,d and k,i) temperature (shading) and specific humidity (g/kg) in contours; (e,f,m,n) and (g,h,o,p) wind vectors and relative vorticity (shaded) at 600 hPa and 975 hPa, respectively. Results are only shown if they are significant at 1% significance under a two-tailed t-test. 47

3.6 (a) Overall cyclone center density during the boreal winter for 20 years. (b) same as (a) except for MTC centers. (c) same as (a) except for LTC centers. (d) $\frac{b-c}{b+c}$, only shown if total density exceeds 3. Note that the colorbar panel (a) is different from that in (b) and (c). 49

3.7 Composites of anomalies for MTCs (left column) and LTCs (right column) in the Southern Indian Ocean (a,b,c,d,e,f,g,h) and Australia (i,j,k,l,m,n,o,p); (a,b and i,j) Relative vorticity (shaded) and contours of potential vorticity (10^{-1} PVU); (c,d and k,i) temperature (shaded) and specific humidity (g/kg) in contours; (e,f,m,n) and (g,h,o,p) wind vectors and relative vorticity (shaded) at 600 hPa and 975 hPa, respectively. Results are only shown if they are significant at 1% significance under a two-tailed t-test. 51

3.8 (a) Joint PDF of P_ξ and $\xi_m - \xi_l$ of all 91,283 cyclonic centers from 30°N to 30°S in 20 years of data. Notation follows Figure 2.1. (b) PDF of P_ξ; (c) PDF of $\xi_m - \xi_l$. 53

4.1 Lag correlation of OLR anomaly over the shown domain with the Arabian Sea ($15 - 22$°N to $68 - 72$°E) mean OLR anomaly time series from June to September, 1980-2019. Shading denotes the regions which are significant at 99% confidence using t-test. 58

4.2 Composites of rainy days ($P_{WI} > 7.6$ mm/day) (a) composite rain anomaly (b) composite precipitable water anomaly (contours: kg/m2) and June-September climatology (colors); (c) composite geopotential height anomaly at 950 hPa for rainy days; (d) same as (c) but for 600 hPa; (e), (f) composite total geopotential heights at 950 and 600 hPa, respectively; (g) is the static stability parameter at 800 hPa; (h) anomalous strength of inversion $\Delta T_{ano} = T_{a750} - T_{a950}$, where T_{a750} and T_{a950} are temperature anomalies at 750 and 950 hPa. heights are in meter and rainfall in mm; the white regions are where topography crosses the geopotential surface of analysis. 60

4.3 Composite height anomaly of 700 hPa surface (m) from $k-$means clustering for Regime 1 (a) to Regime 4 (d). The respective composite winds are shown as arrows, units are m/s. 62
4.4 Lag composites of the four $k-$means clustering regimes from Day -4 to Day 0; row 1 to row 4 represent Regime 1 to 4, respectively. Here, Day zero represents the Day when the cluster was detected. Color shading represents the composite 600 hPa height anomaly (m), dotted shading represents the OLR anomaly, and arrows represent the composite wind anomaly. OLR and height fields are only shown if they are significantly different from climatology at 0.1 significance. Wind vectors are shown if any wind component is significantly different from zero at the 0.1 significance level under the two-tailed t-test. 64
4.5 Domains Specifications: Red box: Arabian Sea; Black box: Bay of Bengal 67
4.6 Northeast Arabian Sea (NEAS) system classification based on their genesis as discussed in method section. A total of 191 long lived systems (life $>$ 3 days) satisfy the rainfall criteria (cyclone following composite rain and rain over western India ($18°$N-$22°$N, $68°$E-$74°$E) during life of cyclone is grater than or equal to 7.6 mm/day) and exist over western India and adjoining Arabian Sea for at least 24 hours (red box, Figure 4.5). Type 1 systems are those which originate in the Bay of Bengal (black box, Figure 4.5). Type 2a MTCs are the *in-situ* forming systems with a preceding the Bay of Bengal LPS. Type 2b are *in-situ* born MTCs which precede the formation of a Bay of Bengal system. Type 2c represents *in-situ* MTC formation with no cyclonic activity in the north Bay of Bengal (black box). 68
4.7 Lag composites of four variants of Arabian Sea systems via cyclone tracking from Day -4 to Day 0. Rows 1, 2, 3 and 4 represent Type 1, 2a, 2b and 2c, respectively. Zero days represent the Day of the heaviest rainfall in western India. Color shading represents the composite 600 hPa height anomaly (m), dotted shading is the OLR anomaly, and arrows represent the composite wind anomaly. Height anomaly and OLR have shown only if they are significantly different from climatology at 0.1 level of significance and arrows if any wind component is significantly different from zero at 0.1 significance. 69
4.8 Mean composite rainfall during cyclone life over the region ($18°$N-$22°$N $68°$E-$74°$E) (a) Gaussian Kernel Density Function (KDF) of mean composite rainfall; (b) box diagram of mean composite rainfall of four variants (Type 1, 2a, 2b and 2c). 72
4.9 Monthly frequency of occurrence of all four variants of Arabian Sea systems. (a) Type 1 ; (b) Type 2a; (c) Type 2b; (d) Type 2c. 73
4.10 Track density (color), mean cyclone motion vector (arrows) and cyclone genesis density (dashed contours) (a) Type 1, (b) Type 2a, (c) Type 2b, (d) Type 2c. Motion vectors are shown if any propagation vector component is significantly different from zero at 0.1 significance. 73
4.11 Left Column: Phase diagram of BSISO during the genesis of each of the four variants of Arabian Sea systems; each dot represents the phase of BSISO during the genesis of a particular system of each category. Right column: Frequency distribution of phases of BSISO during the genesis of each category of synoptic systems. 76

5.1 Lag composite of anomaly of Type 2a systems (mean 800-400 hPa) from Day -6 to Day 0, (a) precipitable water; (b) relative vorticity; (c) potential vorticity; (d) geopotential height; dotted region show where fields are significantly different from zero at 0.1 significance. Wind vectors are only shown if any of the wind component is significantly different from zero at 0.1 significance. 85
5.2 Type 2a composites from Day -3 to Day 0. Row 1: Potential vorticity anomaly, Row 2: Relative vorticity anomaly, Row 3: Zonal wind anomaly, Shading denotes regions which are significant at 0.1 significance level under two tailed student-t test. The cross section of vorticity and PV is at $18.5°$N and of wind component is at $22°$N. 87
5.3 Type 2a lag composite time series at $22°$N and $72°$E. (a) Zonal wind anomaly mean in 600-500 hPa (ms^{-1}); (b) Relative humidity anomaly mean in 600-500 hPa; (c) static stability parameter mean in 700-800 hPa (10^{-5} K/Pa); (c) height anomaly (m) at 500 hPa; shadings are widths of one standard deviation. 88

5.4 Type 2a composite Skew-T, log-P diagram mean over the region $18°$N-$22°$N $68°$E-$72°$E; (a) Day -6; (b) Day -4; (c) Day -2; (d) Day 0. Red lines represent atmospheric sounding, blue lines are dew point temperature, dashed green are constant mixing ratio lines and solid green are saturated adiabats, arrows are winds at different levels. 90
5.5 Type 2a lag composites from Day -6, Day -4, Day -2 and Day 0 ; Row 1: Specific humidity anomaly. Row 2: Relative Humidity anomaly. Row 3: Temperature and static anomaly (contours); Row 4: Equivalent potential temperature anomaly. Dotted shading denotes the regions which are significant at 0.1 significance under two-tailed student-t test. The cross section is at $22°$N. 91
5.6 Composite moisture budget of Type 2a formation; mean budget term over the region ($18°$N-$22°$N $70°$E-$72°$E), are shown in column-1 (a,e,i,m), red bars are the 95 % upper and lower confidence bound derived from student t-test, (a) $-[\nabla \cdot (q\mathbf{V})]$; (e)$-[\nabla \cdot (q_c\mathbf{V}')]$; (i) $-[q_c(\nabla \cdot \mathbf{V}')]$; (m) $-[\mathbf{V}' \cdot \nabla q_c]$; b to d are composite perceptible water anomaly; f to h are $-[\nabla \cdot (q_c\mathbf{V}')]$; j to l are $-[q_c(\nabla \cdot \mathbf{V}')]$; n to p are $-[\mathbf{V}' \cdot \nabla q_c]$ plan view respectively for Days -4, -2 and 0. 93
5.7 Model domain for the numerical simulation of MTCs 95
5.8 Locations of 21 bogus vortices grouped in four sets: A1, A2, A3, A4; group A1 contains nine members; group A2-A4 each contains 4 members. 95
5.9 Geopotential height at 600 hPa of nine members (A11-A19) of group A1 after 24 hours of simulation. 97
5.10 Geopotential height at 600 hPa of nine members (A11-A19) of group A1 after 63 hours of simulation. 98
5.11 Geopotential height at 600 hPa of twelve members of group A2 (row 1) to group A4 (row 3) after 24 hours of simulation, respectively. 99
5.12 Geopotential height at 600 hPa of twelve members of group A2 (row 1) to group A4 (row 3) after 96 hours of simulation, respectively. 100
5.13 Composite time series of various term of Vorticity Budget of group A1, averaged over the MTC region between 500-600 hPa. Zero hour represents the time of maximum intensification rate, $(\frac{\partial \xi}{\partial t})_{max}$, shading represents standard deviation among A1 assemble members. 103
5.14 Plan view of composite terms in the vorticity budget of group A1, averaged between 500-600 hPa for first 24 hours of simulation; dashed contours represent convergence, and solid contours are divergence in (a) and (b); contours in (f) are $\frac{\partial \xi}{\partial t}$. Symbols have their usual meaning. 104
5.15 Plan view of various terms in the vorticity budget of group A1, averaged between 500-600 hPa for 24-48 hours of simulation; dashed contours represent convergence, and solid contours are divergence in (a) and (b); contours in (f) are $\frac{\partial \xi}{\partial t}$. Symbols have their usual meaning. 105
5.16 Composite moisture fields mean over MTC region; (a) Static stability parameter at 800 hPa; (b) $T_{900} - T_{700}$; (c) mean relative humidity at 500-600 hPa; (d) zonal wind mean at 500-600 hPa. . 106
5.17 Geopotential height at 600 hPa of control ensemble members for the July 2020 MTC. Row 1 to row 4 are simulations initialized on 1 July at 00, 06, 12, and 18 UTC, respectively. 108
5.18 Initial conditions (a) cold Gaussian SST blob over Bay of Bengal, (b) Water Vapor (WV) mixing ratio at 1000 hPa — dry east India and BOB. 109
5.19 Geopotential height at 600 hPa of control ensemble members of cold-dry Bay of Bengal experiment. Row 1 to row 4 are simulations of 00, 06, 12, 18 UTC respectively. 110

6.1 Summary of the thesis. 113

A.1 Cyclone tracks with six. hourly sampling (red) and with 24 hour sampling (blue). Red dots indicate genesis location and green dot denotes lysis; black dots represents the 6 hourly position of cyclone. 121
A.2 Overall-center, LTC, MTC center density and MTC to LTC fraction from June to September 2000-2019; left panel (a, c, e, g) without P_ξ constraints; Right panel (b, d, f, h) with all constraints, respectively. 122

Keywords

Middle Tropospheric Cyclones, Indian Monsoon, Monsoon Lows, Cyclone tracking, k-means clustering.

List of Abbreviations

AEW	African Easterly Wave
BSISO	Boreal Summer Intraseasional Oscillations
ISO	Intraseasional Oscillations
IIOE	International Indian Ocean Expedition
LTC	Lower Tropopshere Cyclones
LPS	Low Pressure System
MTC	Middle Tropopshere Cyclones
MD	Monsoon Depression
MJO	Madden–Julian Oscillation
PV	Potential Vorticity
RH	Relative humidity
TC	Tropical Cyclones
WHOI	Woods Hrtical pressure velocity

r_m	Bogus vortex radius of maximum wind
v_m	Bogus vortex maximum wind
ψ	Stream function
ϕ	Geopotential
f	Coriolis parameter
V	Wind vector
w	Vertical velocity
q	Specific humidity

Chapter 1

Introduction

1.1 Middle Tropospheric Cyclones

Indian summer monsoon rainfall exhibits significant variability in space and time (Goswami, 2005). This variability is a result of various interacting phenomena that include the Boreal Summer Intraseasonal Oscillation (Nanjundiah et al., 1992; Wang and Xie, 1997; Sikka and Gadgil, 1980), influence of the Madden-Julian Oscillation (Annamalai and Slingo, 2001), the quasi-biweekly mode (Krishnamurti and Bhalme, 1976), synoptic-scale low pressure systems and their more intense form known as Monsoon Depressions (MDs, Mooley, 1973). Monsoon lows and depressions contribute significantly to Central Indian rainfall (Hurley and Boos, 2015; Hunt and Fletcher, 2019; Adames and Ming, 2018b; Vishnu et al., 2020). These systems primarily move west or northwest from the Bay of Bengal to the Indian landmass (Godbole, 1977; Krishnamurthy and Ajayamohan, 2010; Boos et al., 2015a). The genesis of these low-pressure systems (LPSs) has received enormous attention in the last few decades, and various mechanisms for their formation have been proposed (Krishnamurti et al., 1977; Shukla, 1978; Goswami et al., 1980; Adames and Ming, 2018a; Meera et al., 2019; Diaz and Boos, 2019a,b); further, recent work has brought forth the role of Intraseasonal Oscillations (ISOs) in creating a favorable environment for the genesis of these systems (Karmakar et al., 2021; Deoras et al., 2021). In fact, during the summer monsoon, LPSs over the Bay of Bengal have been classified as being born *in-situ* or associated with downstream

development of South China Sea disturbances (Krishnamurti et al., 1977; Chen and Weng, 1999; Meera et al., 2019). Moreover, global analyses have noted that systems occur throughout the monsoonal regions of the tropics (Hurley and Boos, 2015).

In contrast, Western India receives a considerable amount of rainfall from moist synoptic disturbances called Middle Troposphere Cyclones (MTCs, Carr, 1977; Choudhury et al., 2018). MTCs are tropical synoptic-scale systems with middle troposphere vorticity maximum and weak signature in the lower troposphere accompanying a northeast to southwest tilt with height. Moreover, MTCs exhibit warm and cold temperature anomalies above and below the mid-level center, respectively. The maximum convergence exists below the center, and divergence is observed in the upper troposphere (Miller and Keshavamurty, 1968). Further, MTC's dynamical and thermodynamic structures differ significantly from the monsoon lows and tropical cyclones. Compared to MTC's middle-level vorticity maximum and vertical tilt, monsoon lows are characterized by an upright, deep tropospheric relative vorticity structure with wind and convergence maxima in the lower troposphere (Hunt et al., 2016). Similarly, Tropical Cyclones (TCs, Wang and Jiang, 2019) are another prominent example of synoptic systems with upright vorticity structure and maximum intensity in the lower troposphere. Though, compared to lows and depressions, which usually show a shallow near-surface cold-core (Hunt et al., 2016), TCs have a warm temperature anomaly through the depth of the troposphere (Hawkins and Rubsam, 1968; Frank, 1977; Wang and Jiang, 2019). The structural differences of MTCs compared to other tropical systems are significant and require separate treatment and analysis (Carr, 1977).

Most of our knowledge about the Arabian sea MTCs comes from the data collected during the International Indian Ocean Experiment (IIOE, Miller and Keshavamurty, 1968) from 2-10 July 1963. The derived composite kinematic structure of MTC at 600 hPa and near-surface is shown in Figure 1.1. This clearly shows a synoptic-scale cyclonic circulation at 600 hPa. However, no such cyclonic vortex or closed circulation is evident near the surface except for a weak trough near the coast of Mumbai. Vertical cross-sections through the composite center are shown in Figure 1.2. The vorticity is maximum in the middle troposphere, weak in the lower troposphere, and anticyclonic above 300 hPa. Moreover, the convergence maximum is in the middle troposphere with a compensating divergence signature in the upper troposphere. Figure 1.2 suggests that the MTC center slopes

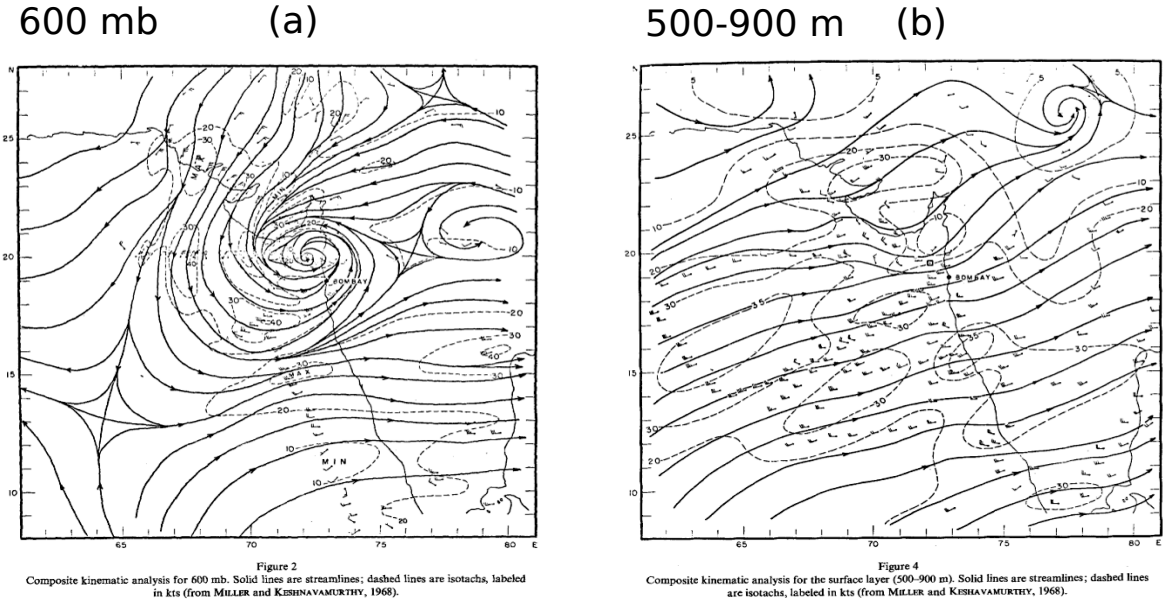

Figure 1.1: Composite kinematic structure of July 1963 MTCs from Miller and Keshavamurty (1968). Streamlines and isotachs are shown at (a) at 600 hPa and (b) 500-900 meter near-surface layer.

south and west with height, consistent with the temperature gradient in the mean environment (Carr, 1977). Interestingly, apart from occasional slow westward movement, this MTC mostly remained quasi-stationary during its life cycle for several days over the northeast Arabian Sea. This resulted in heavy rainfall along the west coast of India (Miller and Keshavamurty, 1968). More recent work has also pointed to this stationary nature of Arabian Sea MTCs and associated heavy rain events over the west coast (Choudhury et al., 2018).

1.2 Motivation

MTCs form throughout the monsoon season over western India (Gujarat, Maharashtra). As mentioned, these systems are responsible for a significant proportion of western Indian monsoon rain and are associated with extreme rainfall events (Choudhury et al., 2018; Miller and Keshavamurty, 1968). Indeed, the west coast of Maharashtra state in western India and the adjoining Arabian Sea generally receives moderate-intensity orographic rain throughout the primary monsoon months (Miller and Keshavamurty, 1968; Ramage, 1971; Kumar and Bhat, 2017). However, it has been observed recently that almost every year, parts of the state (especially Mumbai city and Konkan) face flooding due to MTCs (Shyamala and Bhadram, 2006; Francis and Gadgil, 2006; Kumar

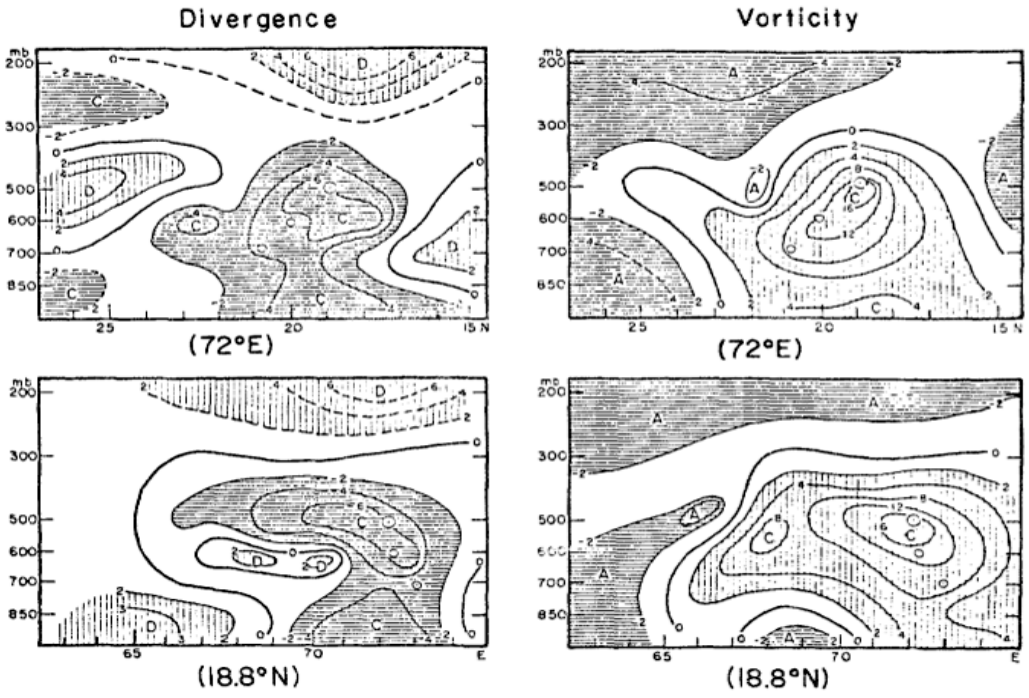

Figure 5
Meridional (top panels) and zonal (bottom panels) cross-sections of divergence and vorticity through the 500 mb composite center (18.8°N, 72°E). Both divergence and vorticity are given in units of 10^{-5} sec^{-1}. The circled dots represent the composite centers of the MTC at different levels (from MILLER and KESHAVAMURTY, 1968).

Figure 1.2: Composite kinematic structure of July 1963 MTCs from Miller and Keshavamurty (1968). Left column divergence and right panel vorticiy.

et al., 2008; Choudhury et al., 2018; Ray et al., 2019). As cyclonic systems over western India and the northeast Arabian Sea are confined to the middle troposphere during most of their life cycle, they remain unrecognized by traditional surface weather charts (Kushwaha et al., 2021), and are underestimated by tracking algorithms that use lower troposphere fields as identifying markers (Miller and Keshavamurty, 1968; Ramage, 1971; Kushwaha et al., 2021).

Apart from social-economic impact, understanding MTC's dynamic structure and formation mechanism may also significantly help understanding tropical convective systems of similar scales (Krishnamurti and Hawkins, 1970). Since they remain quasi-stationary during their life cyclone, these systems may be helpful in understanding and validating the convective quasi-equilibrium hypotheses (Krishnamurti and Hawkins, 1970). Recently, Choudhury et al. (2018) suggested the role of stratiform cloud diabatic heating distribution in shaping the vertical structure of MTC vorticity. Thus, how the dominant cloud types and their relative fraction alter the system's dynamics and

their genesis cycle will help to improve our understanding of the influence of cloud diabatic processes in tropical system dynamics. Understanding MTC formation aspects may also help gain insight into the development of tropical cyclones from mid-level vortices (Bister and Emanuel, 1997; Raymond et al., 2014a). Thus, studying the processes that lead to their formation and where and how frequently these systems occur compared to other synoptic tropical systems is crucial to furthering our understanding of tropical meteorology.

1.3 Regions of MTC Occurrence

From June-July 1963, to support the International Indian Ocean Expedition (IIOE), the US Weather Bureau Research Flight Facility (RFF) aircraft were deployed over the North Indian Ocean. A tropical synoptic system was observed over the central Bay of Bengal on 1 June and 2 June 1963, with a vigorous cyclonic circulation at 500 hPa and weak or no signature in the lower troposphere. The vorticity profile is accompanied by a warm above the cold-core structure near the center. This system was referred to as subtropical cyclone by Ramage (1971, 1964). However, later, it was realized that the structure of this system was significantly different from subtropical cyclones and needed to be placed in a separate class, i.e., a Middle Troposphere Cyclone (Carr, 1977). This was perhaps the first observational evidence of the presence of MTCs over the Bay of Bengal. Later in the month, the IIOE observation network was extensively deployed over the northeast Arabian Sea to understand the monsoon dynamics. A system was observed over the northeast Arabian Sea with intense middle troposphere circulation and almost no signature near the surface. This was the first discovery of MTC over the Arabian sea. This system remained quasi-stationary over this region from 28 June to 10 July 1963. Extensive data collation through the IIOE network allowed the study of this MTC in unprecedented detail, which is reported in Miller and Keshavamurty (1968). Other similar cases of MTCs were also reported off the west coast of India (Thiruvengadathan, 1972). Further Indian Meteorological Department every year inspects the weather charts and reports the existence of Arabian sea MTCs in their annual monsoon reports. Some significant MTCs which affected western India are listed in Choudhury et al. (2018). In addition to the Arabian Sea and Bay of Bengal, MTCs have been documented over southern Indochina (Krishnamurti and Hawkins, 1970). Apart from a subtle difference in motion, Indochina MTCs also exhibit similar characteristics as Arabian Sea MTCs, i.e., mid-level

vorticity maxima and warm above the cold-core temperature anomalies at mid-level center (Krishnamurti and Hawkins, 1970).

In the tropics, another example of a system with a pronounced mid-tropospheric signature and a deep cold-core in the lower troposphere is the African Easterly Wave (AEW; Burpee, 1972; Reed et al., 1977; Jenkins, 1995; Russell and Aiyyer, 2020). These waves contribute significantly to the West African Monsoon's intraseasonal variability from June to September (Nicholson and Grist, 2003), during which this receives almost 95% of its annual rainfall (Mohr, 2004). The West African Monsoon is characterized by a low-level westerly jet, large north-south temperature gradient, middle (850-600 hPa), upper level (300-150 hPa) easterly jet. The movement of AEWs is primarily controlled via the background flow that is dominated by a mid-tropospheric jet known as the African Easterly Jet (Russell et al., 2020; Russell and Aiyyer, 2020). Occasionally, AEWs develop into hurricanes as they reach over the Atlantic Ocean (Hopsch et al., 2010; Thorncroft and Hodges, 2001). While barotropic and baroclinic processes are essential in the genesis of AEWs (Thorncroft and Hoskins, 1994), their mid-tropospheric nature could be related to the generation of potential vorticity (PV) through meridional and vertical gradients of convective diabatic heating (Hsieh and Cook, 2008; Thorncroft et al., 2008; Russell et al., 2020; Russell and Aiyyer, 2020). Recent work on Arabian Sea MTCs and AEWs highlights the crucial role of stratiform convection in enhancing their mid-level circulation and vorticity (Choudhury et al., 2018; Russell et al., 2020). Further, case studies of easterly waves near Central America (Simpson et al., 1967; Reed and Recker, 1971), the Western Atlantic (Shapiro, 1986), and the Eastern Pacific (Raymond et al., 1998) regions have reported prominent mid-tropospheric signatures, though not necessarily a closed cyclonic circulation.

A Global Tropical Survey of MTCs

As discussed, few case studies of MTCs are available over South Asia (Miller and Keshavamurty, 1968; Krishnamurti and Hawkins, 1970; Thiruvengadathan, 1972; Choudhury et al., 2018), and most of them are limited to the Arabian Sea region. Thus their climatological frequency, motion, and robust structural aspects are poorly understood. It is unclear whether these systems mostly form over the Arabian sea or occur in other regions. Further, given that the mid-tropospheric nature of African Easterly Waves is similar to that of MTCs over South Asia, it

is worth asking what the differences are in middle tropospheric systems over different regions of the globe. Considering this background, we first pursue a global tropical survey of MTCs (Chapter 3). As with the recent study of monsoon lows by Hurley and Boos (2015), a better and more general understanding of these mid-troposphere systems can be attempted with this global tropical perspective.

1.4 Arabian Sea MTC Formation

The Arabian Sea region is one of the hot spots for heavy rain-producing MTCs over the global tropics (Choudhury et al., 2018; Kushwaha et al., 2021). In fact, over South Asia, the maxima MTCs activity is observed over the northeast Arabian Sea (Kushwaha et al., 2021). Despite MTCs being a critical driver of rains, what leads to their genesis remains poorly understood.

Initially, with the aid of the steady-state monsoon models, it was argued that the heat low to the west and north of the Arabian Sea exports vorticity at middle levels, which in turn triggers the formation of Arabian Sea MTCs (Ramage, 1966); in fact, the strength of this heat low is known to be partly connected with cyclonic activity over the Bay of Bengal through the subsidence warming of northwest India (Rodwell and Hoskins, 1996; Ramage, 1966, 1971). The local formation of synoptic systems in this region is further complicated by the presence of deserts to the west and north and narrow western Ghat mountains to the east (Krishnamurti et al., 1981; Varikoden et al., 2019). Despite this, fundamental dynamical instability investigations have probed the *in-situ* formation of MTCs (Goswami et al., 1980; Brode and Mak, 1978; Mak, 1975, 1983; Mak and Jim Kao, 1982); however, complexities in identifying proper mean state for instability analysis in an evolving monsoon flow have plagued these efforts (Carr, 1977). Apart from attempts at identifying the *in-situ* formation of Arabian Sea systems, surveys of satellite images showed MTCs over the Arabian Sea to be remnants of monsoon lows moving westward from the Bay of Bengal (Carr, 1977). Recently, detailed manual tracking of MTCs over South Asia using modern reanalysis data spanning sixteen years clearly showed that many MTCs originate as monsoon lows over the Bay of Bengal and later behave like MTCs once they reach the Arabian Sea (Kushwaha et al., 2021). Thus, in addition to in situ genesis, downstream development of LPSs from the Bay of Bengal is a potential route for forming MTCs over the northeast Arabian Sea and western India.

Additionally, during the formation of the 1963 MTC formation, one of the essential meteorological phenomena noted was the coexistence of an LPS over the Bay of Bengal throughout the life cycle of the Arabian Sea MTC. In addition, Miller and Keshavamurty (1968) analyzed conditions during three additional instances of Arabian Sea MTCs. In all cases, again, the coexistence of a warm core monsoon LPS in the Bay of Bengal was a persistent phenomenon. Further analysis of the lead-lag times series of relative vorticity suggested that the cyclonic anomaly in the Bay of Bengal preceded the extreme rain events and vorticity enhancement over the Arabian Sea and western India (Miller and Keshavamurty, 1968; Ramage, 1971). Along similar lines, Choudhury et al. (2018) examined 20 heavy precipitating MTCs over western India from the India Meteorological Department (IMD) data and found that 90% of them formed in the presence of westward-moving LPS over the Bay of Bengal. They also noted that during the formation of most of the MTCs, the $30-60$ day ISO mode was in an active phase over western India.

Thus, given their importance, there is a pressing need to understand what conditions lead to MTC formation, or what their precursors, are using a large sample size afforded by modern reanalysis data. This will allow for a proper investigation of local instability mechanisms for specific classes of MTCs and, more broadly, open a doorway for the potential predictability of extreme rainfall events over western India.

Classification of Arabian Sea MTCs

As discussed, *in situ* genesis and downstream development of LPSs from the Bay of Bengal are the two potential dominant routes for forming MTCs over the northeast Arabian Sea and western India. Further, during *in-situ* MTC formation, the presence of a monsoon low to the east of India and the Bay of Bengal appears to be the most persistent meteorological condition. However, as these observations were based on case studies and with limited duration data, the robust percentage of each class remained unclear. For instance, it is unclear how many of these systems form locally and what fraction results from downstream development of LPSs from the Bay of Bengal. Moreover, specific categories of MTCs prone to producing heavy rainfall need to be explored from a practical standpoint. In the second part of this thesis, we elucidate the formation routes of Arabian Sea MTCs by analyzing the characteristics of rainy days in western India (Chapter 4) and whether there are distinct weather patterns

associated with a bulk of the precipitating events. To prove this unbiasedly, we adopt an unsupervised machine learning (k-means clustering) technique to extract possible clusters of weather patterns on rainy days. Further, we use an independent cyclone tracking method to identify and track middle tropospheric systems, classify them as per their formation mechanism, and compare the results with the k-means methodology. Moreover, given the apparent link between cyclonic activity over the Bay of Bengal and Arabian Sea systems, we systematically explore this propensity of coexistence in terms of how many Arabian Sea MTCs form in the presence of cyclonic system over the Bay of Bengal. Precipitation characteristics and monthly frequency of the different categories within a season are explored, and the modulation by ISOs of each category is also studied.

1.5 Arabian Sea MTCs and cyclonic activity over the Bay of Bengal

The aircraft of the US Weather Bureau Research Flight Facility (RFF) and the Woods Hole Oceanographic Institution explored the northeast Arabian Sea from the surface to 14 km in June-July 1963. As discussed, an MTC was observed from 28 June to 10 July within the range of the observation network. The observation suggested that a warm-core monsoon low formed on 24 June in the Bay of Bengal (around 15N, 97E) with the establishment of the monsoon circulation. In the next two days, the system moved northwestward and crossed the Odisha coast on 26 June around 17°N, and for the next three days system remained stationary north of Tamil Nadu and south Odisha over the East coast. During this time, Rawin reports at Mumbai and Ahmadabad suggested an enhancement of cyclonic shear between 700-500 hPa layers. An MTC was observed on 28 June over the Konkan coast and adjoining the northeast Arabian Sea within the shear zone. With the formation of MTC, an east-west trough formed in the middle troposphere extending from the Arabian Sea to the Bay of Bengal through peninsular India, and a significant active phase of the Indian Monsoon occurred during 2-10 July. The detailed analysis of (Miller and Keshavamurty, 1968) suggested that the presence of MTC was the most significant feature during the active phase of the July 1963 monsoon over western India. Strengthening of westerlies south of 20°N and extension of easterly down to 850 hPa north of 20°N were also observed. Miller and Keshavamurty (1968) compared flow at various vertical levels and concluded that surface layer charts alone failed to yield a satisfactory explanation for the extreme rain which fell after 1 July along the west coast and extended into the Arabian Sea. Since there

was hardly any change in the direction and strength of southwest winds, low-level convergence prior to the sharp increase in the rainfall over the northeast Arabian sea prior to the onset of the heavy rainfall, the MTC was the only significant feature to which this transition to extreme rainfall could be attributed.

Further, Miller and Keshavamurty (1968) noted that desert air from north and west was overriding the moist surface layer during the genesis of MTC. Ship and aircraft observations showed the presence of extensive stratocumulus over the Arabian Sea west of $65°$E, suggesting the trapping of moisture in the lowest 2 km under a strong temperature inversion brought about by differential temperature advection from desert air over cold marine air. Indeed, dropsondes released at 500 hPa during the RFF flight revealed the presence of inversion at 900 hPa. However, the low-level inversion disappeared over the northeast Arabian Sea when the MTC intensified. Following this, there was an increase in moisture content within the system's 700 hPa to 500 hPa layer.

The low-level inversion is primarily due to warm air advection in the middle tropospheric from arid regions to the west and north over relatively cold moist southwesterly monsoon winds in the lower troposphere (Narayanan et al., 2004; Muraleedharan et al., 2013; Das et al., 2021), which is aided by subsidence warming (Narayanan et al., 2004). This low-level inversion inhibits the vertical motions and vertical advection of moisture. Further, the cold SSTs over western Arabian due to subsurface ocean upwelling and evaporating cooling in the western Arabian Sea forced by strong low-level monsoon winds also suppress convection over western Arabian sea compared to east (Izumo et al., 2008; Kumar et al., 2016). As a result of both inversion and cold SST, the western Arabian Sea exhibits a very shallow moist layer and dry middle troposphere. However, as SST increases towards the east and inversion weakens, the depth of the moist layer increases towards the East Arabian Sea (Menon et al., 2018). These moisture gradients not only affect local convection but have far-reaching implications — for instance, quite frequently, advection of dry air in the middle troposphere influences the variability of middle troposphere moisture over western India, which controls rainfall variability in this region (Fletcher et al., 2018; Hunt et al., 2021). Given dry regions to the west and north, the moistening of the middle troposphere, in the absence of *in-situ* deep convection, can only be possible through advection from the east and south (Ramage, 1971). In fact, during the monsoon, the climatological flow over the northeast Arabian Sea is westerly or southwesterly below 600 hPa and easterly above; thus, the direction of winds plays a vital role in the moisture control of the middle

troposphere in western India (Menon et al., 2018). Indeed, abundant middle troposphere moisture and entropy are the necessary conditions for tropical convection (Raymond, 2000; Raymond et al., 2009), and are expected to affect the evolution of MTCs over the Arabian Sea and western India.

Thus, the outstanding questions these raises are, what causes the inversion to weaken, which processes lead to the development of the easterlies north of 20°N, and what causes the moistening of the middle troposphere over the northeast Arabian Sea. In essence, the dynamical cause of the features noted during MTC formation by Miller and Keshavamurty (1968) remains largely unanswered. In all, these observations indicate that Arabian Sea MTCs form in the complex dynamic and thermodynamic environment, and apart from downstream formation, quite frequently, *in-situ* MTC formation occurs with the Bay of Bengal system LPS, so does the low over the Bay alter the Arabian Sea dynamic and thermodynamic environment to facilitate the genesis of an MTC?

Influence of Bay of Bengal LPS on the genesis of Arabian Sea MTCs

The precedence and coexistence of a monsoon low over the Bay of Bengal is the most common feature during the life cycle of Arabian Sea MTCs. After quantifying the number of MTCs that form in such situations, we ask whether this is a coincidence or whether the Bay of Bengal low plays an indirect or direct role in forming and maintaining Arabian Sea MTCs. This issue is addressed in the third part of this thesis (Chapter 5), where we will explore the role of the Bay of Bengal system in the genesis of Arabian Sea MTCs using observations and the Weather Research and Forecasting Model (WRF). Proper understanding of the role of the Bay of Bengal in the formation and maintenance of the Arabian Sea system will also help in better prediction and understanding of extreme rainfall events associated with them. To probe this issue, a "Bogus Vortex" or LPS is introduced over the June-July climatological background flow over the Bay of Bengal. By creating a suitable ensemble of such simulations, we examine the flow evolution and, in particular, see if the low over the Bay leads to the genesis of an MTC over the Arabian Sea and western India. In another set of experiments, we take an actual representative case of coexisting Arabian Sea and Bay of Bengal systems; here, we artificially cool the Bay and dry the overlying atmosphere. As a result, the intensification of the Bay of Bengal system is suppressed, and the question is to see if the MTC develops even in the absence of suppressed cyclonic conditions over the Bay? In essence, this latter

experiment is a mechanism denial simulation where we suppress the low over the Bay to rule out its influence on the conditions over the Arabian Sea.

In summary, the rest of the thesis is organized as follows: Chapter 2 discusses the data and methods used throughout the thesis. Chapter 3 covers the global tropical survey of MTCs and their comparison to LTCs. Chapter 4 probes the classification of Arabian Sea MTCs using cyclone tracking and k-means clustering. In Chapter 5, we explore the role of an LPS over the Bay of Bengal in forming an Arabian Sea MTC using WRF model simulations. Finally, Chapter 6 summarizes the results and presents avenues for future research.

Chapter 2

Data and Methods

In this chapter of the thesis we present details of the data used in our analysis, as well as the techniques developed and employed in various stages of our work. This spans a range of reanalysis products including Modern-Era Retrospective Analysis for Research and Application (MERRA-2), the ECMWRF Research Analysis data (ERA-5), satellite derived rainfall data such as the tropical Rainfall Measuring Mission (TRMM) and outgoing longwave radiation from the National Oceanic and Atmospheric Administration (NOAA). Each of these is described in detail along with their suitability for the present work. The techniques we have developed or utilized to study MTCs and LTCs includes the objective identification of such cyclonic systems, cyclone tracking algorithms (both manual and automated), cyclone metrics and k-means unsupervised learning methodology. Finally, we describe the Weather Research and Forecasting (WRF) model setup, the "Bogus Vortex" Scheme which is used to simulate the influence of a LPS in the Bay on the development of an Arabian Sea MTC and the formulation of the moisture and vorticity budgets that is used to see the import of moisture during the formation of an Arabian Sea MTC and what terms of vorticity dominates during the formation of MTCs.

2.1 Data

2.1.1 MERRA-2 Data

One of the principal data sets we use is the daily Modern-Era Retrospective analysis for Research and Applications Version-2 (MERRA-2) reanalysis spanning years 2000-2019 (Gelaro et al., 2017). The data is available at an approximate resolution of $0.625^\circ \times 0.5^\circ$ on a longitude-latitude grid and on 72 hybrid-eta levels from the surface to 0.01 hPa. The MERRA-2 system retains many of the basic features of MERRA (Rienecker et al., 2008) with several essential updates such as aerosol data assimilation, changes to the forecast model, and bias correction using aircraft observations (Gelaro et al., 2017). In particular, significant improvements have been noted in MERRA-2, especially post the year 2000; for example, in the representation of TC wind, mean sea-level pressure intensities (Hodges et al., 2017), outer size, and overall wind structure (Schenkel et al., 2017). Given the above improvements, we have selected the data from 2000-to 2019 for our study.

Data on 25 vertical levels between 1000 hPa and 100 hPa is used with a resolution of 25 hPa from 1000-700 hPa and 50 hPa at upper levels from 700-100 hPa. As the studied systems are larger than 150 km in scale, the data sets are interpolated to a 1.5° grid prior to application. Such reduced resolution usually filters out small-scale vorticity centers, which generally introduces errors in tracking features of interest (Bengtsson et al., 2007). Further, for tracking synoptic-scale systems, the use of daily data, rather than finer temporal resolutions, does not affect the nature of results in the manual tracking procedure (see Figure A.1). Moreover, for a given computational capacity, this also allows for the use of high vertical resolution global data and reduces the labor of manual tracking of systems.

2.1.2 ERA5 Data

We also utilize ECMWF ERA-5 fifth-generation atmospheric reanalysis data set (Hersbach et al., 2020), which is generated using 41r2 of the Integrated Forecast System (IFS) model. IFS system utilizes a four-dimensional variational data assimilation scheme and takes advantage of 137 vertical levels and a horizontal resolution of 0.28125° (31 km, or TL639 triangular truncation). The data is stored at every hour of model integration. In

our analysis we use six-hourly winds, vorticity, divergence, temperature, and moisture fields on pressure levels from $1000 - 100$ hPa and native horizontal resolution. However, we use interpolated data on 1.5 degrees latitude-longitude gird for synoptic charts. Apart from a high spatial and temporal resolution, ERA-5 has several important updates to its predecessor ERA-I, which was terminated in 2019. These include the use of ozone, satellite radiance, aircraft, and surface pressure data in the assimilation scheme. One of the important changes in ERA-5 is using an all-sky approach instead of the clear sky approach used in ERA-I, thus providing additional information about precipitation and cloud distribution. These updates, along with others, have resulted in more consistent sea-surface temperature and sea-ice compared to ERA-I (Hersbach et al., 2020).

The latest high-resolution reanalysis products, such as ERA-5 and MERRA-2 that ingest large amounts of satellite and ground-based observations, have been successfully employed in detecting and tracking Indian monsoon LPSs and understanding their contribution to monsoon rainfall (Hurley and Boos, 2015; Hunt et al., 2016; Boos et al., 2015a; Hunt and Fletcher, 2019). In fact, modern reanalysis data has allowed for reliable investigations of different structural aspects of monsoon lows, such as their vertical thermal and dynamical features and motion characteristics (Hunt et al., 2016; Hunt and Fletcher, 2019; Sørland and Sorteberg, 2015). Of course, despite significant improvement in reanalysis products, there are still several caveats to be kept in mind; these include unresolved low-level structure and an exaggerated cold-core in the lower troposphere (Manning and Hart, 2007; Wood and Ritchie, 2014), and at times, unrealistic thermal structures, especially in regions of the globe that have a paucity of observations (Janiga and Thorncroft, 2013). Further, the intensity of systems, their temporal coherence, and structure is likely to differ among different reanalysis products (Hodges et al., 2003). Nevertheless, in light of several improvements, we believe that ERA-5 will be suitable for the present goals (Mahto and Mishra, 2019; Nogueira, 2020; Yeasmin et al., 2021; Bian et al., 2021). It is important to note that, as a precaution, we use the reanalysis in conjunction with satellite-based products for robustness and to avoid false detection of rain-bearing systems.

2.1.3 ISO Index

To understand the role of large-scale environmental conditions in Arabian Sea MTCs formation, we utilize intraseasonal Boreal Summer Intraseasonal Oscillation (BSISO) indices which are available at `http://iprc.soest.hawaii.edu/users/kazuyosh/Bimodal_ISO.html` [Accessed May 2021]. This includes the first two normalized principal components ($PC1$ and $PC2$) with their respective magnitude ($\sqrt{PC1^2 + PC2^2}$) and phase (Kikuchi and Wang, 2010; Kikuchi et al., 2012; Kikuchi, 2020), that explain about 25% variance of the Outgoing Longwave Radiation (OLR) and wind fields at intraseasonal scales (Wheeler and Hendon, 2004). This data is available at a daily temporal resolution from 1979-to 2020. Each phase of this intraseasonal oscillation (ISO) corresponds to a specific location of enhanced moist convection over South Asia, and its amplitude represents the strength of this enhanced convection. In particular, phase 2 to phase 3 of BSISO corresponds to enhanced convection over the southern Arabian Sea and the southern Bay of Bengal. Phases 4 & 5 are when the Indian subcontinent goes through a wet spell and convection shifts to the northern Bay of Bengal and the northern Arabian Sea. During Phases 6 through 8, convection weakens, representing the dry or break phase over the Indian subcontinent. Several authors have suggested that the BSISO phase and amplitude modulate various meteorological phenomena, including the onset of monsoon, formation of cyclones, and monsoon lows (Wheeler and Hendon, 2004; Karmakar et al., 2021; Hunt et al., 2021; Deoras et al., 2021). Thus, it is worth exploring whether the BSISO also influences the formation of synoptic systems in the Arabian Sea and western India. Two components usually describe ISO modes — the eastward-moving Madden-Julian Oscillation, which dominates in boreal winter (December-May), and the northward propagating BSISO, which is prominent during the boreal summer (May-October). As we are dealing with the summer monsoon, we mainly use the BSISO index to represent the strength and phase of intraseasonal activity.

2.1.4 Rainfall and OLR data

We use Tropical Rainfall Measuring Mission (TRMM) data for rainfall estimates (Huffman et al., 2007, 2010). In particular, the TRMM Multi-satellite Precipitation Analysis (TMPA)-3B42 Version 7 product with a horizontal resolution of $0.25^\circ \times 0.25^\circ$ is used from 1998-to 2019. The improvements in Version 7 of this product are

described in Prakash et al. (2013). Rainfall data is utilized to distinguish rainy cyclonic systems from dry ones and to understand the quantum of precipitation in different classes of systems. Finally, satellite measured OLR data at 2.5° spatial and daily temporal resolution from the National Oceanic and Atmospheric Administration (Liebmann and Smith, 1996) is used as a proxy for moist convection.

2.2 Detection of MTCs and LTCs

In order to study MTCs and LTCs, at the outset it is essential to have objective criteria to identify cyclonic systems and differentiate between the aforementioned classes. The identification of a cyclonic low has a long history and we follow traditional methods as described by Sinclair (1994); Lambert (1996). The distinction between MTCs and LTCs requires an additional crucial step of differentiating between systems based on the vertical position of their relative vorticity maximum. System identification starts with checking each grid point of the 600 hPa geopotential height field to locate local minima. We choose the 600 hPa geopotential height surface for identification since MTCs (Carr, 1977; Choudhury et al., 2018), monsoon lows (Hurley and Boos, 2015; Hunt et al., 2016) and tropical cyclones (Wang and Jiang, 2019) all exhibit a robust signature at this level. System centers are identified along with their properties including, latitude, longitude, level of vorticity maximum (P_ξ), mean middle (650-500 hPa), lower layer (1000-850 hPa) vorticity (ξ_m and ξ_l) and mean middle layer-specific humidity (Q_m). Further, the differential vorticity, $\delta\xi_p (= \xi_m - \xi_l)$ is computed for each identified center. These properties are averaged over a $4^\circ \times 4^\circ$ region centered on the storm. An area average is used to ensure that the sign of $\delta\xi_p$ is not an artifact of differences at a single grid point. In fact, this is the typical size of the core of MTCs at 600 hPa level (Carr, 1977; Miller and Keshavamurty, 1968). The classification of cyclonic systems is based on the following constraints:

1. A system is classified as a MTC if its relative vorticity maximum lies in the middle troposphere (i.e., $650 \geq P_\xi \geq 500$ hPa), the mean middle and lower layer vorticity is positive (i.e., $\xi_m > 0$, $\xi_l > 0$) and mean middle layer vorticity exceeds that of the lower layer by a given threshold (i.e., $\delta\xi_p > 1.5 \times 10^{-5} s^{-1}$).

2. A system is classified as a LTC if its relative vorticity maximum lies in the lower troposphere (i.e., $1000 \geq$

$P_\xi \geq 700$ hPa), the mean lower and middle level vorticity is positive (i.e., $\xi_m > 0$, $\xi_l > 0$) and mean lower layer vorticity exceeds that of the middle layer by a given threshold (i.e., $\delta\xi_p < -0.8 \times 10^{-5} s^{-1}$).

3. Further, only moist and intense systems of each category are considered by imposing threshold values of $Q_m > 2$ g/kg (Holloway and Neelin, 2009) and $\xi_m > 1.5 \times 10^{-5} s^{-1}$, respectively.

The choice of the thresholds mentioned above for layers, intensity, and moisture content is justified in the following section.

2.2.1 Selection of Identification Parameters

Apart from a few case studies (Miller and Keshavamurty, 1968; Krishnamurti and Hawkins, 1970), to our knowledge, the only MTC events cataloged are by the IMD during the years 1998-2008 over the Northeast Arabian Sea (Choudhury et al., 2018). Here, we utilize the 35 middle troposphere circulation events listed in Choudhury et al. (2018) to estimate the properties of MTCs. Since MTCs in the Arabian Sea usually co-exist with MDs over the Bay of Bengal (Carr, 1977; Choudhury et al., 2018), we extend the region of inspection to cover both the ocean basins (i.e., $5°$N to $25°$N and $50°$N to $95°$E) to sample a spectrum of monsoon systems. During these 35 middle troposphere events, the detection algorithm identifies 725 non-topographic[1] strong cyclonic centers. The joint probability distribution of $\delta\xi_p$ and P_ξ of these 725 systems is shown in Figure 2.1 wherein the correlation among them is -0.7. This implies that the more substantial the positive/negative difference between middle and lower layer vorticity (i.e., $\delta\xi_p$), the larger is the possibility that the level of vorticity maximum situated in higher/lower levels and vice versa. Figure 2.1 shows two regions of high cyclone probability; one at middle levels (500–700 hPa) and the other at lower levels (700–1000 hPa) with a fair amount of spread in $\delta\xi_P$. The natural emergence of these two distinct regions lends credence to studying mid and lower tropospheric systems separately. Note that the two peaks in the probability density function become more apparent when considering relatively large samples of systems from the global tropics.

Considering the features in Figure 2.1 and guided by previous work (Rios-Berrios and Torn, 2017; Ditchek et al.,

[1]Note that MERRA-2 does not extrapolate data below the surface; instead, it lists data undefined. Here, we reject any system as topographic if it has missing vorticity values at the center or if any velocity component has missing values within four degrees east, west, north, or south of the center in the lower layer.

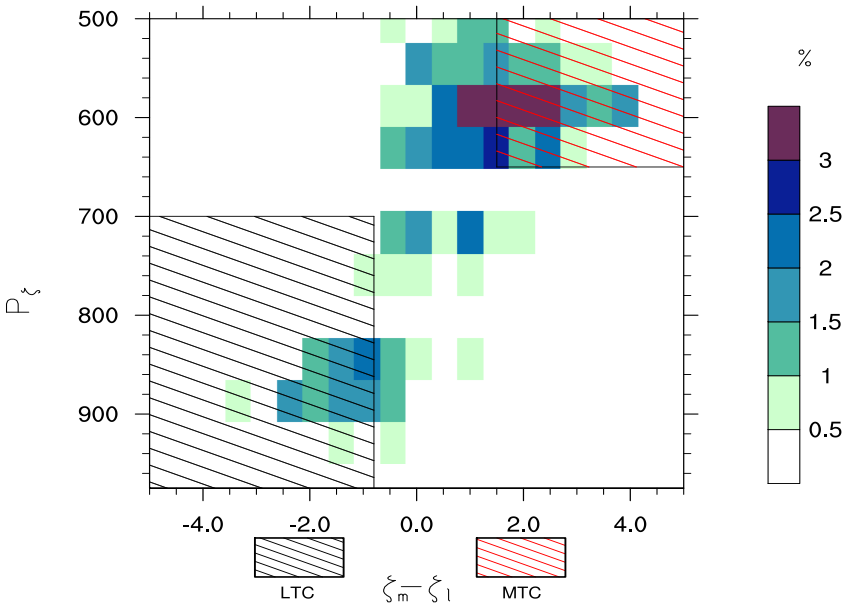

Figure 2.1: Joint probability distribution of $\delta\xi_p = \xi_m - \xi_l (\times 10^{-5} s^{-1})$ and the level of maximum relative vorticity (P_ξ), in hPa for 725 strong & moist cyclonic centers detected during the dates of 35 IMD MTC events over the region 5°N–25°N, 50°E–95°E. Red and black hatching indicates bounds of MTCs and LTCs, respectively.

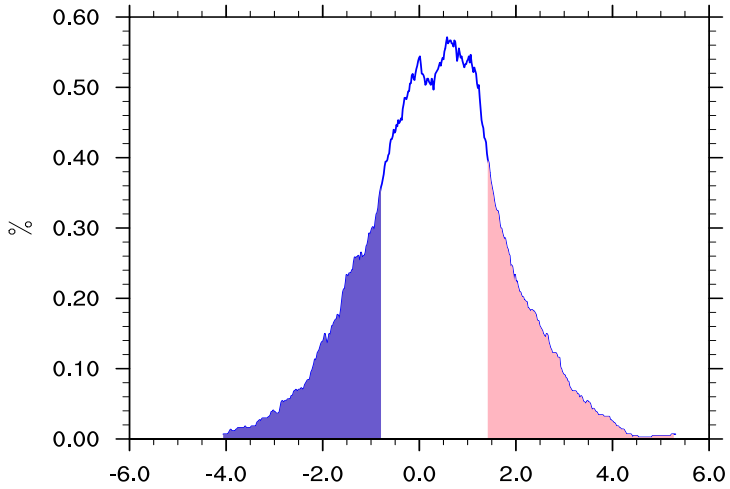

Figure 2.2: Probability distribution of differential vorticity ($\delta\xi_p$, $\times 10^{-5}$ s^{-1}) cyclonic centers as in Figure 2.1. Light blue shaded region denotes lower 20th percentile (i.e., below -0.8×10^{-5} s^{-1}) and the light pink region denotes upper 20^{th} percentile (i.e., above 1.5×10^{-5} s^{-1}).

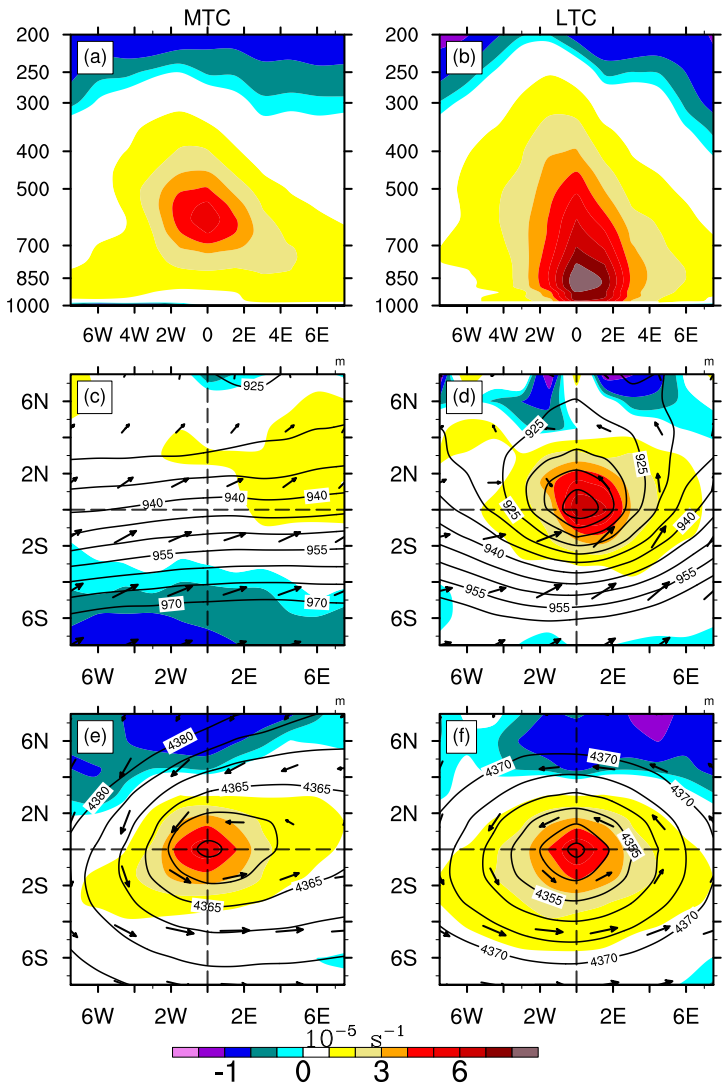

Figure 2.3: Relative vorticity composite from 121 middle troposphere cyclonic centers (Left Panels: a, c, e) and 126 lower tropospheric cyclone centers (Right Panels: b, d, f) from the Indian region. (a), (b) East-West-vertical cross-section through composite center y-axis is pressure in hPa. (c), (d) Horizontal cross-sections at 975 hPa and (e), (f) at 600 hPa. Dashed lines indicate axes through the composite center. Vectors indicate the composite wind of MTC and LTCs and contours represent the composite geopotential height at respective levels in m. Units of the x-y axes of sub-figures c-f are degrees east and degrees north with respect to composite cyclone center, respectively.

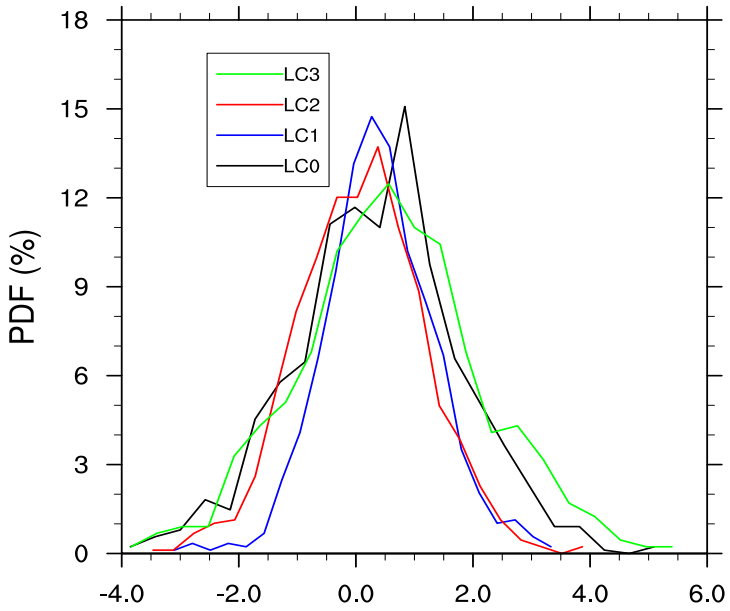

Figure 2.4: Sensitivity of the distribution of differential vorticity ($\delta\xi_p$) to different choices of layers combinations. LC0: lower layer 1000–850 hPa, middle layer, 650–500 hPa; LC1: lower layer 1000-850 hPa, middle layer, 850–500 hPa; LC2: lower layer 1000–650 hPa, middle layer, 650–500 hPa and LC3: lower layer, 900 hPa, middle layer, 600 hPa.

2019), we select the upper 20^{th} percentile of $\delta\xi_p$ (=$1.5 \times 10^{-5}s^{-1}$) as a threshold for MTCs and the lower 20^{th} percentile of $\delta\xi_p$ ($= -0.8 \times 10^{-5}s^{-1}$) as a threshold for non-MTCs (Figure 2.2). Indeed, there can be stricter criteria to separate the MTC and non-MTC categories more clearly, but these will be at the expense of reducing the number of systems sampled. We have settled on these specific numbers as they successfully contrast and differentiate between the two classes of systems. Further, to ensure that the vorticity maximum is confined within specific layers of interest, constraints of $500 \leq P_\xi \leq 650$ for MTCs and $700 \leq P_\xi \leq 1000$ for non-MTCs are applied. Most of the non-MTC category systems have a vorticity maximum in the lower troposphere and are called lower tropospheric cyclones (LTCs). This category excludes heat lows, which are generally dry and confined below 700 hPa (Spengler and Smith, 2008). Though MTCs show vorticity maximum between 700-500 hPa (Figure 2.1), we use a slightly stricter criterion that P_ξ should be above 650 hPa to avoid the cyclonic shear corresponding to the African Easterly Jet, which exhibits maximum intensity around 700 hPa (Burpee, 1972; Reed et al., 1977). In essence, the MTCs and LTCs defined by the above thresholds are shown by red and black shading in Figure 2.1, respectively. These criteria ensure that the identified systems have a robust cyclonic circulation and are moist.

Further, as shown in Figure 2.3, composites of cyclonic centers defined as MTCs and LTCs in Figure 2.1, validate the choice of thresholds—composite MTC vorticity maxima are in the middle troposphere and LTC in the lower troposphere. The sensitivity of $\delta\xi_p$ to different choices of layers in Figure 2.4 shows that this does not affect the form of the probability distribution of $\delta\xi_p$, though, as expected, this influences the number of MTCs and LTCs. The sensitivity of the number of MTCs and LTCs to moisture and vorticity thresholds is shown in Table A.1. It is important to note that these thresholds should be treated as tuning parameters and might need adjustment for different data sets, especially with different horizontal resolutions. Throughout the manuscript, a two-tailed Student-t-test is utilized to ascertain the statistical robustness of results (Wilks, 2016). The test statistics are calculated from the daily mean anomaly fields derived with respect to daily climatology from 2000-to 2019. Results are shown if they are significantly different from daily climatology at 1% significance.

2.2.2 Manual Tracking of MTCs

Following Grigoriev et al. (2000), given its accuracy (Gulev et al., 2000), MTCs are tracked manually in the boreal summer season for 16 years from 2000-2015. This approach is similar to manual tracking of mesoscale convective systems (Davis et al., 2002). The tracking method can be summarized as follows:

1. Daily maps of the 600 hPa geopotential height and streamlines are examined for local minima. These constitute the detected centers of cyclonic systems.

2. These detected centers are labeled, and maps are examined for 1952 days (122$\times$ 16 = 1952; the number of days in a season $\times$ number of years).

3. Cyclones are tracked by comparing labeled sequential daily maps.

4. The first occurrence of an MTC is considered its starting location within the domain provided $\xi_m > 1.5 \times 10^{-5}s^{-1}$ for at least two consecutive days and $\xi_m - \xi_l > 1.5 \times 10^{-5}s^{-1}$ for a minimum of two days within its life cycle.

5. Tracks are terminated when the cyclone shows $\xi_m < 1.5 \times 10^{-5}s^{-1}$ for two successive days. Further, only systems that last for more than three days are considered in the study.

In essence, the first step is to detect geopotential minimum (system center) and calculate properties such as ξ_m and $\delta\xi_p$ associated with it. Then tracks are constructed wherein conditions 3, 4, and 5 are repeated for each center.

2.2.3 Cyclone Metrics

Two measures of cyclone activity namely *cyclone center density* and *track density* are used in this study (Sinclair, 1994). The cyclone center density counts the number of cyclonic centers of all tracks passing within a specific area. When a sufficiently large number of cyclones from multiple years are considered, this measure becomes proportional to the probability of an area being under cyclonic conditions (Sinclair, 1994). For the computation of cyclone matrices, we use 8° catchment area surrounding each grid point, which leads to a smoothing of patterns and ensures continuity of variables in the resulting maps. The second measure, track density, counts the number of cyclone tracks passing within an area centered over each grid point. When derived from sufficiently long data sets, track density becomes proportional to the probability of a cyclone passing in the vicinity of a grid point (Sinclair, 1994). In addition, we define MTC-phase ($\delta\xi_p > 1.5 \times 10^{-5}s^{-1}$) and LTC phase ($\delta\xi_p < -0.8 \times 10^{-5}s^{-1}$) track density as a count of track segments passing within 8° box that belong to the MTC-phase and LTC-phase, respectively. Cyclone motion vectors are also computed for each track point to quantify the motion characteristics of MTCs. All tracks are interpolated spatially to ensure that at least one track point appears in a cell of 1.5° resolution.

2.3 Classification of western Indian weather patterns using k-means

In this section, we deal with the tools which are utilized in the identification of various classes of MTCs and the associated weather patterns. The identification of distinct weather patterns associated with rainfall over western India is achieved by clustering of daily 600 hPa geopotential height anomaly maps by an unsupervised machine learning method known as k-means (Hartigan and Wong, 1979). Prior to applying the method, only moderate or higher intensity rain days are retained by removing dry and light rain days using the threshold $P_{WI} > 7.6$ mm/day, as defined by the Indian Meteorological Department; where P_{WI} is the mean TRMM rainfall over western India bounded by 68°E–72°E and 15°N–22°N; this region of averaging is similar to that of Choudhury

et al. (2018) with a slight reduction of eastern boundary and increase to the south to avoid the effect of topographic rainfall since we are primarily interested in precipitation from synoptic-scale systems.

In the recent past, k-means clustering has proved to be a useful tool in a variety of meteorological applications (Awan et al., 2015; Jiang et al., 2016; Pope et al., 2009; Clark et al., 2018). Broadly, clustering is an approach wherein similar data vectors (daily 600 hPa height anomaly maps in this study) are placed into unique groups or clusters. In k-means, a set of x observations, $[X = X_1, X_2, X_3....X_i...X_x]$; which are real vectors, each having N dimensions are sorted into k clusters, $[K = K_1, K_2, K_3, ...K_i....K_k]$. Here, we use daily geopotential height anomalies of 600 hPa pressure surface from the domain $0 - 30°$N and $60 - 100°$E as the set of vector arrays, with each observation having dimension $N = m \times n$; where m and n are the number of latitude and longitude points in the domain. As similar data vectors will have small Euclidean distances, they will be placed into the same clusters. In the context of this work, this amounts to placing height anomaly patterns with similar spatial distribution and intensity into the same cluster. Note that the domain on which we perform k-means includes the dominant regional features of monsoon: specifically, the monsoon trough, heat low to the north, the Bay of Bengal to the east, and low-level monsoon jet to the south.

Essentially, the k-means clustering algorithm involves the following steps:

1. Randomly assigns k data points as initial cluster centroids.

2. Compute the Euclidean distance of all data points from each cluster centroid.

3. Assign each data point to a cluster centroid with the minimum Euclidean distance.

4. Recalculate the cluster centroids and repeat steps 2 and 3 until each cluster centroid becomes stable.

This method heavily relies on the parameter k, i.e., a number of user-defined initial clusters. Therefore, it is crucial to select the appropriate number of clusters k; a too-small value of k may result in merging different clusters, which may have essential differences and thus be susceptible to the loss of important weather patterns; too large a value may result in multiple clusters which may be only slightly different in intensity or spatial patterns. Here we used two complementary methods to select k; the silhouette coefficient (Rousseeuw, 1987) and elbow

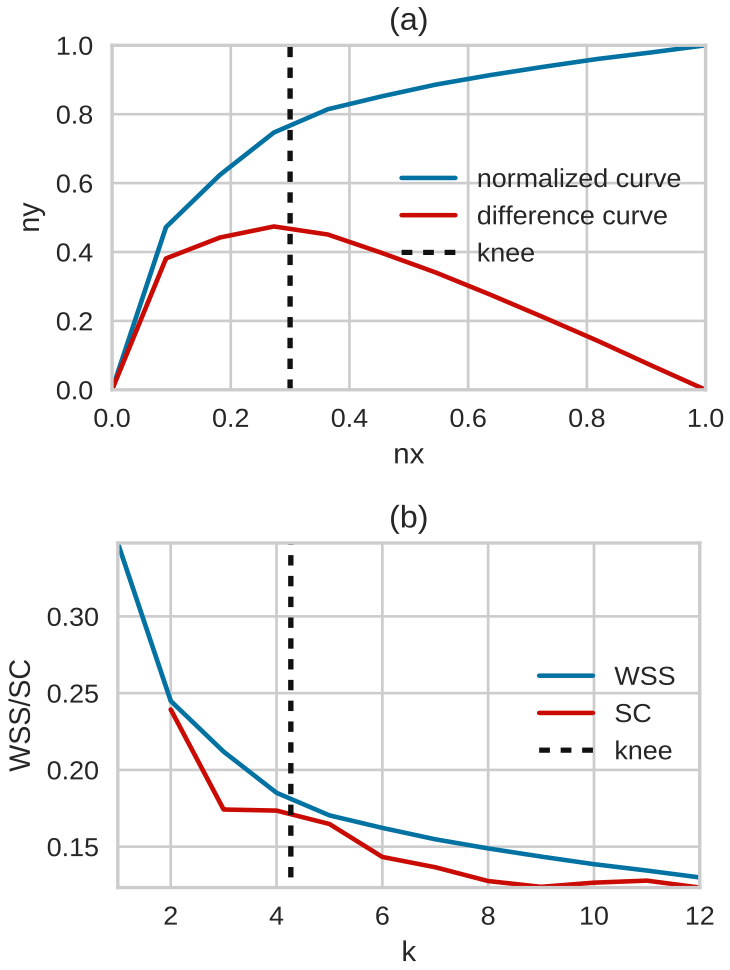

Figure 2.5: Selection of value of optimal cluster from 622 days of height anomalies at 600 hPa as data vectors using Elbow and Silhouette Coefficient (SC) methods Rousseeuw (1987); Satopaa et al. (2011). (a) "nx" is the normalized number of clusters k (i.e., $\frac{k_x - k_{min}}{k_{max} - k_{min}}$). Blue curve ("$ny$"): normalized within cluster sum of square (WSS) of all data vectors; Red (ny): normalized difference curve (i.e., y-axis component of perpendicular Euclidean distances of WSS values to the diagonal from first to last data point following Satopaa et al. (2011). Dotted black line: knee point at the maximum value of normalized difference curve (i.e, $nx = 0.28$); (b) Blue is the total within cluster sum of squares (WSS $\times 10^{-6}$) with varying number of clusters (k). Red: the mean SC Rousseeuw (1987) of data vectors with varying number of clusters (k), ranging from 2 to 12. Black dotted line: value of optimal $k(= 4.27)$ corresponds to the maximum of normalized difference curve (Figure S1a, red) calculated using the kneedle program Satopaa et al. (2011). Further details can be found in Section-III and Figure-2 of Satopaa et al. (2011).

method (Bholowalia and Kumar, 2014; Syakur et al., 2018). The mean silhouette coefficient (SC) is calculated for different values of k (2 to 12) shown in Figures 2.5b (red curve). The silhouette coefficient is defined by the following formula (Clark et al., 2018):

$$s(i) = \frac{b(i) - a(i)}{max(a(i), b(i))}$$

where a(i) is the mean distance of an data point to the remaining data points in the cluster and b(i) is the distance to the next closest cluster. In general, higher positive values of SC indicate better clustering. Here, a relatively high value of SC is found from $k = 2 - 4$, and it drops sharply after that. Hence, from SC, we say that $k \in [2, 4]$ can be used as an appropriate choice. To further constrain the value of k, we then use the elbow method. In this method, the elbow point of normalized error (i.e., Within Cluster Sum of Squares Distances: WSS) curve is taken as the optimal value k, i.e., the value of k at the elbow point. The location of the knee point in our analysis is calculated by a widely used objective method called kneedle (Satopaa et al., 2011), which suggests a knee point at $k = 4.27$ (Figures 2.5a b). Apart from object guidance for the selection of k, it is appropriate to check for the physical significance of obtained clusters (Clark et al., 2018). Indeed, once the cluster analysis was completed, we assessed that the physical meaning of the obtained patterns was consistent with our knowledge of Arabian Sea systems. With both the objective methods and the inspection of their physical validity, the value $k = 4$ was deemed most appropriate for our analysis.

We used the python toolbox "kmeans" to implement the k-means clustering algorithm. The model is initialized with k random data points as initial centroids. Since convergence occasionally becomes sensitive to initialization, we ran the model for 600 random initial centroids and finally selected one which minimizes the sum of the cluster of squares distances (i.e., inertia). Further, 100 iterations are used for every single run. For a data vector considered, the WSS decreases for the first 20 or so iterations and then settles down with no further change in centroids. Hence, 100 iterations are sufficient to ensure that the algorithm has converged to a solution.

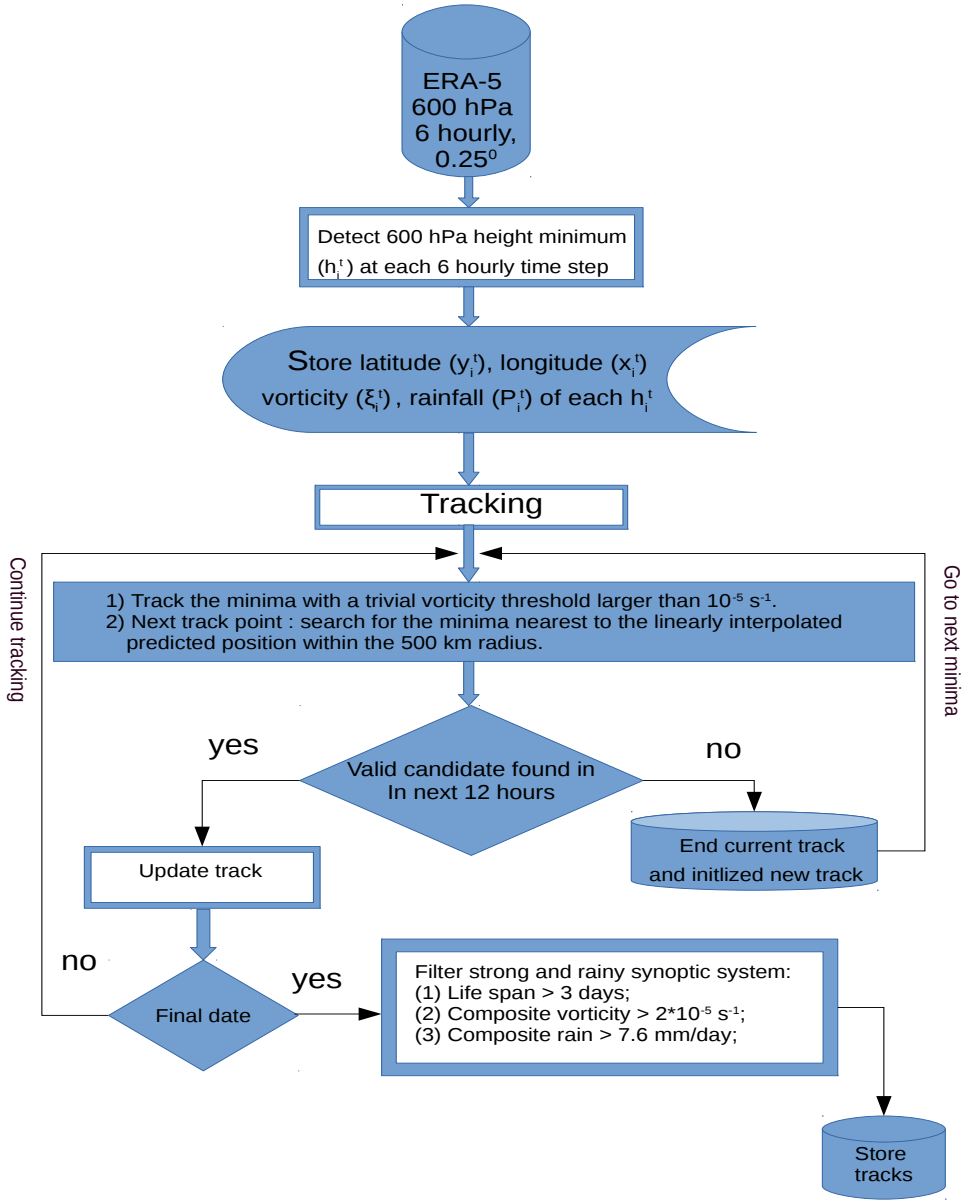

Figure 2.6: Schematic of tracking procedure

2.4 Automatic tracking of systems and their classification

The manual tracking of cyclonic systems is time consuming and not feasible for large data sets. Thus, we have also developed an automated detection and tracking methodology that involves using 600 hPa geopotential height field as Arabian Sea and western Indian systems are known to show maximum intensity in the middle troposphere (Kushwaha et al., 2021). At each six-hourly time step, a local minimum of geopotential height is detected as a system center. After that, only strong system centers are retained for the formation of tracks by applying the threshold $\xi_m > 1 \times 10^{-5} s^{-1}$, where ξ_m is the mean vorticity around 4° area around the detected centers (Kushwaha et al., 2021). The formation of tracks from the above cyclone centers is achieved by a standard nearest neighborhood method. In particular, we use the first guess method of Hanley and Caballero (2012), initially used for extratropical system tracking (Wernli and Schwierz, 2006). Variants of this method have also been employed in the tropics for tracking monsoon lows (Praveen et al., 2015).

In this method the first-guess location of cyclone candidate is a reduced linear continuation of the track in geographical longitude-latitude: $P^*(t_{(n+1)})$ = $P(t_n) + q \times [P(t_n) - P(t_{n-1})]$, where P is a latitude-longitude coordinate pair, t_n is the nth time step and q is a factor which weights the forward speed of the cyclone. A cyclone center located at P at time t_{t+1} regarded as the new position if it minimizes the distance among all cyclones present at t_{n+1} within the radius D_0. For robustness, we also employed vorticity threshold wherein the difference between predicted vorticity, $\xi^*(t_{(n+1)})$ = $\xi(t_n) + r \times [\xi(t_n) - \xi(t_{n-1})]$ and the vorticity of the nearest neighbour candidate must be less then a threshold value of $\xi^*(t_{n+1})$ - $\xi_{n+1} < 5 \times 10^{-5} s^{-1}$. Here, we use tuning parameters $q = 1$ and $r = 0.75$ for optimal tracking (Hanley and Caballero, 2012; Praveen et al., 2015). If no valid candidates are found for consecutive 12 hours, then tracks are terminated. Further, only tracks that last for more than three days are retained. For clarity, a schematic of the tracking procedure is shown in Figure 2.6. We note that results from automated tracking are validated by comparing with manual track maps from extended MTC data sets (Kushwaha et al., 2021), and those of monsoon lows (Hunt et al., 2016; Praveen et al., 2015). Moreover, we also check individual tracks for selected cases against the daily motion of cyclones using six-hourly map animations.

Table 2.1: Model Specifications

Sr.No	Attribute	Attribute Characteristic
1	Model	Weather Research And Forecast Model (WRFV4.0)
2	Model Mode	Non-Hydrostatic
3	Time step for Integration	50 second
4	Number of Domain	Single Domain
5	Central point of the domain	$20^{\circ}N, 80^{\circ}E$
6	Horizontal grid distance (Model Grid Resolution)	57 km
7	Map Projection	Mercator
8	Numberof grid points	X- direction 100 Y- direction 68
9	Horizontal grid distribution	Arakawa C-grid
10	Nesting	No nesting
11	Vertical model level	Terrain-following hydrostatic-pressure coordinate (33 sigma levels up to 50 hPa)
12	Spatial differencing scheme	6th-order centered differencing
13	Initial condition	Three-dimensional real-data $(1^{\circ} \times 1^{\circ} FNL)$
14	Lateral boundary conditions	WRF specified option
15	Time integration	3rd-order Range-Kutta
16	Micro Physics	WRF Single–moment 6–class Scheme
17	Surface Layer	MM5 Similarity Scheme
18	Planetary Boundary Layer (PBL)	Yonsei University Scheme (YSU)
19	Radiation	RRTMG Shortwave and Longwave Schemes
20	Land surface Model	Unified Noah Land Surface Model
21	Cumulus parameterization schemes	New Tiedtke Scheme
22	Turbulence and mixing option	Evaluates 2ed order diffusion
23	Eddy coefficient option	Horizontal smagorinsky first order closure
24	6th order numerical diffusion	No
25	Eddy coefficient option	Horizontal smagorinsky first order closure
26	6th order numerical diffusion	No
27	W-damping	No damping
28	Base temperature	290K
29	Upper level damping	No damping

2.5 Numerical Modeling

2.5.1 Weather Research and Forecast Model Setup

We utilize the Weather Research and Forecasting (WRF) Model version 4 to perform a set of numerical experiments that aim to investigate the influence of a LPS in the Bay of Bengal on the formation of Arabian Sea and western Indian MTCs. Our aim is not to simulate fine-scale convection or rainfall but rather to understand large-scale interactions. Therefore a relatively coarse resolution of 57km has been used in horizontal and 33 vertical

hybrid sigma levels in vertical; this resolution captures synoptic-scale systems and saves significant computational resources and time. First, we calculate the 20 June to 10 July climatology of 16 years (2000-2015) at each six-hourly time step of FNL data interpolated by the METGRID program. This duration has been chosen because most of the input variables are consistent in dimensions and resolutions during the 2000-2015 time window, outside of which there are differences in the soil levels and vertical levels of input data. The calculated six-hourly climatologies serve as the lateral boundary conditions for our simulations. Note that we retained the diurnal cycle while calculating the climatology meaning no daily mean is performed. This reduces the noise which may arise due to differences in the diurnal cycle of the inner domain and climatological lateral boundary conditions if daily mean were used. Sea surface temperature and soil moisture also kept to their climatological value. Since we are interested in the dynamics of tropical MTCs and monsoon lows, we used a combination of physics schemes in WRF, which are well tested and named "TROPICAL SUITE" in the namelist option. TROPICAL SUITE includes the Kessler Scheme for microphysics parameterization, the Tiedtke Scheme used for cumulus parameterization, the Unified Noah Land Surface Model used for land surface processes, and RRTMG Shortwave and Longwave Schemes used for short wave and longwave radiation parameterization. The details of all physics used are shown in Table 2.1. Each simulation was initialized with six hourly climatological lateral boundary and initial conditions of FNL data.

2.5.2 Bogus Vortex Scheme

To understand the effect of the Bay of Bengal LPS in the formation of Arabian Sea MTC, we superimposed a cyclonic vortex as a perturbation over the June-July climatology of NCEP Final Reanalysis (FNL-data). This modified data was then used as initial conditions for the vortex initialization simulations. The construction of the vortex has been done using NCAR-AFWA tropical cyclone (TC) "bogussing" scheme (Davis and Low-Nam, 2001; Fredrick et al., 2009; Low-Nam and Davis, 2001). This method is not computationally expensive, and follows the vorticity removal and inversion method to remove preexisting vortex and inserts a prescribed vortex in nonlinear balance. This method has been widely used as a "bogussing" scheme in the fifth-generation National Center for Atmospheric Research–Pennsylvania State University (NCAR–Penn State) Mesoscale Model (MM5) system. An updated version of which has been implemented in Weather Research and Forecast Model (Fredrick

et al., 2009; Davis et al., 2002). In particular this method is widely utilized in enhancing the description and details of tropical cyclones initialization (Jian and Wu, 2008) and in correcting the location and intensity of the cyclone precursors (Ding et al., 2004; Kuester et al., 2008; Yang et al., 2008; Van Nguyen and Chen, 2011; Wang et al., 2008; Komaromi et al., 2011). The scheme essentially runs in two primary steps. The first step aimed to remove the incorrect vortex and find the background state by removing the perturbation fields associated with the cyclone by solving the series of Poisson's equations. In the second step, a user-defined balanced vortex of prescribed winds and moisture profiles is placed in the specified location. Since our background state is already known as climatology, we only use the vortex addition part of the scheme. In particular, the process of construction of a vortex is based on the following assumptions,

1. The vortex is assumed to be axis-symmetric.
2. The mass and momentum fields are assumed to be in nonlinear balance.
3. Radius of maximum wind is specified.
4. The core of the system is assumed to be near saturated.
5. Maximum winds of bogus storms are a predetermined fraction of maximum winds observed.

The user specified vortex winds profile is given by the simple Rankine vortex, namely,

$$v = A(z)F(r) \tag{2.1}$$

$$F(r) = \frac{v_m}{r_m} r \quad ; (r \leq r_m) \tag{2.2}$$

$$F(r) = \frac{v_m}{{r_m}^{\alpha}} r^{\alpha} \, ; (r > r_m) \, , \tag{2.3}$$

where v_m is the maximum winds at a radius of maximum wind, r_m, $\alpha = -0.75$ is the empirical constant used to reduce the mismatch between the vortex winds and the influence of other systems at large radii. Vortex winds' amplitude and height dependence are defined by $A(z)$. The assumption used here is that the maximum azimuthally averaged wind is $0.75V$, where V is the user-defined maximum wind. The vertical weighting function,

$A(z)$, is defined as 1 up to 600 hPa and decreases linearly to 150 hPa and above. Within the radius of maximum wind, the relative humidity is assumed to be nearly saturated. Outside of twice the radius of maximum wind, climatological humidity is prescribed, and between the two, radii humidity is linearly relaxed from saturation to climatology. Once the vortex winds are defined, the stream-function is known. Then the equation of nonlinear balance (Equation 2.4, which relates the stream-function and geopotential height fields) has been used to calculate the geopotential height perturbation (Charney, 1955).

$$\nabla^2\psi + \nabla\psi.\nabla f - \frac{2}{f}\left[\left(\frac{\partial^2\psi}{\partial x\partial y}\right)^2 - \frac{\partial^2\psi}{\partial x^2}\frac{\partial^2\psi}{\partial y^2}\right] = \frac{\nabla^2\phi}{f} \tag{2.4}$$

The above Poisson equation can be solved numerically provided that the appropriate solution strategy is being used to ensure the convergence (Arnason, 1958; Ames, 2014). In Equation 2.4, ψ represent the stream function, ϕ represents the geopotential height, f is Coriolis parameter. Finally, once the geopotential height perturbations are known, they are used to calculate the temperature perturbations by hydrostatic balance ($\frac{\partial\phi}{\partial(d\ln p)} = -RT$).

2.6 Moisture and Vorticity Budget

2.6.1 Moisture Budget

To understand the source of water vapor during the MTC formation, the water vapour budget is estimated via the equation (Chou and Neelin, 2004; Zhou et al., 2019; Trenberth, 1997),

$$\frac{\partial W}{\partial t} = -\nabla\cdot\mathbf{Q} + E - P + R, \tag{2.5}$$

where W is vertically integrated atmospheric water vapor (i.e., precipitable water), $W = \int_{p_t}^{p_s} q\frac{dp}{g}$, g is gravitational acceleration of 9.8 m s^{-1}, q is the specific humidity (kg kg^{-1}), and p is pressure level (Pa); p_s is surface pressure and p_t is the pressure of top of the atmosphere; P and E are the precipitation and evaporation respectively. $\frac{\partial W}{\partial t}$ is the time derivative of the column integrated moisture, $-\nabla\cdot\mathbf{Q}$ is the horizontal convergence of column integrated water vapor fluxes (i.e., $-\nabla\cdot\mathbf{Q} = -\nabla\cdot\int_{p_t}^{p_s}\mathbf{V}q\frac{dp}{g}$, where $\mathbf{V}$ is the horizontal wind velocity vector), and R is a residual term related to spurious water vapor tendencies due to the data assimilation cycle

while generating reanalysis products.

The column integrated moisture convergence term ($-\nabla\cdot\mathbf{Q}$) on the RHS of Equation 2.5 does not provide information about the advective and convergent flux components separately. This can be achieved by taking the divergence operator inside the integral, i.e.,

$$-\nabla\cdot\mathbf{Q} = -\nabla\cdot\int_{p_t}^{p_s}(\mathbf{V}q)\frac{dp}{g} = -\int_{p_t}^{p_s}q(\nabla\cdot\mathbf{V})\frac{dp}{g} - \int_{p_t}^{p_s}(\mathbf{V}\cdot\nabla q)\frac{dp}{g} - q_s\mathbf{V}_s\cdot\nabla p_s, \tag{2.6}$$

this introduces extra surface moisture forcing term (last term of Equation 2.6), which remains relatively small compared to other terms and is usually ignored in the analysis of synoptic systems (Trenberth and Guillemot, 1995; Seager and Vecchi, 2010; Seager et al., 2007; Seager and Vecchi, 2010; Seager and Henderson, 2013; Adames and Ming, 2018a). where subscript s denotes the surface quantities. A detailed derivation of moisture budget equation and its decomposition can be found in Trenberth and Guillemot (1995). The convergence term depends upon the mass convergence of moisture and peaks in the lower troposphere where atmosphere mass and specific humidity are high, and the advective component depends upon the direction of winds and moisture gradients (Trenberth and Guillemot, 1995).

Further, the vertically integrated meridional (v_q) and zonal moisture (u_q) transports can be written as,

$$u_q = \int_{p_t}^{p_s}(uq)\frac{dp}{g};\;\; v_q = \int_{p_t}^{p_s}(vq)\frac{dp}{g}, \tag{2.7}$$

and they determine the direction of column integrated moisture fluxes. To investigate the separate role of dynamical and thermodynamic processes, anomalies in moisture transport due to winds and moisture are further partitioned following Yan et al. (2020); Zhou et al. (2019) as $\mathbf{V} = \mathbf{V_c} + \mathbf{V}'$ and $q = q_c + q'$, where subscript c denotes a 22 years daily climatology, and primes are deviation form the daily climatology. Substitution in Equation 2.6 yields,

$$-\int_{p_t}^{p_s}\nabla\cdot(\mathbf{V}q)\frac{dp}{g} = -\int_{p_t}^{p_s}\nabla\cdot(\mathbf{V}'q_c)\frac{dp}{g} - \int_{p_t}^{p_s}\nabla\cdot(\mathbf{V_c}q')\frac{dp}{g} - \int_{p_t}^{p_s}\nabla\cdot(\mathbf{V}'q')\frac{dp}{g} - \int_{p_t}^{p_s}\nabla\cdot(\mathbf{V_c}q_c)\frac{dp}{g}. \tag{2.8}$$

This allows the quantification of the contribution to the moisture flux from the mean flow and transient eddies.

Using the shorthand $[.] = \int_{p_t}^{p_s} \frac{dp}{g}$, Equation 2.8 can be further expanded as,

$$-[\nabla\cdot(\mathbf{V}q)] = -[q_c(\nabla\cdot\mathbf{V}')] - [(\mathbf{V}'\cdot\nabla q_c)] - [\nabla\cdot(\mathbf{V_c}q')] - [\nabla\cdot(\mathbf{V}'q')] - [\nabla\cdot(\mathbf{V_c}q_c)]. \tag{2.9}$$

The first two terms in Equation 2.9 are the convergent and advective components of climatological moisture convergence by anomalous winds; the third term is the anomalous moisture convergence by climatological wind, and the fourth term is the convergence of anomalous moisture by anomalous winds; this term is the product of two small quantities, and thus relatively small compared to other terms. The last term is the climatological moisture convergence by climatological winds, which does not change over synoptic time scales, and is relatively unimportant in the analysis of transient systems.

2.6.2 Vorticity Budget

To understand the intensification of Arabian Sea MTCs we use a vorticity budget (Raymond and López Carrillo, 2011; Holton, 1973; Carr, 1977; Boos et al., 2015b). The Eulerian inviscid relative vorticity (ξ) budget equation in pressure coordinates reads,

$$\frac{\partial\xi}{\partial t} = -\xi\nabla.\mathbf{V} - f\nabla.\mathbf{V} - \mathbf{V}.\nabla\xi - \beta v - \omega\frac{\partial\xi}{\partial p} + \left(-\frac{\partial\omega}{\partial x}\frac{\partial v}{\partial p} + \frac{\partial\omega}{\partial y}\frac{\partial u}{\partial p}\right) + \text{Res.} \tag{2.10}$$

Here, the first two-term terms on the RHS represent the vorticity generation (destruction) by convergence (divergence) of horizontal winds when coupled with the relative and planetary vorticity, respectively. The third term represents vorticity advection by the horizontal wind ($\mathbf{V}$), the fourth term is the coupling between differential planetary vorticity and meridional wind (the so-called β-term), the fifth term represents the vertical advection of relative vorticity via upward or downward motion, and the sixth term is the tilting term which is the change in vorticity due to horizontal gradients in the vertical velocity or vice versa. Finally, the last term is a residual that arises due to the parameterised physics and numerical approximations in post processing of the data being used. To understand the formation and intensification of MTC, each term of the vorticity equation is calculated and compared to deduce the dominant contributions to the systems' growth.

Chapter 3

A Global Tropical Survey of Middle Tropopsheric Cyclones

In this chapter, we begin our exploration of MTCs. In particular, analysis is carried out over the global tropics ($30°\text{N}-30°\text{S}$) in the boreal summer (June-September) and winter (December-March) for 20 years (2000-2019). Along with MTCs, we also keep track of tropical systems with lower troposphere vorticity maxima, which include monsoon lows, MDs, and TCs (together referred to as lower tropospheric cyclones; LTCs), and the relative fraction of these two types of systems (i.e., MTCs and LTCs) is also analyzed. In essence, this chapter addresses the following questions:

1. What are the frequency and statistical characteristics (starting locations, lysis, cyclone motion vectors, and track density) of MTCs over South Asia?
2. Apart from South Asia, which tropical regions support MTCs activity, and what are the common features?
3. What are the differences between the dynamic and thermodynamic structure of MTCs and LTCs?
4. Are MTCs fundamentally independent from tropical lows (i.e., LTCs)? Or do MTCs and LTCs appear in different stages of the life cycle of tropical cyclonic systems?

Specifically, in Section 3.1, we present the statistical characteristics and structure of manually tracked MTCs over South Asia. We then move to the global tropics in Section 3.2 — regions of MTC and LTC occurrence are identified, and their structure is compared among basins during the northern and southern hemispheric summer seasons. In Section 3.3 we will discuss the robustness of the results, and in Section 3.4 we summarize the principal findings of this chapter.

3.1 MTCs over South Asia

We begin our analysis with South Asia because MTCs have been frequently reported over the Arabian Sea (Carr, 1977; Choudhury et al., 2018) and, to a lesser extent, over the Bay of Bengal (Ramage, 1964, 1971), and the South China Sea (Krishnamurti and Hawkins, 1970). Since most systems identified as MTCs show middle and lower tropospheric vorticity maxima in different stages of their life cycle; the notation we have adopted from here on is that, all systems that show $\delta\xi_p > 1.5\times10^{-5}s^{-1}$ at least for two days are MTCs; the specific days when they show $\delta\xi_p > 1.5 \times 10^{-5}s^{-1}$ is referred to as their MTC-phase and days when $\delta\xi_p < -0.8 \times 10^{-5}s^{-1}$ is called their LTC-phase. As vorticity maxima can shift from one level to another, we refrained from imposing constraints on P_ξ during tracking. We have verified that this relaxation does not alter results qualitatively (Figure A.2) ; however, as expected, there is an effect on the actual number of MTC centers.

Using MERRA-2 reanalysis data from 2000–2015, a total of 261 MTCs are tracked, which contain 2414 track points. Of these, 1109 track points satisfy MTC-phase criteria, and 401 satisfy LTC-phase criteria. As we aim to differentiate between the properties of middle and lower tropospheric systems, quite naturally, there are a fair number of "intermediate" systems (37%) that do not fall in either category. These numbers indicate that mid-tropospheric vorticity maxima frequently occur over South Asia. Specifically, 261 systems in 16 years, 2000 to 2015, June to September, implies about 3–4 systems per month. Moreover, many track points in the LTC phase suggest that MTCs can exhibit lower tropospheric maxima during a significant portion of their life cycle; this implies a conversion between the MTC and LTC phases of these systems. In fact, this type of intermittent shift of vorticity maximum among different vertical levels or interaction between the middle and lower troposphere circulation was observed during some tropical cyclones' formation (Bister and Emanuel, 1997; Raymond et al.,

2014b).

Composites of relative vorticity, PV, temperature, wind vectors, and specific humidity anomalies of MTC and LTC phases are shown in Figure 3.1. These composites are derived from a large sample size, thus providing a robust structural view of systems over South Asia. The vertical cross-sections and plan views of composites of MTCs and LTCs phases show a localized vorticity maximum in the middle and lower troposphere, respectively. This is consistent with systems over the Arabian Sea and the Bay of Bengal (Figure 2.3).

Further, the relative vorticity, PV, moisture, and temperature anomalies of the LTC-phase composite are stronger than that of the MTC-phase. The MTC composite's temperature structure shows warm anomalies above the MTC center (at 600 hPa) and cold anomalies below it (Figure 3.1c). LTCs, on the other hand, shows a warm anomaly from the middle to the upper troposphere and a negative anomaly squeezed below 800 hPa (Figure 3.1d). It should be kept in mind that the low-level anomaly might be influenced by the coarse resolution of reanalysis data (Manning and Hart, 2007). The westward tilt of MTCs is apparent in the vorticity and specific humidity anomaly structure, while LTCs do not show such a pronounced tilt with height. The PV anomaly of MTCs has a single peak with a maximum localized in the middle troposphere, while that of LTCs extends down to the surface and has two peaks. Specifically, similar to monsoon lows (Boos et al., 2015b; Hunt et al., 2016), the LTC PV structure has one maximum in the middle troposphere and another in the lower troposphere. The confinement of MTC's PV in the middle troposphere may be related to the high fraction of stratiform heating (Choudhury et al., 2018; Russell and Aiyyer, 2020). Whereas the PV of LTCs is likely influenced by deep convective heating (Murthy and Boos, 2019). Consistent with the vertical distribution of vorticity, the plan views at 600 and 975 hPa confirm that MTC's anomalous relative vorticity and circulation at lower levels are significantly weaker than the middle troposphere and located to the east of the middle-level center. On the other hand, LTCs show comparable or even stronger signatures near the surface, which are collocated with the mid-level anomalies.

3.1.1 Track density, starting location density, and cyclone motion vector

The track density (color shading), starting location density (contour lines), and motion vectors of all systems identified as MTCs and their LTC and MTC-phases are shown in Figure 3.2a, b, c, respectively. Note that the

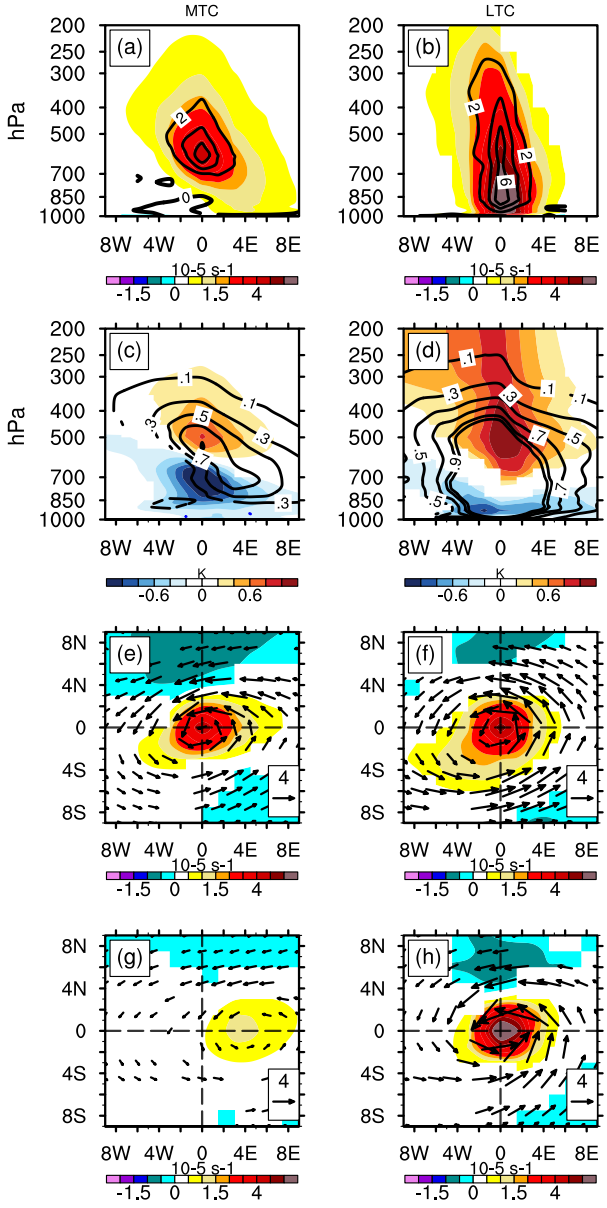

Figure 3.1: South Asian composites from 1107 MTC-phase track points (a) Relative vorticity (shaded) and PV anomaly in contours (c) Temperature anomaly (shaded) and specific humidity anomaly (contours). In both (a) and (c), positive contours are solid, and negative are dashed. Panels (e) and (g) are plan views of vorticity (shaded) and wind vectors at 600 and 975 hPa, respectively. Panels (b), (d), (f) and (h) are the same quantities as (a), (c), (e) and (g) but constructed from 401 LTC-phase track points. Units of PV is 10^{-1} PVU, and specific humidity is g/kg. Results are only shown if they are significant at 1% significance under a two-tailed t-test.

starting location is the first point in the domain where the system is detected, and the actual genesis location may fall outside the domain. The highest starting density of MTCs (dashed lines, Figure 3.2a), is over the Arabian Sea, followed by the Bay of Bengal and the South China Sea. The Arabian Sea starting location density is more spread out than the Bay of Bengal, and the maximum over the South China Sea is the most southward and geographically concentrated. The starting density over the north Bay of Bengal (1-2 per summer, contour lines) is comparatively less than that reported in previous studies (5-10 per summer, Hurley and Boos, 2015). This is primarily because we have considered only systems that show $\delta\xi_p > 1.5 \times 10^{-5} s^{-1}$ at least for two days. On the other hand, despite only considering MTCs, the Arabian Sea density is significantly larger than in previous reports. This difference is due to our use of the 600 hPa geopotential as MTCs show a robust signature in the middle troposphere, and many have little or no near-surface signature. In contrast, earlier work used sea level pressure or low-level vorticity as an identifying marker (Hurley and Boos, 2015).

Similar to starting location density, the track density also shows the same three maxima in South Asia. The highest total and MTC-phase density are over the Arabian Sea, while the LTC-phase track density peaks inland and over the Bay of Bengal. Comparing the total MTC and LTC phases suggests that the MTC phase contributes a significant portion of the Arabian Sea's total density. While from northwest Bay of Bengal to inland, the total density is dominated by the LTC phase. The geographical location of maximum MTC-phase density is qualitatively consistent with the previous literature, which reports MTCs primarily over the North-East Arabian Sea (Carr, 1977; Choudhury et al., 2018). These regions match with enhanced regions of monsoon synoptic activity (Hurley and Boos, 2015), indicating that MTCs are found in regions where Indian summer monsoon lows occur. A notable difference is that MTCs show more activity, where monsoon depressions and lows show less activity and vice versa. For instance, over the Arabian Sea, MTCs have the highest frequency while monsoon lows have only a modest presence (comparing Figure 3.2 with Fig-2 of Boos et al., 2015b). Comparing LTC and MTC phases (Figure 3.2), it appears that the MTC phase occurs with a relatively higher density equatorward compared to the LTC phase. Together, it is likely that, in their life cycle, MTCs show LTC and MTC phases; however, there is a preferred range of latitudes for the respective phases.

From the cyclone motion vectors in Figure 3.2, cross basin motion from the Bay of Bengal to the Arabian Sea

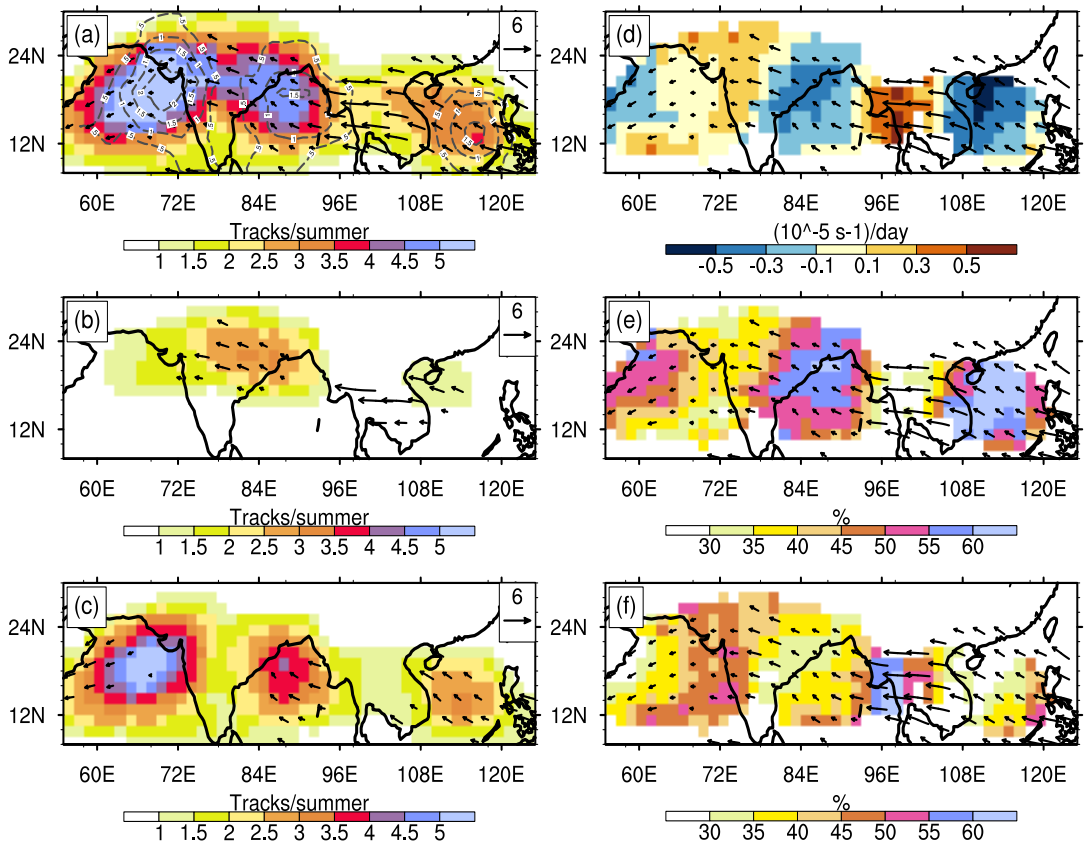

Figure 3.2: (a) Track density (shaded) and starting location density (contours) of 261 MTCs over South Asia. Arrows denote the cyclone motion vectors; arrow length is proportional to the propagation speed in m/s. The vectors are shown only if any wind components are significantly different from zero at 1% significance under a two-tailed t-test. (b) Same as (a), except calculation is done for each track segment if it is in the LTC-phase (c) is same as (a) except results are for the MTC-phase. (d) the mean of change in along-track differential vorticity of all tracks. (e) and (f), percent of systems at every 8 degrees with the negative and positive rate of differential vorticity change, respectively. Here, negative values denote an increase in low-level cyclonic vorticity, and positive values show an increase in mid-level cyclonic vorticity. Velocity vectors in (d,e,f) are the same as in (a) and are shown to guide the eye.

and from the South China Sea to the Bay of Bengal is evident. This is consistent with previous work wherein frequent conversion of Bay of Bengal monsoon low-pressure systems into MTCs over the Arabian Sea was observed (Carr, 1977). This cross basin propagation, followed by a conversion from LTC-phase to MTC-phase, makes the origin of many of these systems nonlocal. Specifically, an MTC over the Arabian Sea could have originated as a depression in the Bay of Bengal. Further, cyclone motion vectors of MTCs show a northwest orientation over the Bay of Bengal and the South China Sea with a reasonably large magnitude and relatively slow westward movement over the western Arabian Sea. Neither the LTC phase nor the MTC phase shows a preferred statistically significant direction of motion over the northeast Arabian Sea, which supports the observation of their quasi-stationary behavior in this region (Miller and Keshavamurty, 1968; Carr, 1977). Further, the spatial density of MTC and LTC phases is not uniform. The regional changes in these phases can be quantified in terms of the rate of change of differential vorticity ($\delta\xi_p$) along each track. The average tendency of $\delta\xi_p$ along all tracks in an 8-degree grid is shown in Figure 3.2d. This measure, in a broad sense, characterizes regions of enhanced low level (negative rate of change of $\delta\xi_p$) or middle level (positive rate of change of $\delta\xi_p$) vorticity. Based on this, at every location, the percentage of systems that exhibit low and middle-level vorticity enhancement is shown in Figures 3.2e,f, respectively. Figures 3.2e,f suggest that western India, the eastern Arabian Sea ($\approx 55 - 60\%$), southeast Bay of Bengal, and Myanmar ($\approx 60 - 90\%$) show the largest tendency of systems to transition from LTC to MTC phases. Whereas east India ($\approx 60 - 80\%$), western half of the Bay of Bengal ($\approx 60 - 90\%$), northwest South China Sea ($\approx 60 - 90\%$) and western Arabian Sea ($\approx 50 - 60\%$) show a pronounced tendency for systems to transition into LTCs phases.

3.1.2 Starting location and intensity distributions

Figure 3.3a, b, and c shows the monthly probability of occurrence of MTCs over the three basins in South Asia. Starting locations of the Arabian Sea MTCs peak in June (42%), then reduce during July (20%) to August (13%) but increase in the late part of the monsoon in September (23%). The high probability of occurrence of MTCs in the early phase of monsoon over the Arabian sea has been linked with the export of middle-level vorticity from the heat low over northwest India (Ramage, 1966; Carr, 1977). Over the Bay of Bengal, the highest probability of MTC occurrence is also in the first half of the monsoon (June and July), while, over the South China Sea, MTCs

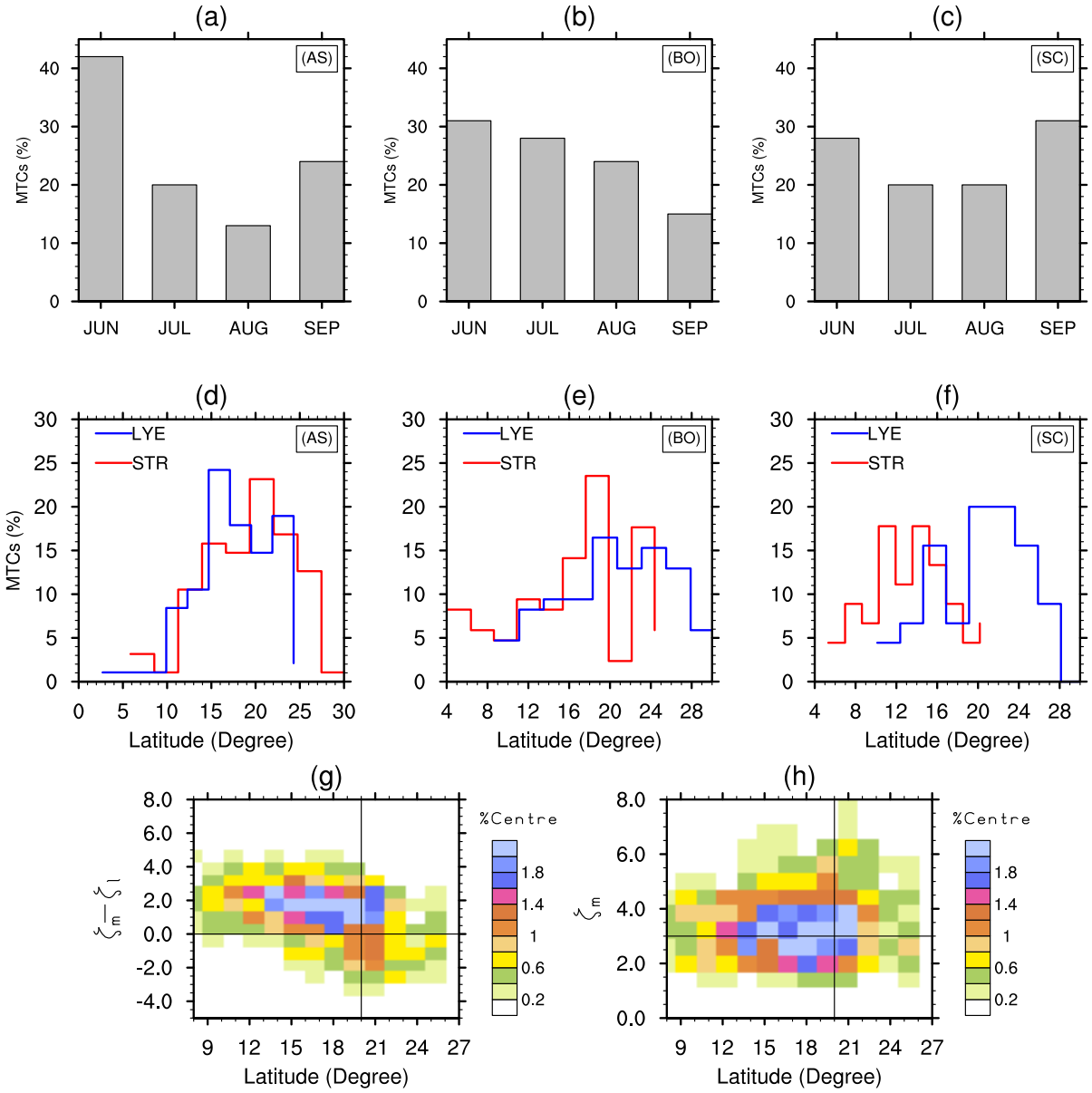

Figure 3.3: Monthly starting location probability (in percent) of 261 South Asian MTCs over (a) Arabian Sea (AS),(b) Bay of Bengal (BO) and (c) South China Sea (SC). Panels (d), (e), (f) follow (a), (b) and (c) but show the initial location (red, STR) and lysis (blue, LYE) probability distribution with latitude for the three regions. (g) and (h) show the joint probability distribution of $\delta\xi_p$ and ξ_m respectively with respect to latitude for all 261 tracks.

probability is significant in the early (June) and late (September) portions of the summer season. Figure 3.3d,e, and f show the latitudinal starting location and lysis probability distribution over the Arabian Sea, the Bay of Bengal, and the South China Sea. In the latter two regions, the mean starting locations are equatorward compared to lysis latitudes. This is consistent with the noted northwestward propagation tendency of these systems. On the other hand, the starting locations and lysis distributions over the Arabian Sea largely coincide however there is slightly southwards shift of lysis peak compared to starting location, agreeing with a quasi-stationary character or a slow westward motion here. Curiously, there is a peak in these systems' starting locations between $15 - 17°$N for all three basins.

Figures 3.3g,h show distributions of $\delta\xi_p$ and ξ_m with latitude, respectively. As indicated earlier in Figure 3.2, the MTC-phase probability is higher towards the equator, which is also evident in Figure 3.3g. In fact, equatorward of 15°N, almost all the systems center show $\delta\xi_p > 0$. On the other hand, Figure 3.3h suggests that cyclonic centers tend to become stronger with latitude (up to about 21°N). In other words, Figures 3.3g,h indicate that away from equator systems are more intense and less localized in the middle troposphere (LTC-phase). Whereas near the equator, systems are less intense but more localized in the middle troposphere (MTC-phase).

3.2 MTC statistics over globe

3.2.1 Boreal Summer

In this section, the occurrence of MTCs and LTCs over global tropics (30°N–30°S) is explored by examining daily 600 hPa geopotential surfaces during the boreal summer for 20 years. Note that imposing multiple criteria to track synoptic systems can result in a considerable amount of inconsistency among different reanalysis products (Hodges et al., 2003). Further, as the manual collection of tracks worldwide is time-intensive, we use cyclone center density to identify regions that support MTCs or LTCs. Since tracks are not formed, MTC and LTC phases of systems are not accessible; instead, we get quantitative maps of middle and lower tropospheric cyclonic center density.

A total 49,580 non-topographic moist cyclonic systems with $\xi_m > 1.5 \times 10^{-5}\text{s}^{-1}$ are found in these 20 years.

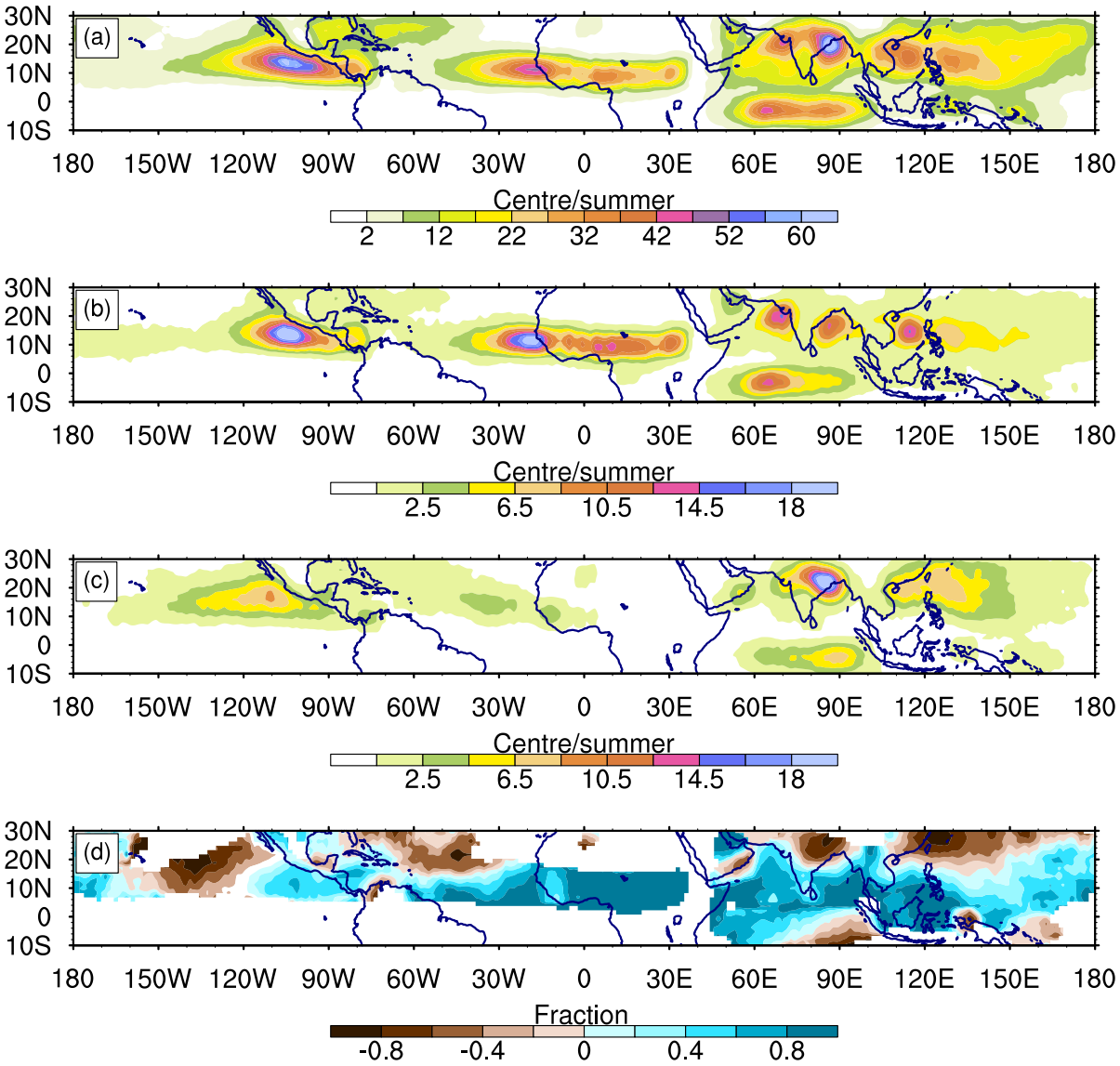

Figure 3.4: (a) Overall cyclone center density during boreal summer for 20 years. (b) same as (a) except for MTC centers. (c) same as (a) except for LTC centers. (d) $\frac{b-c}{b+c}$, only shown if total density exceeds 3. Note that the colorbar panel (a) is different from that in (b) and (c).

The cyclone center density of these systems is shown in Figure 3.4a. Of these, 10,406 systems satisfy MTC criteria, and 6,381 systems satisfy LTC criteria. Since we consider only system centers with well-defined middle and lower tropospheric characteristics, about 66% of the system centers remain unclassified. The cyclone center density of systems classified as MTCs and LTCs is shown in Figure 3.4b,c. The dominant regions of cyclonic activity in South Asia are the Arabian Sea, the Bay of Bengal, and the South China Sea. The South China Sea's maximum extends and connects to the West Pacific maxima, which extends up to the central Pacific. These regions are consistent with manual tracking results presented in the previous section (Figure 3.2). As expected from the nature of center density, high cyclone center density regions have minimum cyclone speed. Apart from South Asia, additional maxima are evident over East-West Africa and the East Pacific. The fractional or relative cyclone center density of MTCs and LTCs suggests that most of the West Pacific and East Indian region cyclones are LTCs. This is in accord with the relatively high frequency of monsoon lows in these regions (Hurley and Boos, 2015). Finally, another prominent region of cyclone activity lies just south of the equator over the Indian Ocean. This region coincides with the maximum rainfall zone south of the equator during June-September (Adler et al., 2017). Together Figures 3.4b,c, and d suggest that the MTC fraction is high near the equator, while the LTC fraction increases as we move towards the subtropics.

Another significant region of cyclonic activity observed in Figure 3.4a is over the west coast and the east-central continent of Africa, which has also been noted by previous regional studies (Kiladis et al., 2006). Here, mid-tropospheric cyclonic disturbances are driven to the west by the AEJ, and occasionally these systems spin up at lower levels and become warm-core tropical lows over the Atlantic Ocean (Hopsch et al., 2010). Further, the AEWs might be induced downstream by latent heating near the entrance of the AEJ (Kiladis et al., 2006; Thorncroft et al., 2008). Thus, the high cyclone center density observed near the AEJ entrance may result from convective systems which form in this region (Mekonnen et al., 2006). The relative fraction of MTC and LTC densities in Figure 3.4d suggests that over the ocean and near the west coast of Africa, LTC numbers are comparable to MTCs. But, clearly, the MTC fraction is much larger over the continental regions of East and Central Africa. This distribution is consistent with recent studies that suggest that troughs of AEWs over East and Central Africa are usually rich in stratiform convection, thereby enhancing the middle tropospheric maximum of

relative vorticity as captured in Figure 3.4b (Russell et al., 2020; Russell and Aiyyer, 2020). Further, Russell and Aiyyer (2020) suggests that Western Africa and the Atlantic Ocean are rich in deep convection, thus enhancing the low-level circulation in these regions, thereby favoring LTC-type systems (Figure 3.4c).

Composites of middle and lower tropospheric systems over Africa are shown in Figure 3.5. The MTC and LTC composite shows a vorticity maximum in the middle and lower troposphere, respectively, with a baroclinic thermal structure, which is remarkably similar to systems over South Asia (Figure 3.1). Further, the vorticity and moisture anomalies of MTCs extend downwards relatively east of the center, reflecting an east-west tilt of these systems. The PV anomalies of MTCs and LTCs show significant differences wherein the former is confined in the middle troposphere, and the latter extends down to the lower troposphere maintaining an upright structure. Finally, we obtain a very low cyclone density near the Sahara desert, which contrasts with previous studies that suggest high activity over the north and northwest of Africa (Hurley and Boos, 2015). As discussed earlier, this difference may be due to the 600 hPa level for identification, which does not account for shallow, near-surface lows.

Consistent with case studies (Reed and Recker, 1971; Shapiro, 1986), another geographical region of MTC activity is the eastern Pacific off the coast of Central America. This region also shows significant monsoon low-pressure system activity (Hurley and Boos, 2015). Here, MTCs and LTCs are favored close to land and over the open ocean, respectively. Indeed, the fractional density (Figure 3.4d) changes from positive values indicating MTC prevalence between 90°W–120°W to negative values indicating LTC prevalence over 120°W–150°W. A composite of East Pacific systems is shown in Figure 3.5 wherein the distinction between the two types of cyclonic centers is evident. The MTC and LTC composite structures in this region are similar to Africa and South Asia (Figure 3.1). A notable difference is that the anomalies are relatively stronger than in Africa, and LTCs are warm-core throughout the troposphere than African LTCs, which show a low-level cold-core. Further, cyclone activity in the East Pacific shares some interesting features with West Africa. In particular, both the regions are close to the equator and have relatively high MTC density (positive fraction) to the southeast and high LTC (negative fraction) to the northwest of the maximum in total cyclone density. Further, both West Africa and the East Pacific are characterized by low level negative absolute vorticity advection (Tomas et al., 1999). Thus, in

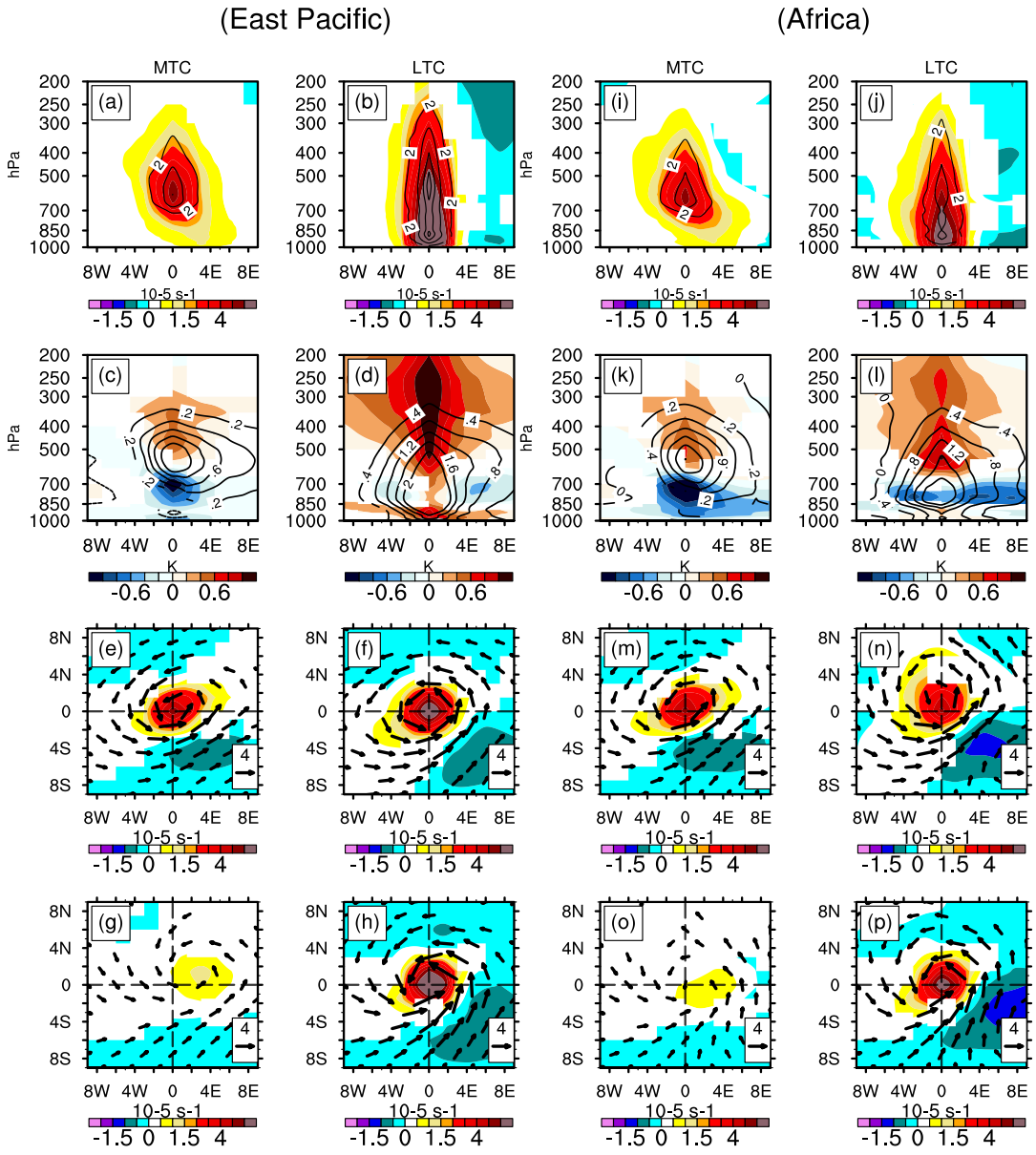

Figure 3.5: Composites of anomalies for MTCs (left column) and LTCs (right column) in the East Pacific region (a,b,c,d,e,f,g,h) and the Africa (i,j,k,l,m,n,o,p); (a,b and i,j) Relative vorticity (shading) and contours of potential vorticity (10^{-1} PVU); (c,d and k,i) temperature (shading) and specific humidity (g/kg) in contours; (e,f,m,n) and (g,h,o,p) wind vectors and relative vorticity (shaded) at 600 hPa and 975 hPa, respectively. Results are only shown if they are significant at 1% significance under a two-tailed t-test.

addition to mid-level cloud heating (Choudhury et al., 2018; Russell et al., 2020; Russell and Aiyyer, 2020), the MTCs profile in these regions might be aided by the lowering of low-level relative vorticity via cross hemisphere low-level vorticity advection.

3.2.2 Boreal Winter

This section focuses on MTCs and LTCs' activity in the boreal winter (December to March; 2000-2019). Following the same methodology, 41,703 cyclonic centers are identified during boreal winters of 20 years. Out of these 41,703 centers, by definition, 6,954 systems are MTCs, and 6,391 are LTCs. These subsets are used to calculate the cyclone center density in Figure 3.6. The dominant regions of cyclonic activity are North Australia, the Southern Indian Ocean, subtropical Africa, and subtropical South America, The former two regions show a relatively high center density compared to the latter. To a large extent, the above cyclone activity regions agree with previous work on monsoon lows and mesoscale systems (Berry and Reeder, 2016; Laing and Michael Fritsch, 1997). A notable difference is near Australia, where previous work highlighted most activity over the southwest part of the continent compared to north Australia (Hurley and Boos, 2015). This difference may be again due to the use of 600 hPa geopotential fields in this work, contrary to 850 hPa vorticity by earlier work, which is strongly influenced by surface heat lows. As in Hurley and Boos (2015), the low system density over South America suggests that rainfall in this region is likely due to small-scale systems which are not resolved in reanalysis or due to open troughs not detectable as geopotential surface minima. Composites of middle and lower tropospheric centers from the South Indian Ocean and Australia are shown in Figure 3.7. Though the MTC composite is mostly similar to other tropical regions, the LTC structure shows some notable differences. Specifically, in the South Indian Ocean, LTCs show almost no sign of a cold anomaly at low levels.

The highest center density over north Australia is consistent with the active monsoon region, which consists of the westward propagating low-pressure systems similar to Indian monsoon lows (Hurley and Boos, 2015; Clark et al., 2018). The region of maximum cyclonic activity in North Australia extends out to the South Pacific and merges with the South Pacific Convergence Zone (Widlansky et al., 2011). A relatively weak signature of cyclonic activity is also found north of the equator over the South Bay of Bengal, which corresponds to the

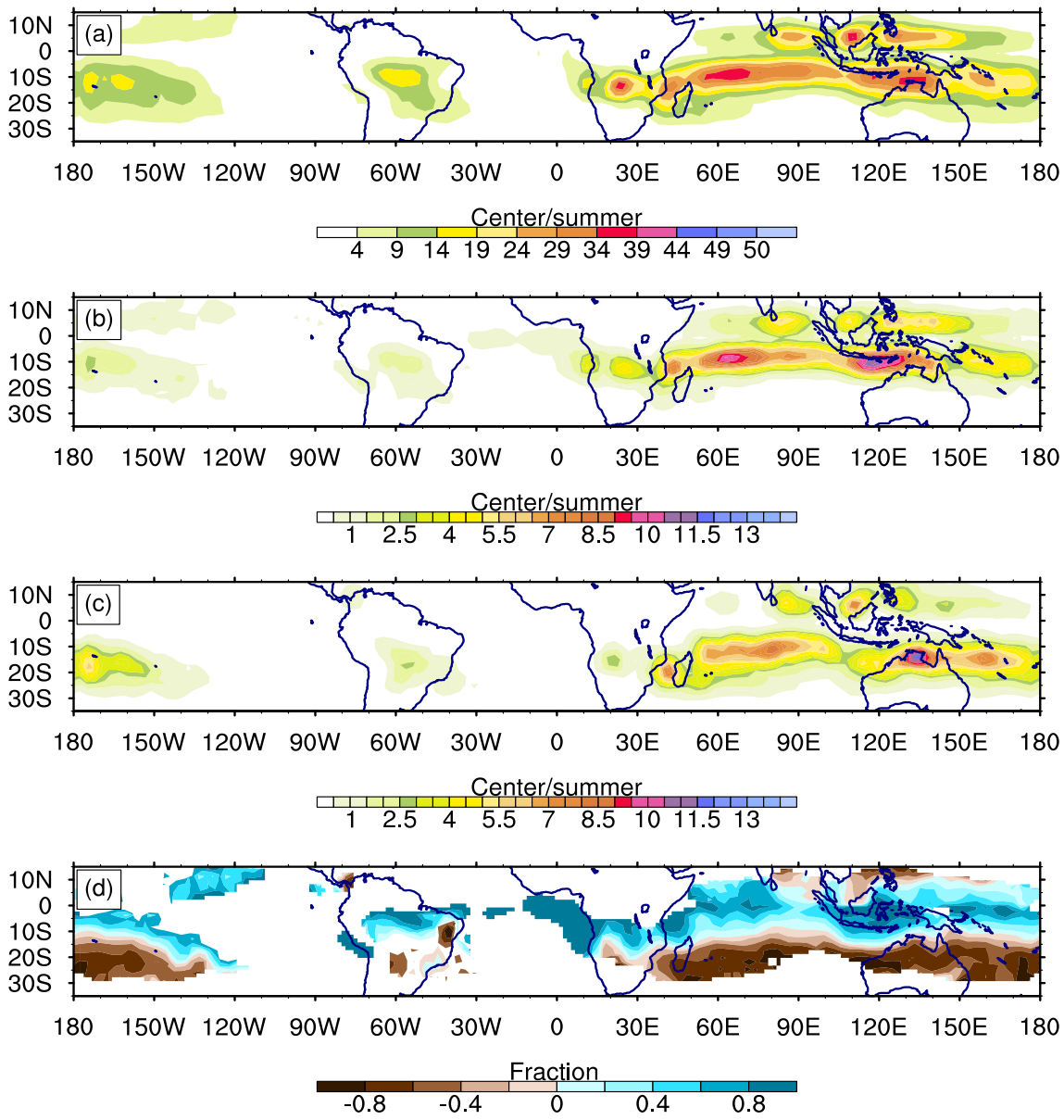

Figure 3.6: (a) Overall cyclone center density during the boreal winter for 20 years. (b) same as (a) except for MTC centers. (c) same as (a) except for LTC centers. (d) $\frac{b-c}{b+c}$, only shown if total density exceeds 3. Note that the colorbar panel (a) is different from that in (b) and (c).

northeast Indian monsoon (Rajeevan et al., 2012). Indeed, Southern India receives most of its rainfall in this season from low-pressure systems that form over the Bay of Bengal and then move westward (Singh et al., 2017). The massive rain event of 2015 that resulted in severe flooding in Tamil Nadu's state is an example of such a weather system (Phadtare, 2018). This region shows both lower and middle tropospheric systems (Figure 3.6c,d). Interestingly, the LTC density is high over North Australia, which is poleward of the maximum in MTC density. Similarly, high LTC density over the Indian ocean is poleward compared to the MTC density maximum. Indeed, Figure 3.6d is similar to its boreal summer northern hemisphere counterpart, wherein the fractional LTC density increases away from the equator, and the MTC fractional density is relatively high near the equator. Thus, the latitudinal preference of MTCs and LTCs is independent of the hemisphere. A common thread is that MTCs are prominent in regions where the seasonal cross-equatorial flow (advecting oppositely signed vorticity at low levels) meets with the monsoon trough, and LTCs are observed further northward in the vicinity of the monsoon trough itself.

Together, during boreal summer and winter total 91,283 moist cyclonic centers with $\xi_m > 1.5 \times 10^{-5}\text{s}^{-1}$ are identified over the entire tropics. A joint pdf of P_ξ and $\xi_m - \xi_l$ and separate pdfs using all these systems is shown in Figure 3.8. This highlights the bimodal nature of moist tropical systems. Indeed, cyclonic centers have clear peaks that align with the LTC or MTC categories. It is evident from Figure 3.8b that cyclonic centers are not counted in either the MTC or LTC categories mainly because P_ξ varies from near-surface values to about 400 mbar, but by definition, only centers from $650 \geq P_\xi \geq 500$ hPa are classified as MTCs and centers in the range $1000 \geq P_\xi \geq 700$ hPa are LTCs.

3.3 Robustness of Results

At this stage, it is worthwhile to examine the robustness of these results and whether the identified regions of MTCs occurrence are artifacts of the reanalysis or they exist in the real atmosphere. Also, the tilt of MTCs raises the concern of whether these are midlatitudes systems formed by baroclinic instability. Apart from the fact that reanalysis post-2000 performs satisfactorily in detecting cyclones (Hodges et al., 2017), the identified regions that support middle tropospheric systems agree with reported MTC locations by the IMD (Choudhury et al., 2018)

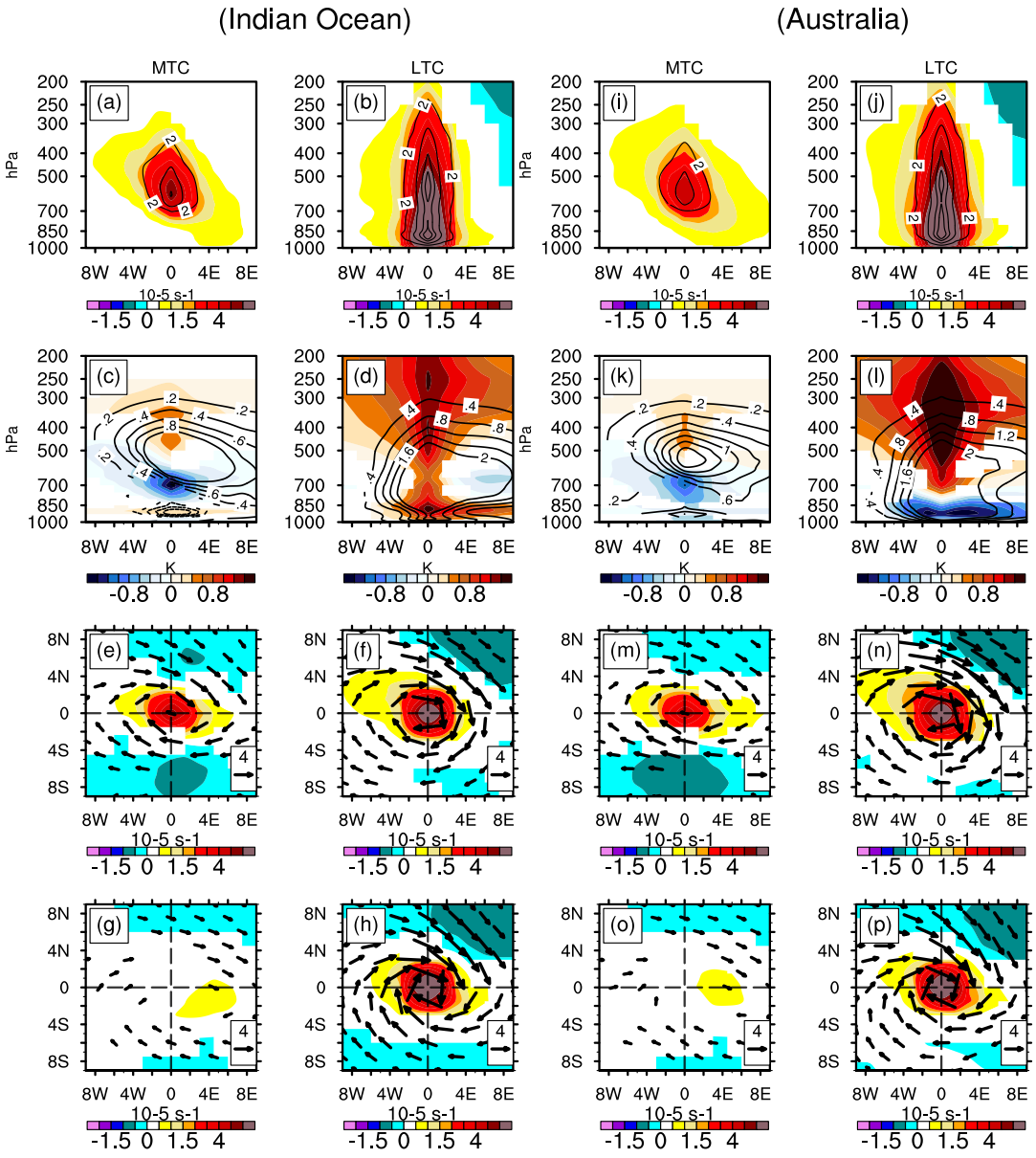

Figure 3.7: Composites of anomalies for MTCs (left column) and LTCs (right column) in the Southern Indian Ocean (a,b,c,d,e,f,g,h) and Australia (i,j,k,l,m,n,o,p); (a,b and i,j) Relative vorticity (shaded) and contours of potential vorticity (10^{-1} PVU); (c,d and k,i) temperature (shaded) and specific humidity (g/kg) in contours; (e,f,m,n) and (g,h,o,p) wind vectors and relative vorticity (shaded) at 600 hPa and 975 hPa, respectively. Results are only shown if they are significant at 1% significance under a two-tailed t-test.

and with the Indian Ocean field experiment over the Arabian Sea (Miller and Keshavamurty, 1968). Even in other tropical regions, there is observational evidence for moist systems with mid-tropospheric vorticity maxima, for instance, during the GATE-III experiment (Reed et al., 1977) and other observational case studies over Africa (Kiladis et al., 2006), near Central America (Simpson et al., 1967; Reed and Recker, 1971), the Western Atlantic (Shapiro, 1986) and the Eastern Pacific regions (Raymond et al., 1998). Indeed, the fact that reanalysis shows mid-tropospheric vorticity maxima in the same regions that these field experiments noted such vorticity profiles is encouraging. Further, the MTC structure's consistency across the tropics and preferential occurrence close to the equator indicate that they are not misidentifications of extratropical baroclinic systems.

In addition to this observational support, we note that reanalysis shows systems with lower and mid-tropospheric maxima in the same regions. The MTC fraction increases towards the equator, but both systems are observed in similar locations throughout the tropics. Nevertheless, it is crucial to note that the low spatial resolution of the underlying model in reanalysis products can lead to a low-level cold-core structure and an under resolved lower tropospheric circulation (Manning and Hart, 2007). Further, due to differences in the physics, resolution, limitation in data assimilation, and initialization used in underlying models, there might be disagreement in structures, exact location, and temporal coherence of these systems among different reanalysis data sets (Hodges et al., 2003). Indeed, it has been noted that there is a mismatch between different reanalyses, especially in diabatic heating and rainfall in regions where observations are sparse, such as for AEWs (Janiga and Thorncroft, 2013). Thus the actual number of MTCs and LTCs, their intensity, and structure in different reanalysis products might differ in such regions.

3.4 Conclusions

A global climatology of Middle Troposphere Cyclones (MTCs) for boreal summer and winter is presented based on 20 years (2000–2019) of reanalysis data. First, we analyze cyclonic systems in the Indian region during the IMD specified dates of middle troposphere circulation events over the Arabian Sea. The probability distribution of the differential vorticity (mid minus lower level) versus the height of vorticity maximum naturally yields two peaks (i.e., bimodal), thus, justifying the separation of cyclones into mid and lower-level systems. The two peaks

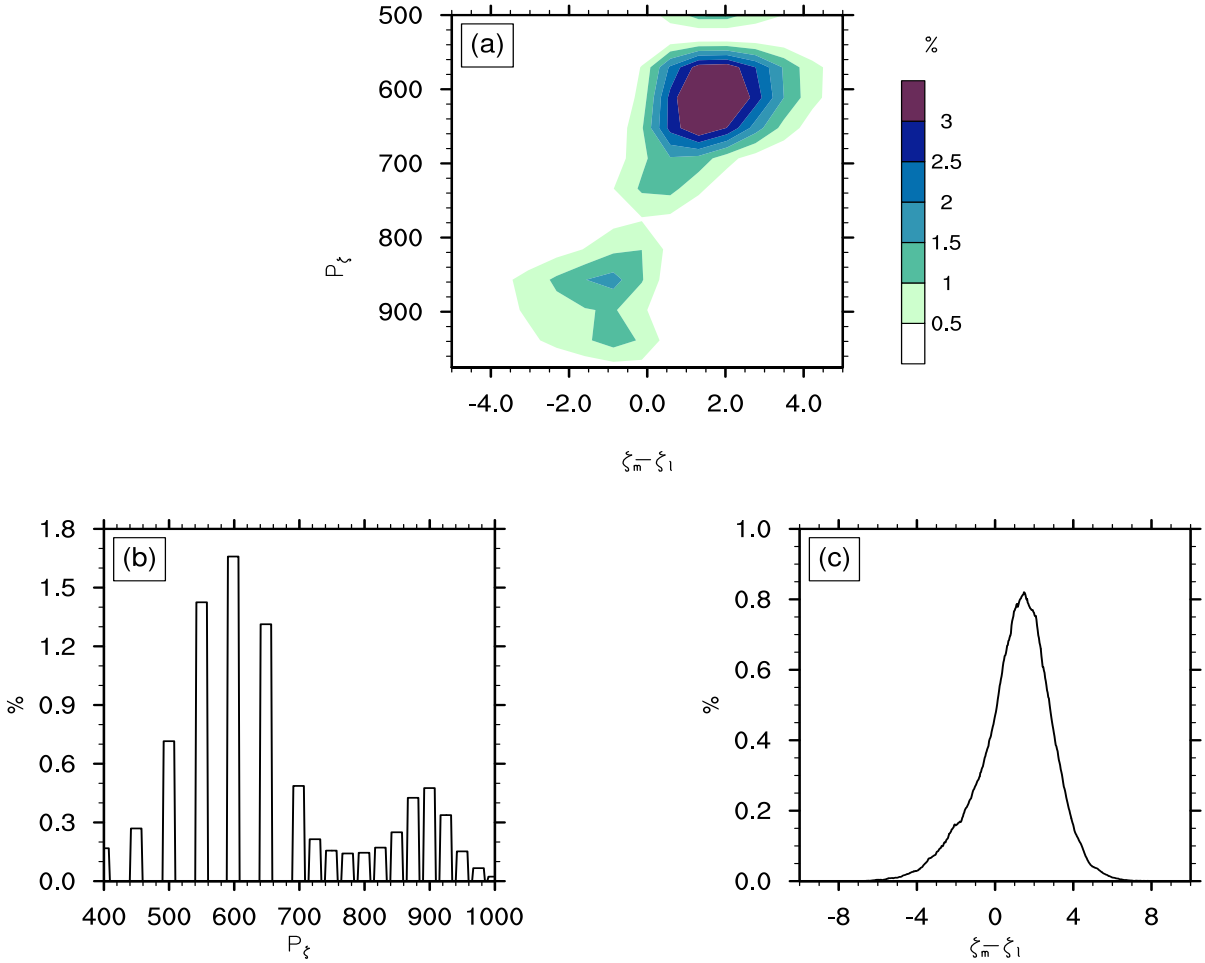

Figure 3.8: (a) Joint PDF of P_ξ and $\xi_m - \xi_l$ of all 91,283 cyclonic centers from 30°N to 30°S in 20 years of data. Notation follows Figure 2.1. (b) PDF of P_ξ; (c) PDF of $\xi_m - \xi_l$.

are used to define thresholds that allow for a separation of cyclonic centers into these two categories. The utility of the selected thresholds is validated by composites of cyclone centers that fall in the two clusters.

Over South Asia, cyclonic systems have been tracked manually for sixteen years. This yields 261 MTCs or about 3-4 systems per month during the summer season. The principal characteristics of these systems are as follows:

1. The highest density of MTCs is over the North-East Arabian Sea, followed by the Bay of Bengal and the South China Sea. Further, MTCs mainly occur during the early part of the summer monsoon (i.e., June and July).

2. MTCs are part of the life cycle of tropical cyclonic systems. In particular, tracks of systems identified as MTCs change their character. Usually, they exhibit a middle (MTC-phase) and a lower troposphere vorticity maximum (LTC-phase) during different periods of their life cycle.

3. Cross basin motion suggests that MTCs observed in a given region can have a nonlocal or remote genesis.

4. Cyclone motion statistics indicate that MTCs move slowly westward or remain quasi-stationary over the Arabian Sea compared to the Bay of Bengal and the South China Sea.

5. Analysis of the differences of middle and lower troposphere vorticity ($\delta\xi_p$) and mean middle tropospheric vorticity (ξ_m) indicates that the MTC and LTC phases are prevalent south and north of 20°N, respectively.

Cyclone center density over global tropics suggests that MTCs form over several monsoonal regions. These include the Arabian Sea, East & West Africa, East Pacific, North Bay of Bengal, and the South China Sea in the boreal summer. During boreal winter North Australia, the South Indian Ocean, South America, and subtropical Africa show significant MTCs activity. Further, near-equatorial regions have more MTCs than LTCs in both hemispheres, while LTCs are more prominent than MTCs away from the equator. In particular, MTCs are dominant equatorward of the monsoon trough, and LTCs are prevalent in the vicinity of the monsoon trough itself. Together, the probability density function of differential vorticity versus the height of peak vorticity of cyclonic centers over global tropics is bimodal, with one peak (for MTCs) in the middle and another (for LTCs) in the lower troposphere.

Composites from different global tropical regions show that, apart from their tilt, which is somewhat region-dependent, MTCs are remarkably similar throughout the tropics. In particular, they show high vorticity, potential vorticity, and moisture anomalies in the middle troposphere. Besides, MTCs show a baroclinic structure with warm temperature anomalies over cold anomalies with significant east-west tilt. Though they have maximum intensity in the middle troposphere, in most places, MTCs also show a weak trough-like surface signature to the east of the middle-level center. LTCs, on the other hand, show a maximum vorticity and moisture anomaly in the lower troposphere with a shallow cold core below 800 hPa and a relatively warm upright temperature structure. It should be noted that the shallow cold-core at lower levels may be an artifact of the coarse grid spacing of reanalysis products. The PV anomalies of MTCs have a single peak in the middle troposphere. In contrast, the PV profile of LTCs usually shows two peaks, one in the middle troposphere and another in the lower troposphere. Further, LTCs show some regional structural differences, primarily in the low-level cold anomaly, which is almost non-existent in the South Indian Ocean and East Pacific and somewhat deeper in other parts of the tropics.

Chapter 4

Classification of MTCs over the Arabian Sea and Western India

In the previous chapter, our global analysis of MTC occurrence showed the Arabian Sea region to be a hot spot for these rainy synoptic systems. This is consistent with the description in the Introduction that western India receives a significant portion of its rainfall from MTCs. In fact, the state of Gujarat and the west coast of Maharashtra are regions that receive more than 70% of their annual rainfall from heavy rainfall events, with the intensity of rain events reaching 80 mm per day (Kumar et al., 2014; Vuruputur et al., 2018). In terms of meteorological and societal impact, not only does western India witness some of the world's heaviest rainfall events and associated floods (Mapes, 2011; Vuruputur et al., 2018; Choudhury et al., 2018), it has also shown an increasing trend in both annual precipitation and in the frequency of extreme rain events in the past few decades (Rajeevan et al., 2008; Pattanaik and Rajeevan, 2010; Vinnarasi and Dhanya, 2016; Roxy et al., 2017). Given the crucial role of synoptic middle troposphere systems in extreme rain events and annual rainfall over western India, we now focus on precursors and formation mechanisms of MTCs in this region.

In particular, in this chapter, we begin by exploring the large-scale evolution of fields and composite weather pattern during rainy days over western India in Section 4.1 and 4.2, respectively. In Section 4.3 we identify

various clusters of rainy days over western India using the unsupervised k-means algorithm. We will then adopt an independent cyclone tracking approach to classify systems in the different groups based on their formation. The intent here is to see if there are common dominant patterns that arise from clustering and tracking that partition the entire set of MTCs into groups that can then be analyzed for genesis mechanisms. Indeed, in Section 4.4 we will look at the characteristics of various categories of MTCs and how intraseasonal oscillations modulate their formation. Finally, we summarize the main results of this chapter in Section 4.5.

4.1 Large Scale Conditions During Western India Rainfall

Before diving into the classification and formation mechanisms of synoptic systems, it is worth exploring the prevalent large-scale conditions during rainfall over western India. The lag-correlation of daily OLR — a proxy for moist convection — in the South-Asian sector with the mean daily OLR time series over western India ($68 - 72°$E, $15 - 22°$N) for 37 years during June through September is shown in Figure 4.1. Here, Day 0 represents the correlation at zero lag. At $8 - 10$ days lag (Figure 4.1a), a large-scale east-west elongated belt of positive correlation appears near the equator — reflecting the presence of the Intertropical Convergence Zone (ITCZ) near the equator or Phase 1 of BSISO (Kikuchi et al., 2012; Lee et al., 2013). This region of positive correlation stretches from the western equatorial Indian Ocean up to the South China Sea. From Day -9 to 0 (Figure 4.1a-e), northward propagation of correlation patterns is pronounced over the Arabian Sea and Bay of Bengal. Interestingly, the Arabian Sea branch appears to advance much faster than its Bay of Bengal counterpart. These differences in propagation result in a northwest to southeast tilt, which has been observed in prior studies (Karmakar and Misra, 2020). The northward movement is seen up to Day 0 over both basins; after which the Bay of Bengal branch shows a west-northwest extension from Day 0 to 3 (Figure 4.1e-f) that is maybe a reflection of relatively high-frequency variability associated with the westward motion of monsoon lows and Rossby waves (Goswami, 1987; Sobel and Horinouchi, 2000; Karmakar and Misra, 2020; Karmakar et al., 2021). Moreover, all the way through Days 0 to 9 (Figure 4.1e-i), while regions of positive correlation gradually weaken, they are seen to remain quasi-stationary, with one maximum over the northeast Arabian Sea and the other over the east coast of India and the Bay of Bengal, indicating the co-existence of convective activity over both these regions.

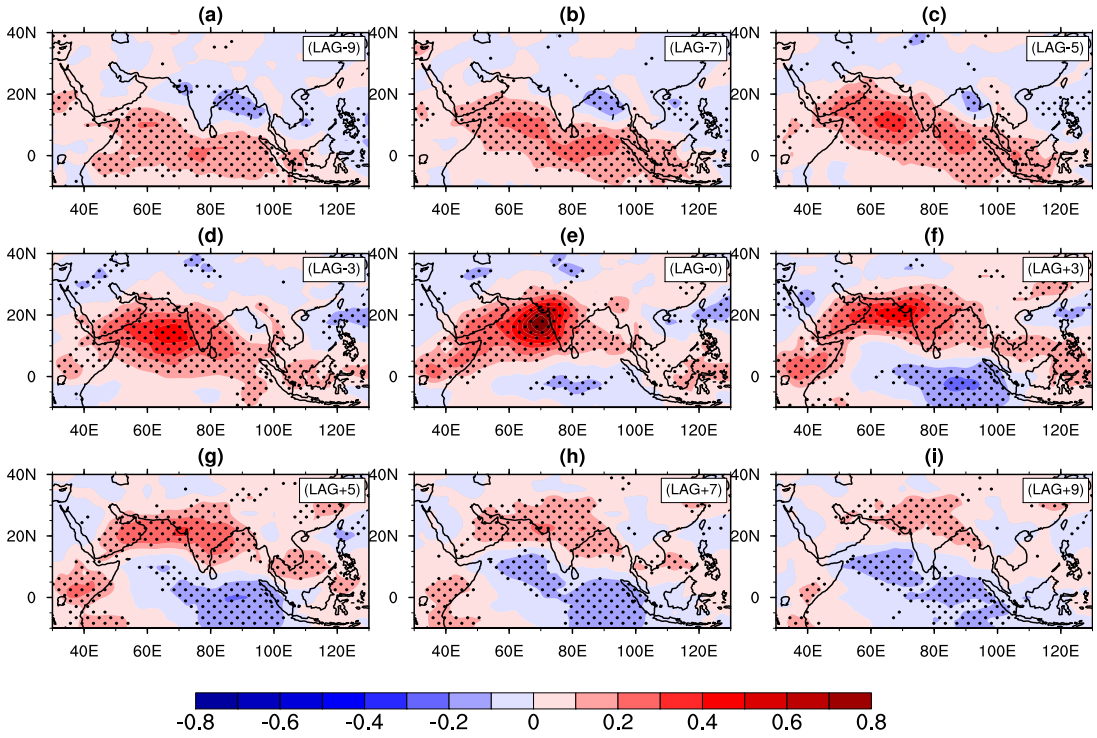

Figure 4.1: Lag correlation of OLR anomaly over the shown domain with the Arabian Sea ($15-22°$N to $68-72°$E) mean OLR anomaly time series from June to September, 1980-2019. Shading denotes the regions which are significant at 99% confidence using t-test.

Since the large-scale correlation pattern concurrently covers both the Arabian Sea and the Bay of Bengal, it suggests favorable conditions for cyclonic systems over both the basins simultaneously. Hence, it is not surprising that prior studies reported the co-existence of synoptic systems over these two regions (Ramage, 1971; Carr, 1977; Choudhury et al., 2018). Although the correlation of OLR anomalies includes the entire spectrum of temporal variability, the Spatio-temporal evolution of these patterns closely resembles those of intraseasonal modes (Kikuchi et al., 2012; Lee et al., 2013). Essentially, these results suggest that the rainfall over western India and the eastern Arabian Sea is likely modulated by northward propagating large-scale OLR anomalies that are similar to the BSISO (Kikuchi et al., 2012).

4.2 Rainy day composites

To understand the dynamical features prevalent during rain events over western India, we now construct composites of meteorological fields on rainy days. In particular, composites of the precipitation anomaly, precipitable water anomaly, total and anomalous wind, and geopotential height anomalies during the rainy days over western India at 950 hPa and at 600 hPa are shown in Figure 4.2; anomalies are with respect to daily climatology constructed from 22 years of reanalysis data.

During rainy days, precipitation anomalies (Figure 4.2a) are largest along the western coast of India but extend up to central and east India. Similarly, precipitable water (Figure 4.2b) is anomalously high over the northeast Arabian Sea and western India, with a positive anomaly up to the Bay of Bengal. The precipitable water anomaly maximum (Figure 4.2b; contours) also coincides with the anomalous circulation, suggesting that anomalous winds might play a role in controlling moisture accumulation. The wind direction over this region is crucial in moisture control, given strong meridional and zonal moisture gradients. Specifically, towards the north-northwest (east), there is a substantial decline (rise) in climatological total column water vapor around 20°N and 70°E (Figure 4.2b; colors). Consistent with the anomalous flow, the height anomalies (Figure 4.2c,d) at 950 and 600 hPa depict a widespread low in the middle troposphere over western India and the northeast Arabian Sea. In addition, the height anomaly and associated cyclonic circulation over the eastern Arabian Sea and western India (Figure 4.2e,f) appears to be the part of the middle-tropospheric zonally oriented monsoon trough, which extends from the Bay of Bengal to the Arabian Sea during the rainy days.

The strength of inversion (Figure 4.2h) — difference of temperature anomaly at 750 and 950 hPa levels ($\Delta T = T_{a750}$-T_{a950}) — weakens during rainy days over the northeast Arabian Sea. This is also reflected in the reduction of the static stability at the 800 hPa level (Figure 4.2g). This is reasonable as the prevailing anomalous northeasterly winds reduce the advection of cold maritime air at low levels, while enhanced easterly winds in the middle troposphere prevent the advection of warm, desert air from the northwest at middle levels, effectively reducing the strength of inversion. Indeed, this is consistent with the noted decrease and increase in strength of inversion in this region during the active and break phases of the Indian monsoon, respectively (Narayanan and Rao, 1981; Dwivedi et al., 2021). In fact, the reduction in strength of inversion was also noted by (Miller and Keshavamurty,

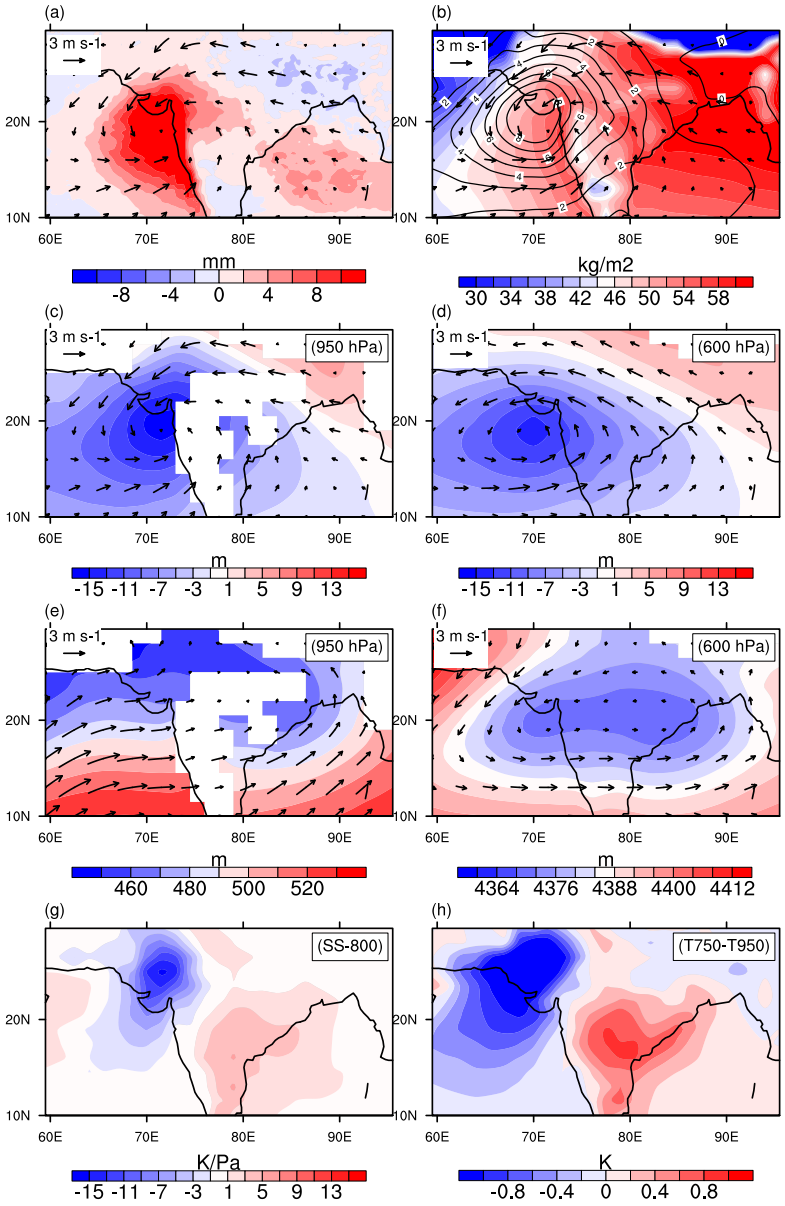

Figure 4.2: Composites of rainy days ($P_{WI} > 7.6$ mm/day) (a) composite rain anomaly (b) composite precipitable water anomaly (contours: kg/m2) and June-September climatology (colors); (c) composite geopotential height anomaly at 950 hPa for rainy days; (d) same as (c) but for 600 hPa; (e), (f) composite total geopotential heights at 950 and 600 hPa, respectively; (g) is the static stability parameter at 800 hPa; (h) anomalous strength of inversion $\Delta T_{ano} = T_{a750} - T_{a950}$, where T_{a750} and T_{a950} are temperature anomalies at 750 and 950 hPa. heights are in meter and rainfall in mm; the white regions are where topography crosses the geopotential surface of analysis.

1968) in their original study of an MTC. The weakened low-level inversion facilitates a favorable environment for monsoon rain in western India. Once the inversion is destroyed, water vapor can rise vertically and trigger deep convection. In addition, consistent with the observations of Miller and Keshavamurty (1968), we note that north and south of about 20°N (Figure 4.2d), the mid-level anomalous circulation is easterly and westerly, respectively.

Thus, as a whole, when western India experiences significant precipitation, the composites clearly point towards the presence of well-developed middle tropospheric anomalies in circulation and the geopotential height, both of which are collocated with the anomalous build-up of precipitable water. Furthermore, the erosion of the usually strong inversion layer over the eastern Arabian Sea is notable and consistent with the occurrence of deep convection.

4.3 Weather Regimes over Western India

To identify dominant weather regimes or patterns associated with rainy days over western India and, in turn, their precursors, we utilize a k-means clustering approach. As discussed in Chapter-2, we choose four clusters ($k = 4$), and the composite 600 hPa geopotential height and wind anomalies of these four weather patterns as identified by k-means are shown in Figure 4.3. As expected, all four dominant weather regimes show anomalous cyclonic circulation and height depression in the middle troposphere over the northeast Arabian Sea and adjoining western Indian region. Regime 1 (Figure 4.3a) consists of a sizeable negative height anomaly oriented northwest to the southeast, which covers both the Arabian Sea as well as the Bay of Bengal. This reinforces the notion that Arabian Sea systems exist with cyclonic conditions over the Bay of Bengal (Miller and Keshavamurty, 1968; Ramage, 1971). Regime 2 (Figure 4.3b) is more compact than Regime 1 and consists of a zonally oriented height anomaly that again extends from the Arabian Sea up to the Bay of Bengal. Regime 3 (Figure 4.3c) consists of a relatively weak broad negative height anomaly accompanied by cyclonic circulation over the northeast Arabian Sea, which extends up to the southwest Arabian Sea and depicts a northwest to northeast orientation. In this Regime, the Bay of Bengal shows a gigantic positive height anomaly and associated anticyclonic circulation. Finally, Regime 4 (Figure 4.3d) shows a zonally elongated negative height anomaly and cyclonic circulation that is closer to the equator and spans a small portion of the southern Bay of Bengal, the southern tip of India and stretches into the

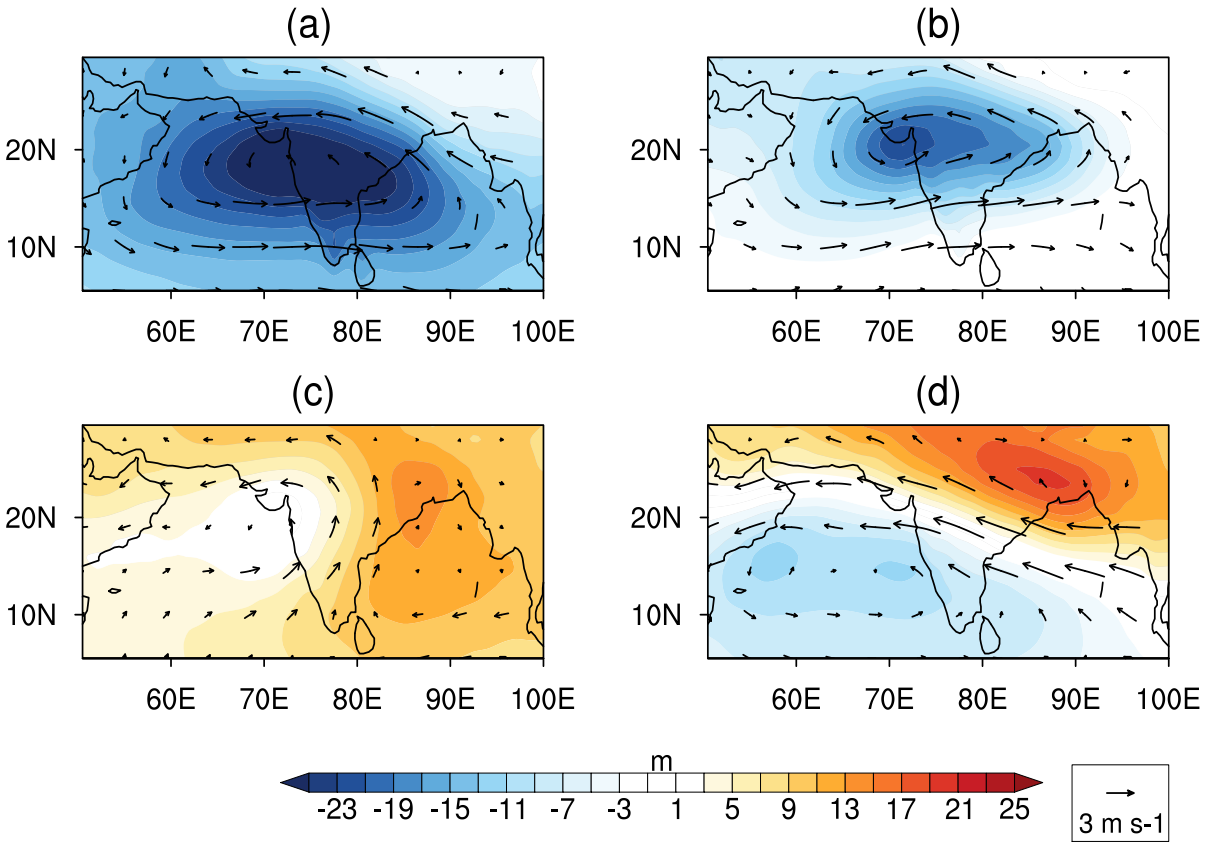

Figure 4.3: Composite height anomaly of 700 hPa surface (m) from $k-$means clustering for Regime 1 (a) to Regime 4 (d). The respective composite winds are shown as arrows, units are m/s.

southern Arabian Sea. Similar to Regime 3, Regime 4 also shows the signature of a positive height anomaly and anticyclonic circulation over northeast India and the North Bay of Bengal; however, in contrast to Regime 3, here, the positive height anomalies are narrow, zonal, and confined to east-central India and foothills of the Himalayas with a maximum over West Bengal. Essentially, the first two regimes indicate cyclonic vorticity and a convectively active environment that ranges from the Arabian Sea & western Indian up to the Bay of Bengal. In contrast, the latter two regimes suggest the existence of Arabian Sea cyclonic anomalies in isolation which remain relatively weak in the absence of convectively active cyclonic conditions over the Bay of Bengal.

For these four patterns (Regimes 1, 2, 3 & 4), precursors are now extracted from daily time-lag composites (Clark et al., 2018); these are shown in Figure 4.4. Lag composite of the Regime 1 (row 1; Figure 4.4) suggests a cyclonic circulation and height depression over the Bay of Bengal accompanied by a weak trough-like signature over the Arabian Sea on Day -4. Subsequently, from Day -4 to -2, the Bay of Bengal height anomalies deepen and propagates northwestwards. Following this, from Day -2 to Day -1, the cyclonic circulation over the northeast Arabian Sea shifts eastwards and merges with the intensifying and northwestwards moving Bay of Bengal anomaly. Essentially, in this Regime, the Arabian Sea cyclonic conditions appear to be the direct result of westward-moving Bay of Bengal cyclonic anomalies. In essence, westward-moving LPSs in the Bay of Bengal and East India are expected to be a precursor for the formation of this particular class of Arabian Sea systems.

The lag composite of Regime 2 (row 2; Figure 4.4) shows two dominant centers of action, one over the Arabian Sea and one over the Bay of Bengal from Day -4 to Day -1. The composite winds and height anomalies of this Regime indicate the presence of twin vortices joined together by an elongated trough line in the middle troposphere with a northwest orientation. This structure is similar to the evolution of the July 1963 MTC wherein, after intensification, the Arabian Sea MTC became joined with the Bay of Bengal LPS by a zonal middle tropospheric trough (Miller and Keshavamurty, 1968). The daily evolution of lag-composite shows that initially (Day -4), there is a sign of cyclonic systems in both basins, but height anomalies (color shading) deepen first over the Bay of Bengal (Day -3), and then the deepening of height anomalies or intensification of the Arabian Sea system follows (Day 0). In fact, a gigantic circulation develops by about Day -2 that encircles both systems. To some extent, the structure, orientation, and propagation characteristics of this Regime resemble that of phases 4 & 5

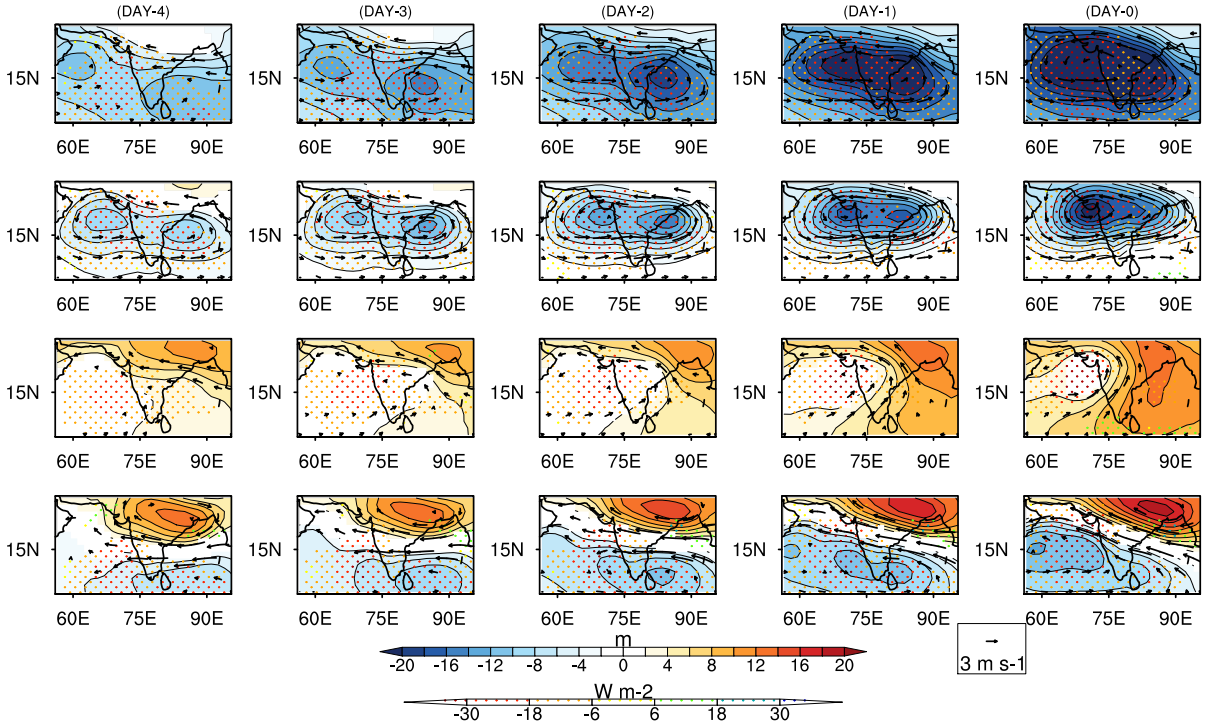

Figure 4.4: Lag composites of the four $k-$means clustering regimes from Day -4 to Day 0; row 1 to row 4 represent Regime 1 to 4, respectively. Here, Day zero represents the Day when the cluster was detected. Color shading represents the composite 600 hPa height anomaly (m), dotted shading represents the OLR anomaly, and arrows represent the composite wind anomaly. OLR and height fields are only shown if they are significantly different from climatology at 0.1 significance. Wind vectors are shown if any wind component is significantly different from zero at the 0.1 significance level under the two-tailed t-test.

of the BSISO (Kikuchi et al., 2012). We anticipate that the co-existence of systems in both basins may have a far-reaching influence on rainfall patterns and intensity by the cooperative intensification through enhanced moisture exchange and an enhanced vorticity-rich environment. In fact, the presence of cyclonic anomaly over both the basins in this Regime is in agreement with the notion that most Arabian Sea systems exist in the presence of Bay of Bengal disturbances (Carr, 1977; Choudhury et al., 2018; Miller and Keshavamurty, 1968). Further, it is important to note that though, on Day -3, Regime-1 and Regime-2 look similar, their evolution is quite different. In Regime-1, the anomalies originated far south of the Bay of Bengal and showed a clear west-northwest motion which finally became Arabian sea MTCs on Day-0. On the other hand, in the Regime-2, the Bay of Bengal system was already present near the coast of Odisha. It did not show much movement throughout, and an independent *in-situ* Arabian sea MTCs formed with this coexisting Bay of Bengal system.

The composite winds, height anomaly, and OLR for Regime 3 are shown in Figure 4.4; row 3. Here, weak negative OLR and height anomalies are seen over most Arabian Sea from Day -4 to Day -3. Then, east India and western regions of the Bay of Bengal also develop a signature of cyclonic circulation around Day -3. Hence, as the Arabian Sea system evolves, we note the appearance of cyclonic activity over the western Bay of Bengal. Subsequently, the Arabian Sea height anomaly moves northwards and by Day 0 becomes a concentrated vortex over the northeast Arabian Sea & west India. In fact, the emergence of this compact vortex causes the cyclonic circulation to withdraw from the Bay, and from Day -1 to Day 0, a positive height anomaly appears in the North Bay of Bengal. Thus, when mature, the Arabian Sea and north Bay of Bengal anomalies exhibit an opposite sense of circulation in Regime 3.

In Regime 4 (row 4; Figure 4.4), the negative height anomaly in the Arabian Sea system is positioned at a lower latitude compared to Regimes 1,2 & 3. Here, the North Bay of Bengal and core monsoon zone are characterized by positive height anomalies, anticyclonic circulation, and absence of convection. In contrast to the North Bay of Bengal, a large region of negative OLR and height anomalies exist in the southern Bay of Bengal on Day -4. Following this, from Day -4 to Day -3, the convectively active region of the South Bay of Bengal moves northwestwards into the Arabian Sea (by Day 0). With the movement of this large-scale envelope of negative height anomaly over the Arabian Sea, the genesis of a cyclonic system is observed over the northeast Arabian

Sea. Similar to Regime 3, Regime 4 also shows a positive height anomaly over the north Bay of Bengal and the Indian monsoon trough region. It is also worth noting that Regimes 3 & 4, characterized by convectively unfavorable conditions over the Bay of Bengal, also show weak OLR and wind anomalies over the Arabian Sea. This suggests that cyclonic conditions over the north Bay of Bengal might be vital in intensifying Arabian Sea systems — as strong Arabian Sea anomalies are only observed in Regimes 1 & 2, where cyclonic conditions persist over the Bay of Bengal.

A common feature of the first three regimes — pronounced in Regimes 1 & 2 and with a weaker short-lived signature in Regime 3 — is the co-existence of a Bay of Bengal cyclonic anomaly during the development of the Arabian Sea system. In comparison, Regime 4 (and Regime 3, when mature) is characterized by an anticyclonic anomaly over the north Bay of Bengal. Interestingly, in all cases, the pattern in the Arabian Sea is poleward compared to the Bay of Bengal, which agrees with the northwest to the southeast orientation of the BSISO (Kikuchi et al., 2012). Broadly, based on the evolution of these regimes and guided by previous work, the formation of systems over the Arabian Sea can be physically grouped into two classes, namely the downstream development of westward-moving lows that originated in the Bay of Bengal (Regime 1) and *in-situ* genesis (Regimes 2, 3 & 4).

4.4 Tracking of Western Indian Cyclonic Systems

Though the lagged composite of clusters in Figure 4.4 provide some insight about weather patterns, identification of individual storms, their precursors, and evolution is now undertaken by tracking systems for 22 years (June-September; 1998-2019). Indeed, tracking of systems allows us to quantify local versus remotely formed systems based on their genesis, lysis, and trajectories. Further, this allows for an independent grouping of rainy systems in this region and thus also confirms the existence of clusters detected by the k-means approach. The tracking algorithm (described in the Method section) results in a total of 191 rainy & long-lived cyclonic systems which pass over the Arabian Sea and western India (a marked red region in Figure 4.5). These systems are now classified based on the location of their genesis and the co-existence or absence of Bay of Bengal disturbances. Specifically, we define four categories as follows: (1) direct downstream intensification of the westward-moving Bay of Bengal

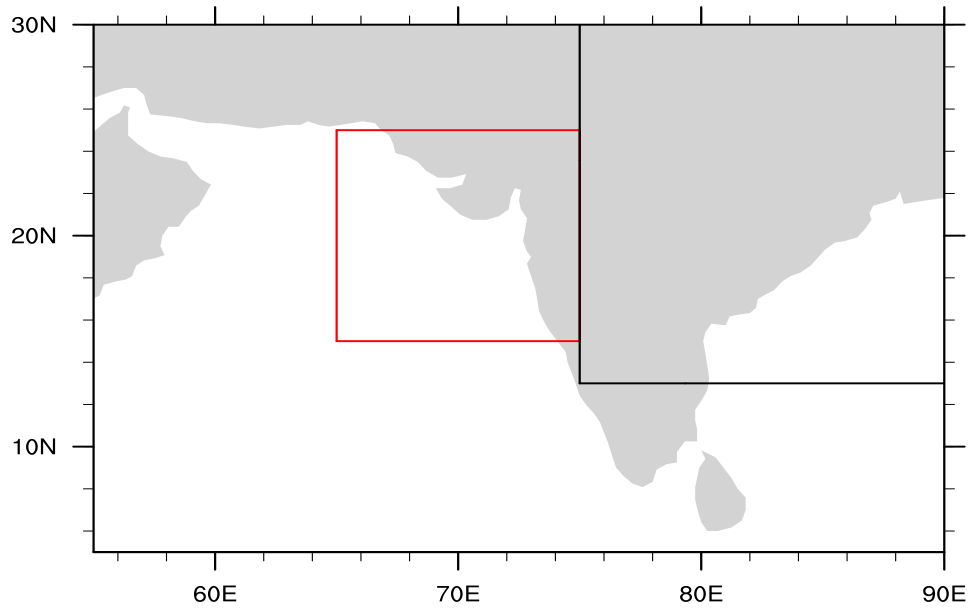

Figure 4.5: Domains Specifications: Red box: Arabian Sea; Black box: Bay of Bengal

system (Type 1); any system falls in this category if its genesis is east of $75^{\circ}E$, the region marked black in Figure 4.5 and lasts in the red marked region at least 24 hours. This accounts for around 51% or 98 systems; (2) *In-situ* formation over the Arabian Sea (Type 2); any system falls in this category if it forms over the Arabian Sea and remains in the marked box at least for 24 hours; this accounts for about 48% or 92 systems. Further, Type 2 is grouped into three sub-categories based on the presence or absence of a monsoon low to the east. In particular, Type 2a comprises of *in-situ* Arabian Sea system formation with a preceding Bay of Bengal system. This accounts for 31% of systems. Type 2b is *in-situ* formation but which precedes a Bay of Bengal system. This accounts for 9-10% of systems. Type 2c is *in-situ* formation in the absence of a system in the Bay of Bengal, and this accounts for the remaining 7-8% of systems.

For clarity, a flow chart of system classification is shown in Figure 4.6. Interestingly, the association of a Bay of Bengal system with Arabian Sea MTC formation becomes apparent as more than 90% of rain-bearing systems in this region fall in Type 1 and Types 2a & 2b categories. Further about 83% of the *in-situ* synoptic systems observed in the Arabian Sea and western Indian region are associated with cyclonic anomalies (either preceding or after) in the Bay of Bengal. This is consistent with previous case studies in that stand-alone formation of rainy systems over the Arabian Sea is relatively rare, and most of the systems develop with a Bay of Bengal LPS.

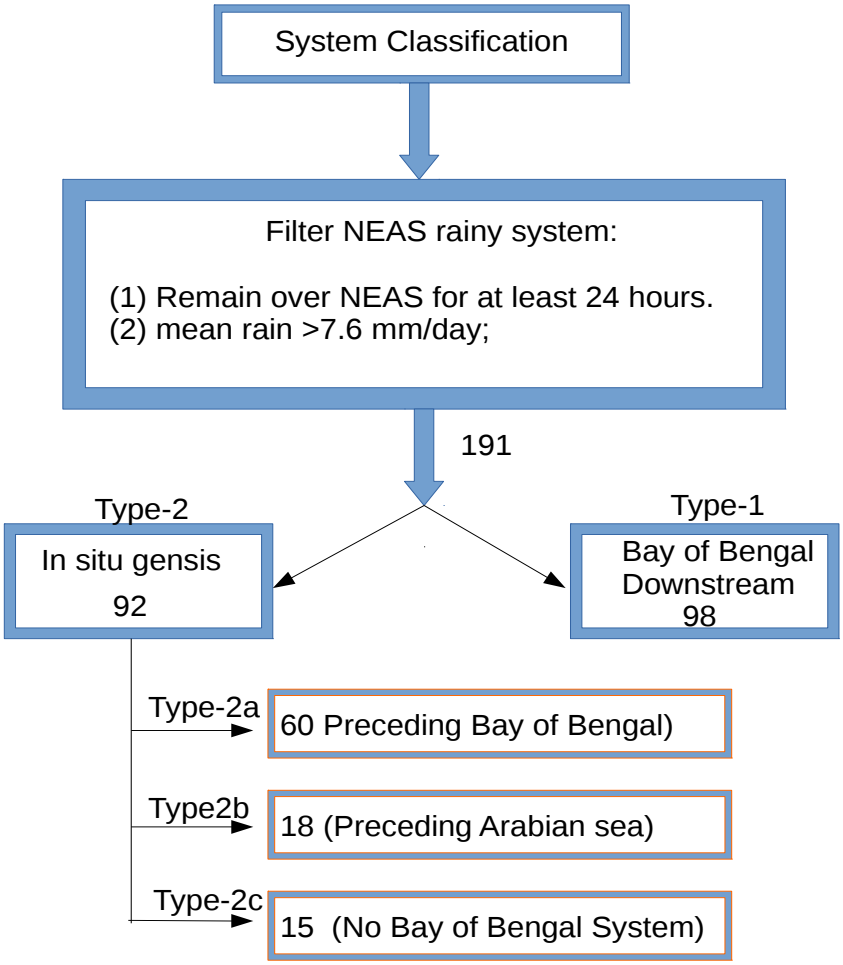

Figure 4.6: Northeast Arabian Sea (NEAS) system classification based on their genesis as discussed in method section. A total of 191 long lived systems (life $>$ 3 days) satisfy the rainfall criteria (cyclone following composite rain and rain over western India (18°N-22°N, 68°E-74°E) during life of cyclone is grater than or equal to 7.6 mm/day) and exist over western India and adjoining Arabian Sea for at least 24 hours (red box, Figure 4.5). Type 1 systems are those which originate in the Bay of Bengal (black box, Figure 4.5). Type 2a MTCs are the *in-situ* forming systems with a preceding the Bay of Bengal LPS. Type 2b are *in-situ* born MTCs which precede the formation of a Bay of Bengal system. Type 2c represents *in-situ* MTC formation with no cyclonic activity in the north Bay of Bengal (black box).

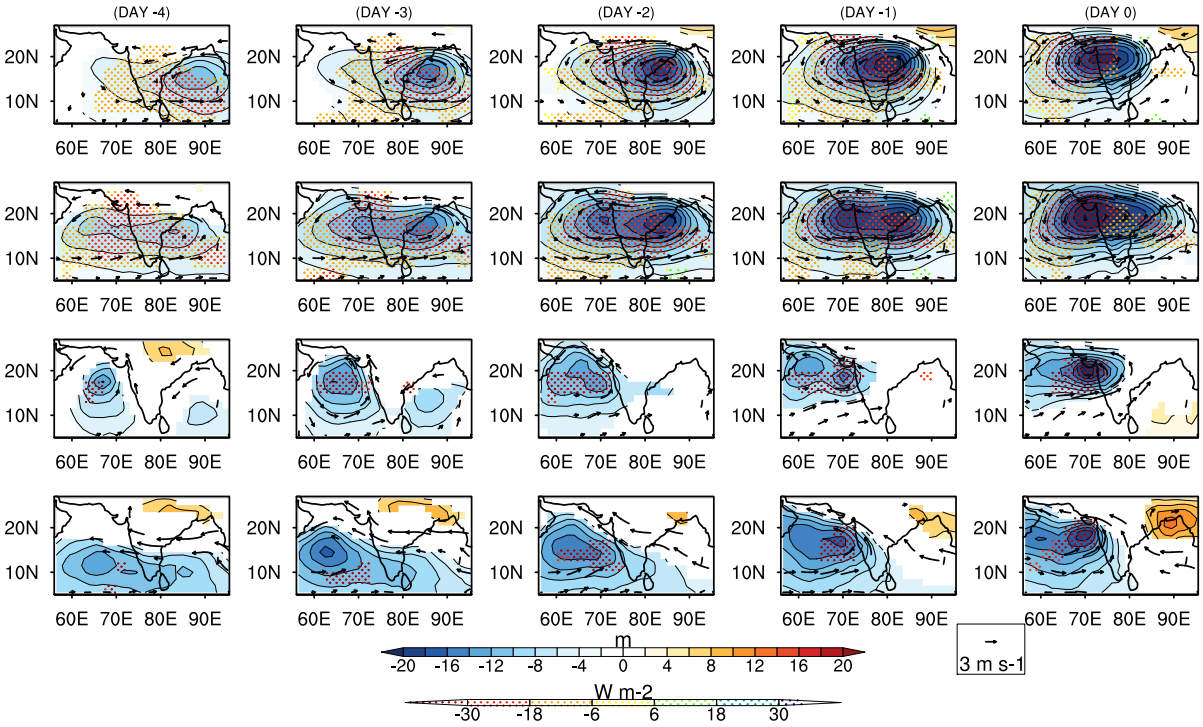

Figure 4.7: Lag composites of four variants of Arabian Sea systems via cyclone tracking from Day -4 to Day 0. Rows 1, 2, 3 and 4 represent Type 1, 2a, 2b and 2c, respectively. Zero days represent the Day of the heaviest rainfall in western India. Color shading represents the composite 600 hPa height anomaly (m), dotted shading is the OLR anomaly, and arrows represent the composite wind anomaly. Height anomaly and OLR have shown only if they are significantly different from climatology at 0.1 level of significance and arrows if any wind component is significantly different from zero at 0.1 significance.

Furthermore, it is comforting to note that the classification of systems based on their genesis and tracks into Type 1, 2a, 2b & 2c matches, at least qualitatively, with the patterns (Regimes 1, 2, 3 & 4) obtained via unsupervised k-means clustering.

4.4.1 Evolution of four categories

The lag-composites of 600 hPa height, OLR, and wind anomalies for the four types of MTCs identified by tracking of cyclonic systems over 22 years (Type1, Type 2a, 2b & 2c) are shown in Figure 4.7. In Type 1 composite evolution (first row; Figure 4.7), initially, a height depression, cyclonic circulation, and associated negative OLR anomaly develop over the Bay of Bengal. This occurs at least four days before the onset and intensification of the system over the Arabian Sea. A westwards extending trough and weak negative OLR anomaly along the west coast of India are also observed prior to system formation. Gradually, the cyclonic circulation over the Bay

intensifies and moves northwestwards, which finally, around Day -1 approaches western India. This category of system formation was found to be most frequent (98 systems) and consistent with previous work, suggesting that, quite often, Arabian Sea systems form from the downstream evolution of westward-moving Bay of Bengal lows (Carr, 1977; Kushwaha et al., 2021). Given that this formation mechanism involves direct downstream development, its frequency is expected to be highly sensitive to the formation of cyclonic systems in the Bay of Bengal. The evolution of this type is qualitatively similar to Regime 1 of k-means clustering.

The composite evolution of Type 2a formation (second row; Figure 4.7) shows that these systems develop locally over the Arabian Sea but in the presence of a monsoonal disturbance over the Bay of Bengal or East India. Four days before the intensification of the Arabian Sea system, a relatively strong cyclonic circulation and height anomaly is observed to develop over the Bay of Bengal, along with a zonally oriented trough and associated negative height anomaly over the Arabian Sea. A negative OLR anomaly accompanies this along the Western Ghats and over the Bay of Bengal in the southwest sector of cyclonic circulation. From Day -4 to Day -3, the Bay of Bengal height anomaly deepens, convection intensifies, and both systems encircle. This is immediately followed by an intensification of the Arabian Sea cyclonic system. Indeed, from Day -3 to Day 0, the Arabian Sea system remains stationary and intensifies significantly. Eventually, from Day -1 to Day -0, the Bay of Bengal system weakens and almost merges with the Arabian Sea system. Notably, the evolution is qualitatively similar to Regime 2 of k-means clustering.

Type 2b formation (third row; Figure 4.7) occurs with weak cyclonic activity over the Bay of Bengal or Eastern India. However, contrary to Type 2a, the genesis of this class of systems precedes the system to the east. From Day -4 to -3, convection and cyclonic circulation appear over the southwest Arabian Sea, gradually moving northwards with a slight eastwards component. From Day -3 to -2, cyclonic shear and a negative OLR anomaly appear in the Bay of Bengal and East India. Interestingly after the weak negative height and OLR anomaly around Day -3 to Day -2, the eastern Bay of Bengal shows signs of positive height anomalies and anticyclonic shear. Gradually, from Day -2 to Day 0, the cyclonic anomaly in the Arabian Sea and associated convection moves northwards parallel to the west coast of India and remains stationary near the coast of Gujarat. Indeed, for Type 2b, when mature, the sense of circulation is opposite in the Arabian Sea and the North Bay of Bengal. Given

the evolution of wind and OLR anomalies, this formation type depicts the prototype monsoon onset vortex, which usually helps the progress of monsoon over western India and the Arabian Sea in the early monsoon months (Krishnamurti et al., 1981). The development of this Type 2b category is similar to Regime 3 of k-means clustering.

Finally, Type 2c (fourth row; Figure 4.7) is a category where the Arabian Sea system appears in the absence of convection and cyclonic circulation over the north Bay of Bengal. However, this is a case of northwestward propagation of an equatorial convective envelope into the Arabian Sea. In particular, on Day -4, a cyclonic flow and negative OLR anomalies existed over the southern Bay of Bengal, south Arabian Sea, and near Sri Lanka. These anomalies then propagate northwestward into the Arabian Sea from Day -4 to Day -2. Once in the Arabian Sea, the movement is predominantly northward along the western coast of India, and the formation of a cyclonic system follows in the northeast Arabian Sea. Notably, while the large-scale anomalies propagate northwestward from the southern Bay of Bengal, the cyclonic system develops locally in the Arabian Sea. Throughout the evolution of this system, positive height anomalies and anticyclonic circulation is observed over the core monsoon zone and north Bay of Bengal, similar to the Regime 4 of k-means clustering.

4.4.2 Meteorological characteristics of the four categories

Having established that rainy MTCs over the Arabian Sea and western India fall into four categories with respect to the formation, the overall nature of which agrees with the k-mean classification scheme, we now examine various characteristics of these categories, including their rainfall distribution (Figure 4.8), monthly frequency (Figure 4.9), track density and motion vectors (Figure 4.10).

Type 1 formation, in terms of mean and extreme rainfall (Figure 4.8), is the second-largest rain-producing category over western India and occurs most commonly in July and August (Figure 4.9). The cyclone motion vectors and genesis density, shown in Figure 4.10a, suggest that most of these systems take shape near the eastern state of Odisha in India, which is a little south of the head Bay of Bengal. As per the notion of their downstream development, motion vectors indicate that this category exhibits northwest movement across central India into the Arabian Sea. In contrast, Type 2a genesis occurs throughout the monsoon season (Figure 4.9); however,

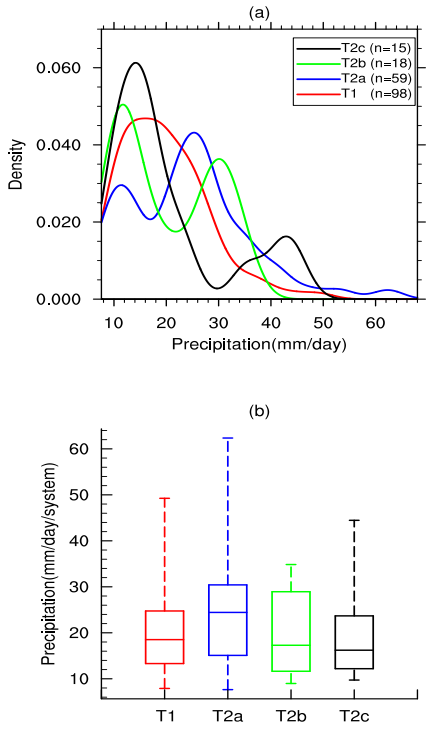

Figure 4.8: Mean composite rainfall during cyclone life over the region (18°N-22°N 68°E-74°E) (a) Gaussian Kernel Density Function (KDF) of mean composite rainfall; (b) box diagram of mean composite rainfall of four variants (Type 1, 2a, 2b and 2c).

this category is most frequent in June, and its occurrence monotonically decreases from June to September. The maximum track and genesis density of this class peaks in the northeast Arabian Sea suggests that these systems do not move much during their life cycle (Figure 4.10b). Indeed, this is a major characteristic of the Arabian Sea synoptic systems during the monsoon (Carr, 1977; Kushwaha et al., 2021).

As these systems remain close to the west coast of Maharashtra during their life cycle, their effect is expected to be more significant over the Indian landmass. Indeed, their slow motion and closeness to the west coast make them the rainiest (in terms of mean and extreme) type of systems experienced by western India (Figure 4.8). In terms of rain rates, Type 2a systems reach intensities that exceed 60 mm/day, as is seen in the tail of the distribution in Figure 4.8. The Type 2b class moves northward parallel to the west coast of India with a slight eastward component towards the Indian landmass (Figure 4.10c). This category's maximum track and genesis density are significantly less than Type 1 and Type 2a and more spread out in a zonal direction. Notably, some systems of this class turn towards Indian landmass, thus having the potential of affecting western India, but overall

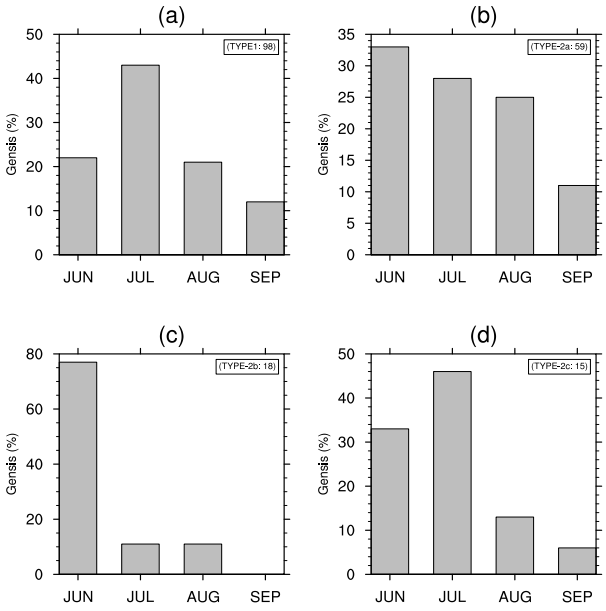

Figure 4.9: Monthly frequency of occurrence of all four variants of Arabian Sea systems. (a) Type 1 ; (b) Type 2a; (c) Type 2b; (d) Type 2c.

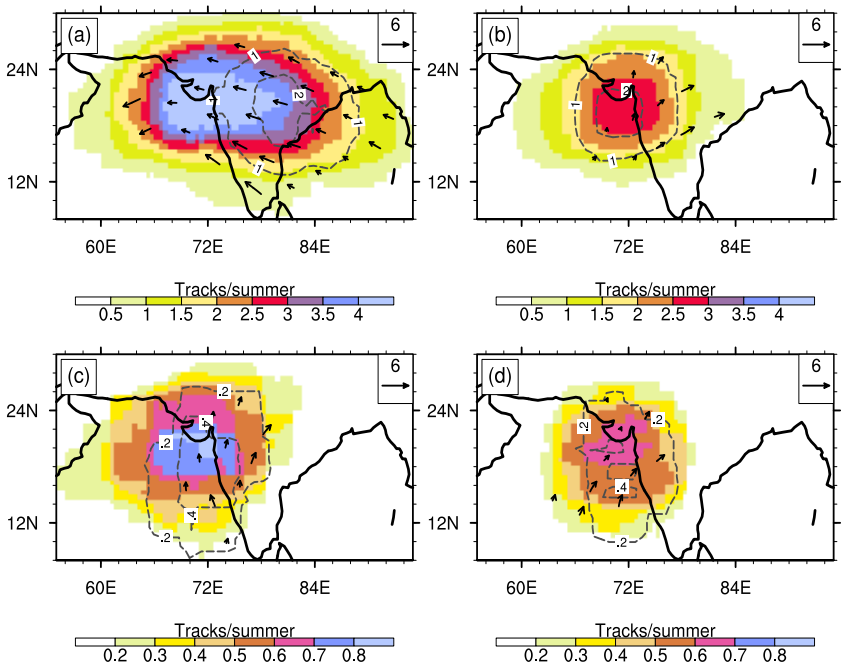

Figure 4.10: Track density (color), mean cyclone motion vector (arrows) and cyclone genesis density (dashed contours) (a) Type 1, (b) Type 2a, (c) Type 2b, (d) Type 2c. Motion vectors are shown if any propagation vector component is significantly different from zero at 0.1 significance.

their contribution to rainfall is lower than either Type 1 or Type 2a categories (Figure 4.8). Further, in terms of the nature of heavy rainfall events, Type 2b is comparable to the Type 2a (Figure 4.8a) and forms almost exclusively in June (Figure 4.9c), bearing a resemblance to the monsoon onset vortex (Krishnamurti et al., 1981; Pearce and Mohanthy, 1984; Yihui and Chan, 2005). Finally, Type 2c systems are the least frequent category forming mainly in July (Figure 4.9d). These systems progress northward along the west coast of India with a motion toward the Indian landmass (Figure 4.9d). As this class is weak and less frequent, it is overall less rain-bearing (Figure 4.8). Interestingly, all the local formation types (Type2a, 2b & 2c) show a bi-modal composite rainfall distribution, where the peaks are separated by almost $20 - 30$ mm/day. This suggests that though Types 2b & 2c are less frequent and overall less rainy, systems in this category that correspond to the second peak may be hazardous. Further, it should be noted that individual rainfall events on a particular station would be might higher than what is presented in Figure 4.8 because it is a composite of precipitation over the life of the cyclone averaged over western India.

4.4.3 Modulation by Intra-Seasonal Oscillations

As seen in Figure 4.1 and 4.2, rainfall over western India and the northeast Arabian Sea does not happen in isolation; rather, it exists with moist convective activity over large regions similar to those seen in summer ISOs. Since ISOs can be effectively predicted on sub-seasonal time scales, this provides a warning for systems with a propensity for genesis in this large-scale environment. Hence, it is useful to explore if different categories of the Arabian Sea and western Indian systems identified so far have specific dependencies on indices that describe the activity of summer ISOs. Figure 4.11 shows the frequency of occurrence of each of the categories (Type 1, 2a, 2b & 2c) with the phase and strength of BSISO during June-September, 1998-to 2019. In particular, the left column of Figure 4.11 represents the phase and magnitude of BSISO during the genesis of each system of the respective category, and the right column shows the corresponding frequency of formation during the respective phases of BSISO. Type 1 system formation occurs during all BSISO phases; however, the maximum frequency is during phases 4 and 5. This is not surprising because, during these phases, convection and cyclonic vorticity are enhanced over the north Bay of Bengal, which supports the formation of cyclonic systems (Karmakar and Misra, 2020; Diaz and Boos, 2021). Since Type 1 systems over the Arabian Sea are a result of downstream development

of Bay of Bengal lows, their frequency is expected to be directly modulated by cyclonic activity over East India and Bay of Bengal, thereby dependent on ISO phases which control low-pressure center formation over the Bay of Bengal (Deoras et al., 2021; Karmakar et al., 2021). Type 2a systems genesis also occurs during all phases of the ISO but shows peak activity during phase 5, followed by phase 4. Thus, Type 2a appears to share the same large-scale environment in terms of ISO phases as Type 1 for development. Moreover, in addition to the similarity with the phases 4 & 5 of the BSISO, Type 2a composite during Days -2 to -1 (Figure 4.7) exhibits remarkable similarity with the phases 2 & 3 of the Quasi-Biweekly Oscillation (QBWO; for example, Figure 10 in Qian et al., 2019).

Type 2b system formation peaks during phases 3 & 4 of the BSISO, during which the maximum convection and cyclonic vorticity enhancement occur over the south-central Arabian Sea and west equatorial India Ocean. This is in accord with the recent work by Deoras et al. (2021); Hunt et al. (2021) which suggests that LPS formation in the Arabian Sea and rainfall are usually enhanced during phases $2-4$ of the BSISO. Finally, Type 2c formation also peaks at phase 3 of BSISO, when the convection over the equatorial Indian ocean is enhanced and migrates northward (Kikuchi et al., 2012). An examination of the evolution of height anomaly and wind fields of Type 2c (Figure 4.7) shows west-northwest motion tendency from the equator to the Arabian Sea during Day -4 to Day -2 and becomes predominately northwards from Day -2 to 0. Gradually, these height anomalies reach the northeast Arabian Sea and intensify into a cyclonic vortex. On Day -4, the height anomaly remains negative south of maximum easterly zonal winds (around 10-15°N) and positive near central and north India (15-25°N). This motion and height anomaly patterns closely resemble those of the QBWO (Chaterjee and Goswami, 2004). In fact, the QBWO is the dominant mode of variability at $15-25$ days time scales during the boreal summer and is known to modulate the active and break phase of monsoon (Kikuchi and Wang, 2009; Qian et al., 2019). In fact, the influence of the QBWO on the formation of synoptic systems has been noted in various ocean basins (Ling et al., 2016; Ghatak and Sukhatme, 2022). The positive height anomaly over central India and negative near the equator (Figure 4.7) is consistent with phase 8 of QBWO (Chaterjee and Goswami, 2004) and phases $1-3$ of BSISO (Kikuchi et al., 2012), which correspond to a monsoon break over the north and central India, and an active spell over the southern part of the country. Thus, Type 2c represents a class of systems whose formation is

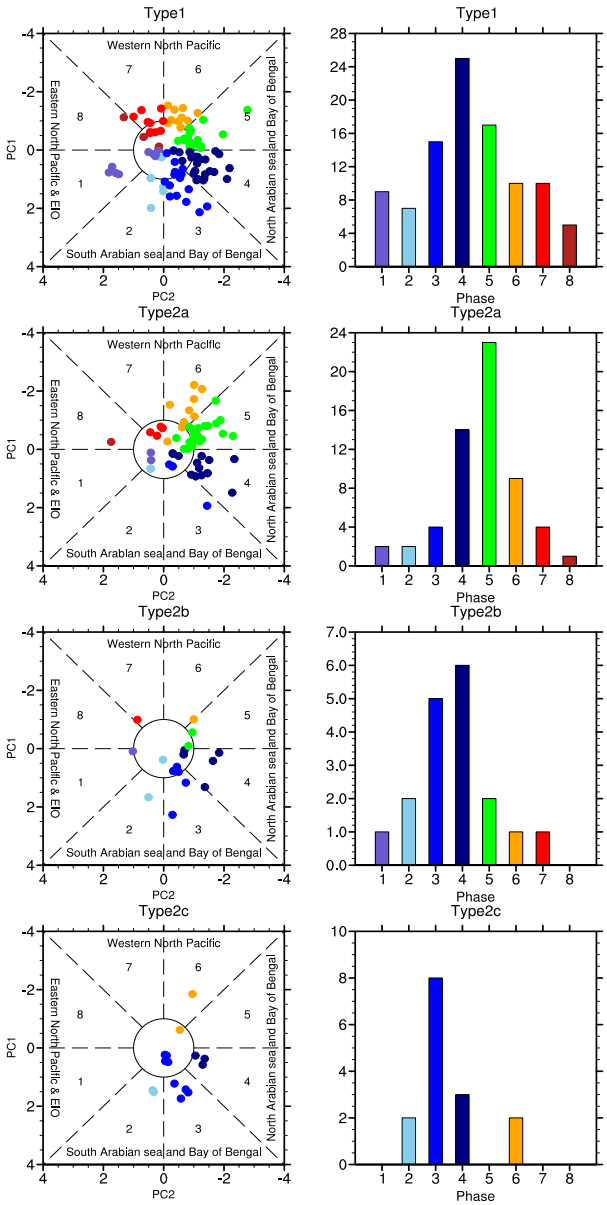

Figure 4.11: Left Column: Phase diagram of BSISO during the genesis of each of the four variants of Arabian Sea systems; each dot represents the phase of BSISO during the genesis of a particular system of each category. Right column: Frequency distribution of phases of BSISO during the genesis of each category of synoptic systems.

triggered during the positive phase of BSISO and QBWO near the equator.

Overall, these results indicate that instances of *in-situ* formation of Arabian Sea & western Indian systems in the absence of Bay of Bengal cyclonic activity occur when the ISOs (BSISO and/or QBWO) are in a favorable phase over this region. Moreover, the genesis of Type 1 and Type 2a, which is tied to cyclonic activity over the Bay of Bengal, is more efficient when the ISO is in an active phase over the north Bay of Bengal. Hence, the active phase of BSISO, and to some extent, the QBWO, and their location are essential for the Arabian Sea and western India system formation and evolution. This sensitivity of system formation on ISO phases is expected to some extent because positive phases of ISOs enhance large-scale moisture, vorticity, and barotropic instability, which are conditions that are required for the formation of synoptic monsoon systems (Karmakar et al., 2021).

4.5 Conclusions

Rain bearing synoptic systems over the northeast Arabian Sea and western India are analyzed by k-means clustering and cyclone tracking methodologies. Over twenty years of summer monsoon data from modern reanalysis is used to obtain a robust view of the systems responsible for a significant portion of the annual precipitation and extreme rainfall events in this part of the world. At the outset, a lag correlation analysis of OLR immediately shows a tendency for moist convection to simultaneously occur over the Arabian Sea and western Indian region, and the Bay of Bengal. Further, the nature of the correlation patterns also suggests that large-scale environmental conditions play a role in favoring the formation of rainy systems in this region.

Dominant patterns during rainy days over the Arabian Sea and western India are extracted by a k-means analysis, which is performed using an optimum of four clusters, as decided by the silhouette coefficient and elbow methods. Each of the four clusters is obtained using daily 600 hPa geopotential height anomaly as input data vectors of western India's rainy days. Physically, all four clusters represent different weather regimes consisting of middle tropospheric cyclonic circulation anomalies over the northeast Arabian Sea and west India. The height anomalies of the first Regime have a northwest orientation and range from the Arabian Sea to the Bay of Bengal. Lagged composites indicate that synoptic systems over the Arabian Sea in this Regime develop from the westward

movement of monsoon lows over the Bay of Bengal. Second Regime shows concomitant cyclonic activity over the Arabian Sea and Bay of Bengal and suggests dynamical interaction between the two circulation patterns. In the third Regime, systems form locally in the South Central Arabian Sea and move northwards with a weak transient cyclonic signature in the Bay of Bengal. Further, lagged composites indicate that the Bay of Bengal system intensification precedes or follows the Arabian Sea system genesis in the second and third regimes, respectively. In fact, in the third Regime, when the Arabian Sea system matures, the circulation in the Bay is anticyclonic. The fourth Regime consists of a large-scale cyclonic envelope that gradually moves northwest from the South Bay of Bengal and leads to the formation of a synoptic system in the Arabian Sea.

With this broad characterization in four clusters, a detailed cyclone tracking methodology is used to track the systems and follow their development. In particular, 191 rainy synoptic systems over the northeast Arabian Sea and western India in 22 years are tracked and classified. The resulting classification brings out four categories: the first (Type 1) accounts for 51% of all systems, and these form from the westward (downstream) development of cyclonic lows over the Bay of Bengal. Second, Type 2a accounts for 31% cases and consists of the formation of MTCs over the Arabian Sea with a coexisting Bay of Bengal system that precedes the Arabian Sea system formation. Third, Type 2b (9-10%) formation is again characterized by the coexisting cyclonic circulations over the two basins. However, in this category, the Arabian Sea system precedes a relatively weak and short-lived cyclonic circulation over the Bay of Bengal. Finally, Type 2c accounts for the remaining 7-8% of systems that form locally in the Arabian Sea from a large-scale cyclonic envelope that propagates northwestward from the southern Bay of Bengal. It is noteworthy that no *a priori* constraint was imposed on the tracking procedure, and it too yields four categories that qualitatively match the patterns captured by the k-means approach.

Tracking also allows for a study of motion vectors associated with synoptic systems and enables quantification of systems rainfall and the monthly frequency of genesis of different categories of systems. We observe that *in-situ* genesis (specifically, Types 2a & 2b) is favored in the early part of the monsoon season (i.e., June). In contrast, downstream development, Type 1 and Type 2c (i.e., *in-situ* Arabian Sea systems triggered from a large-scale cyclonic anomaly of south Bay of Bengal) are most frequently observed in July. Among all categories, Type 2a genesis occurs throughout the monsoon (June-September) and is rainiest, with the highest rain rates in western

India that exceed 60 mm/day. Further, the motion vectors of Type 2a suggest a marked quasi-stationary nature — a hallmark of Arabian Sea MTCs — when over the northeast Arabian Sea and western India, this leads to a large quantum of rain and potential flooding in the continental portion of this region. The westward-moving category (Type 1) moves off from western India to the Arabian Sea, but given its track, it accounts for the second rainiest system in this region. Interestingly, Type 2b, where the Arabian Sea system precedes the Bay of Bengal system, motion vectors indicate the possibility of curving into the Indian landmass; thus, though much less frequent than Types 1 & 2a, they too have an influence on rainfall in the western coastal regions of India. Finally, Type 2c systems usually progress northward into the eastern Arabian Sea and at times make landfall over the west coast; however, they contribute the least out of the four categories to rainfall in western India.

With regard to the large-scale environment, it is seen that each of the four categories is preferentially formed in certain phases of the BSISO, which is the dominant mode of intraseasonal variability in the Indian region during the summer monsoon. In particular, Types 1 & 2a, both of which require the prior presence of a cyclonic system over the Bay of Bengal, are most active in phases 4 and 5 of the BSISO. Indeed, these are precisely the phases of the BSISO when moist convection is favored over the Bay of Bengal. Phases 3 and 4 of BSISO, when convection is active in the western equatorial Indian Ocean, and the central Arabian Sea, are favorable for the genesis of the categories where the Arabian Sea system precedes cyclonic circulation over the Bay (Type 2b) and when the Arabian Sea system develops from the northwest movement of large-scale cyclonic anomalies from the South Bay of Bengal (Type 2c). Apart from an association with the BSISO, Type 2a & 2c systems also show a preference for particular phases of the QBWO; in particular, the large-scale envelope from which Type 2c systems are born closely resembles the boreal summer QBWO. Thus, both intraseasonal modes, the BSISO and the QBWO, appear to aid the formation of synoptic systems over the Arabian Sea and western India.

In all, from the lag-correlation patterns of OLR, the regimes from k-means clustering and tracking systems over twenty monsoon seasons, it is clear that most rainy synoptic systems in the Arabian Sea and western India form with, or from, cyclonic anomalies in the North Bay of Bengal. Indeed, more than 90% of rain-bearing systems in this region fall in Type 1 and Types 2a & 2b categories. Even Type 2c, where the north Bay of Bengal shows unfavorable conditions for the moist cyclonic activity, forms from a large-scale cyclonic anomaly that propagates

into the Arabian Sea from the southern Bay of Bengal. The qualitative consistency in the clusters found by k-means and the groups delineated by cyclone tracking is an encouraging indicator of the robustness of the four basic regimes that encompass much of the rainy spells experienced in western India. We are hopeful that these regimes, their precursors, and the identification of large-scale intraseasonal phases in which they occur will help in the potential predictability and preparedness for extreme events associated with these systems.

Chapter 5

Genesis of MTCs over the Arabian Sea

The classification of Arabian Sea MTCs in the last chapter revealed two dominant formation mechanisms: downstream intensification of Bay of Bengal low pressure systems and *in-situ* genesis. Importantly, 59 out of 92 *in-situ* cases of MTC formation (Type 2a) show precedence and then coexistence of a LPS in the Bay of Bengal. Further 18 Type 2b cases also show a coexisting Bay of Bengal system; however, in this class the Arabian Sea MTC preceded the Bay of Bengal system. Thus, the development of 83% of *in situ* born MTCs occurred with a LPS in the Bay of Bengal. Indeed, as noted in the Introduction, the coexistence of a Bay of Bengal system with an Arabian Sea MTC has also reported in previous studies (Miller and Keshavamurty, 1968; Choudhury et al., 2018). The natural question arises from these observations is whether the coexistence of the Bay of Bengal LPS during MTC formation (specifically, for the Type 2a category) is a coincidence, or does the Bay of Bengal system play a role in the formation of MTCs by altering the dynamics and thermodynamics of the region over the Arabian Sea.

To investigate this issue we focus on Type 2a MTCs, i.e., those that form with a preceding and then coexisting LPS over the Bay of Bengal. In Section 1, we explore the lag composites of dynamical and thermodynamic fields of Type 2a MTC formation, a moisture budget analysis of these systems is then presented in Section 2. In Section 3, we discuss the results of numerical experiments — this utilizes the "bogus vortexing" technique in which an ideal balanced LPS is added over Bay of Bengal and its influence on the dynamic and thermodynamic conditions

over the Arabian Sea is studied. A second suite of numerical experiments consist of suppressing a LPS over Bay in an observed Type 2a formation case; the aim is to validate whether the MTC forms in the absence of the LPS over the Bay of Bengal. We then discuss how Bay of Bengal LPS alters the meteorological conditions over the Arabian Sea and what are the dominant terms in the vorticity budget which help in the intensification of the a MTC. Finally, in Section 4, we summarize the the results obtained in this chapter.

5.1 Type 2a MTC formation

5.1.1 Evolution of Dynamic Fields

Plan views of Type 2a lag-composites of total precipitable water anomaly, relative vorticity, potential vorticity (PV), and geopotential height anomaly with composite wind vectors are shown in Figure 5.1 rows 1, 2, 3 and 4, respectively. All variables are vertically averaged between $800-400$ hPa to ensure that composite anomalies have a coherent vertical structure, and are robust through the depth of the middle troposphere. Clearly, precipitable water anomalies (row 1; Figure 5.1) increase in size and magnitude over the northeast Arabian Sea from Day -6 to Day 0, i.e., till the day of heaviest precipitation. During this period, the wind anomaly (quivers in Figure 5.1) is easterly and slightly northeasterly over the north Arabian Sea where the maximum accumulation of water vapor is observed. The easterly wind is not localized to this region but appears to be the part of a large-scale circulation and height anomaly; indeed, winds originate from the Bay of Bengal and reach up to the Arabian Sea, enveloping the southern peninsula of India. Considering the spatial scale of height anomaly, it is possible that this flow may be related to the branch of cyclonic flow associated with phases $2-3$ of BSISO, when it is active over the southern part of the Bay of Bengal and South India (Kikuchi et al., 2012).

Sequentially, on Day -6, a weak height anomaly envelops the southern tip of India and there is a positive vorticity anomaly over southwest Bay of Bengal (around 15°N, 85°E; row 2; Figure 5.1). The height anomaly over the Arabian Sea has a large scale east-west oriented structure which is restricted to the south of 15°N (row 4; Figure 5.1). The Bay of Bengal height anomaly centered around 15°N to 85°E deepens from Day -6 to Day -4 with the intensification of associated relative vorticity and potential vorticity anomalies (rows 2 & 3 of

Figure 5.1). Following which, an east-west shear zone forms over the Arabian Sea that connects with the Bay of Bengal vortex (rows 2 & 3; Days $-6, -2$; Figure 5.1). Within this evolving shear zone over the Arabian Sea, as seen on Day -4, two significant positive PV and relative vorticity anomaly centers form — one near the west coast of India near $15°$N and $72°$E and another around $65°$E and $18°$N. With further intensification of the system over the Bay of Bengal (Days -4 to -2), the westward situated Arabian Sea vorticity anomaly starts to move eastward and merges with the anomaly over the western coast on India by Day -2. As the height anomaly over the Bay of Bengal deepens and moves northwards from Day -6 to Day -2, concurrently the trough over the Arabian Sea also intensifies, and becomes more localized off the coast of Maharashtra. This is reflected in the rapid intensification of vorticity and PV anomalies over the northeast Arabian Sea from Day -2 to Day 0 (row 3; Figure 5.1).

Overall, the evolution of height, velocity fields, and winds suggest that anomalies over the Arabian Sea and western India are indeed linked with the Bay of Bengal system — but, the anomalies first deepen over the Bay of Bengal and this is followed by intensification of Arabian Sea vorticity anomalies. The intensification of the Bay of Bengal system before the Arabian Sea seems reasonable as during the primary monsoon months, the Bay of Bengal SST and precipitable water are relatively high as compared to the Arabian Sea (Masunaga, 2014; Saikranthi et al., 2019a,b); and these conditions are favorable for development and intensification of cyclonic systems. On the contrary, in a mean sense, deep convection over the Arabian Sea is usually hampered by colder SSTs due to the upwelling of subsurface cold water, and further by a dry middle troposphere and a low-level inversion (Narayanan et al., 2004; Muraleedharan et al., 2013; Das et al., 2021).

The Type 2a circulation (Figure 5.1) also bears a close resemblance with the flow during rainy days over western India (Figure 4.2f); specifically, both are characterized by the westward extending height depression and associated circulation which originates over Bay and ends over the Arabian Sea. Further, the structure of geopotential height at 600 hPa on rainy days (Figure 4.2) and those of composite of various classes of MTCs show a non-circular Bay of Bengal system with a westwards extending trough. This trough shows remarkable similarity with steady-state Rossby response to the off equatorial heating (Goswami, 1987; Gill, 1980). Thus, the apparent link between Arabian Sea MTCs formation and the Bay of Bengal system can be qualitatively explained in terms

of heat-induced circulations or Gill response to off equatorial diabatic heating (Gill, 1980). It is well known that convective diabatic heating shapes various tropical circulations such as monsoons (Hoskins and Rodwell, 1995; Xie et al., 2006) and various remote teleconnections through Rossby waves response to heating (Ma and Franzke, 2021; Xie et al., 2006; Rodwell and Hoskins, 1996). In fact, previous studies observed the remote link between Bay of Bengal heating and western India circulation, wherein when the heating was prescribed over the Bay of Bengal, the cyclonic vorticity and precipitation enhanced over western India and northeast Arabian sea and which was argued to be Rossby wave response to heating (Xie et al., 2006; Choudhury et al., 2018). Similarly, remote induction of synoptic scale systems downstream of a mature tropical cyclone was observed in various ocean basins (Krouse and Sobel, 2010; Schenkel, 2016, 2017). It was augured that the induction of new cyclones could be possible by parent cyclone by the emission of vortex Rossby waves to the east-southeast for northwest moving cyclone (Krouse et al., 2008). However, such formation is only possible in special conditions such as easterly shear and westwards moving cyclones, thus strongly depending on background environmental flow (Krouse et al., 2008). Since MTCs forms to the westwards side of the Bay of Bengal lows as opposed to predicted by the vortex Rossby waves theory in easterly shear for westwards moving system (Krouse et al., 2008), it is unlikely that vortex Rossby waves inducting the MTCs to the westwards side of monsoon lows. Nevertheless, it will be worth exploring whether the generalization of these theories subjected to realistic monsoon flow and diabatic heating can explain the link between Arabian sea MTCs and Bay of Bengal monsoon lows. Thus, to a first approximation, sufficient localized latent heating in the atmosphere above the Bay of Bengal will induce a Gill response consisting of a zonal trough that extends up to the Arabian Sea (Goswami, 1987; Gill, 1980; Choudhury et al., 2018; Xie et al., 2006). Given its rotational character, this Rossby gyre is associated with horizontal shear and cyclonic vorticity. Apart from its fundamental nature, such a response of middle troposphere forced by realistic diabatic heating in this region has been noted in recent general circulation model experiments (Choudhury et al., 2018; Xie et al., 2006). The induced horizontal shear as a result of Gill type response can be critical for the growth and motion of the Arabian Sea system by barotropic instability (Goswami et al., 1980; Goswami, 1987); in fact, moist barotropic instability has been identified as a possible source of energy for the formation of monsoon lows (Diaz and Boos, 2019a,b). In essence, the rapid development of the system over the Bay induces a Gill response that results in enhanced vorticity and shear along with strengthening of easterlies (westerlies) to

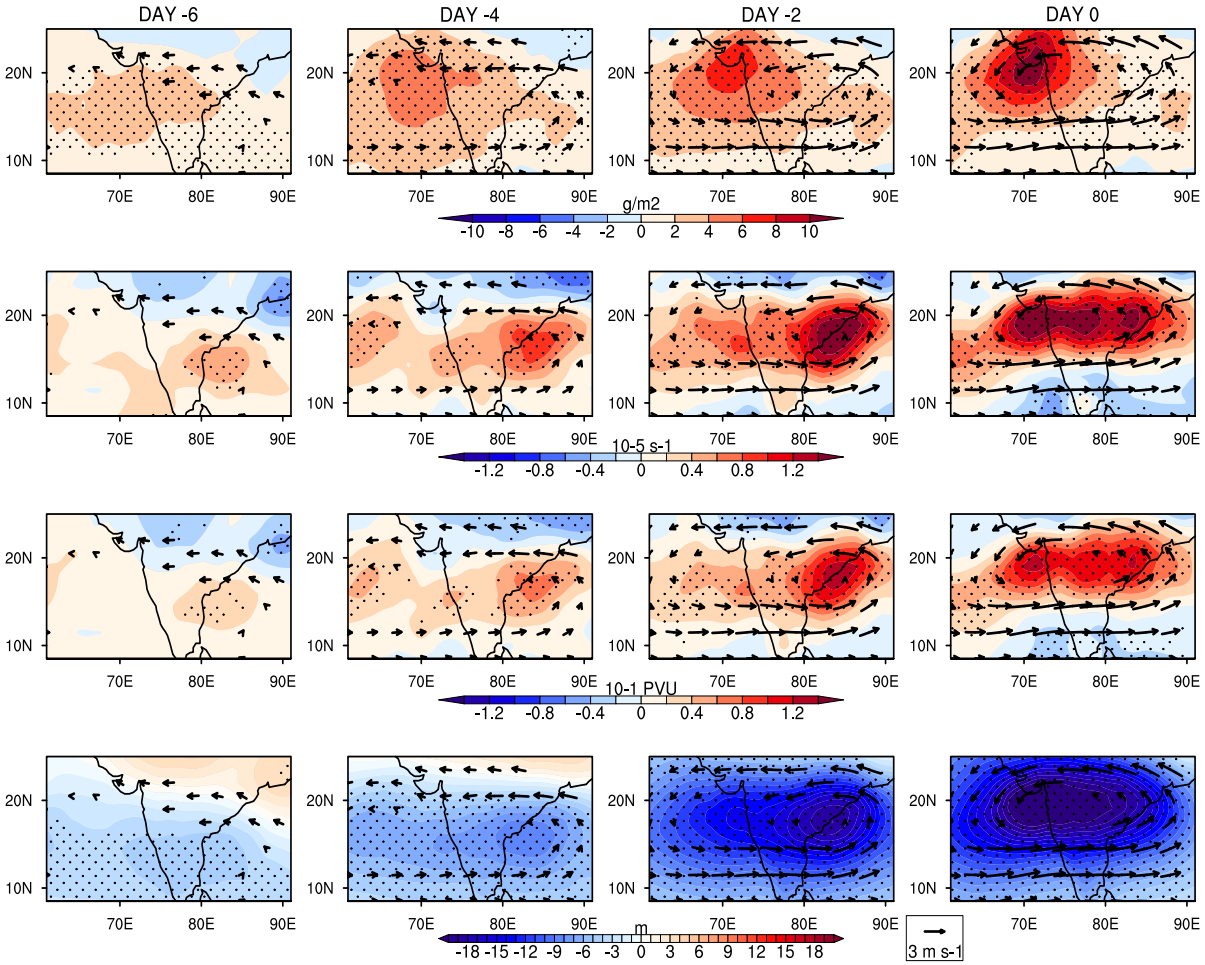

Figure 5.1: Lag composite of anomaly of Type 2a systems (mean 800-400 hPa) from Day −6 to Day 0, (a) precipitable water; (b) relative vorticity; (c) potential vorticity; (d) geopotential height; dotted region show where fields are significantly different from zero at 0.1 significance. Wind vectors are only shown if any of the wind component is significantly different from zero at 0.1 significance.

the north (south) of the northeast Arabian Sea and western India. These features, in turn, appear to promote the growth of a cyclonic system in western India and the Arabian Sea. Further, when the Arabian Sea and Bay of Bengal systems are well-developed, a large-scale cyclonic circulation encompasses both the systems and results in an east-west oriented monsoon trough. Since both systems remain inside this gigantic envelope of circulation, it appears that this protects them from dry low entropy air of outer boundaries — especially from dry air to the west and northwest of India; this is important because conditions over the Arabian Sea alone can not sustain a system given unfavorable local conditions discussed earlier.

Up to now we focused on horizontal evolution of system; to understand the vertical structure during the Type

2a system formation, vertical-horizontal cross sections of relative vorticity, potential vorticity, zonal and meridional winds are shown in Figure 5.2. Before Day -4 (not shown) the relative and potential vorticity is relatively disorganized and weak in much of troposphere over western India. However, as the low-level PV and relative vorticity spin-up over the Bay of Bengal, the corresponding mid-level entities increase in an organized and statistically significant manner over the Arabian Sea (Figure 5.2; row 1 and row 2). At later stages (Day -1 to 0), the vorticity and PV intensify at the lower levels too, reflecting the increasing presence of deep convection in the system (Murthy and Boos, 2019; Russell and Aiyyer, 2020; Kushwaha et al., 2021). The zonal wind (third row; Figure 5.2) shows a significant increase of an easterly wind anomaly in the middle troposphere from Day -3 to Day -1 over western India which extends up to 300 hPa with a maximum around 700 hPa. Thus, it appears as though the anomalous easterlies in the middle troposphere are enhanced by the system in the Bay of Bengal. Further, we suspect that this is accompanied by an increase horizontal shear over western India and the Arabian Sea, and a mitigation of unfavorable thermodynamic conditions such as strength of inversion and prevent dry air mixing from west and northwest India. This in turn allows the development of deep convection and further moistening of the free troposphere over the Arabian Sea.

In fact, the effect of the anomalous easterlies is confirmed in Figure 5.3. From Day -6 to Day 0, middle tropospheric easterlies increase (Figure 5.3a), concomitantly, relative humidity increases over western India (Figure 5.3b). The expected reduction in the low-level inversion is also observed, and this is measured by the static stability (Figure 5.3c) that serves as a proxy for the inversion lid. This reduction in inversion strength and increase in moisture is expected to favor deep convection, which is followed by deepening the height anomaly (Figure 5.3d) and further spinning-up cyclonic anomalies over the Arabian Sea and western India.

5.1.2 Evolution of thermodynamic fields

The thermodynamic environment (Skew-T Log-P diagram) over western India during the formation of Type 2a is presented Figure 5.4. Interestingly, there was hardly any change in temperature and humidity profiles in the boundary layer during the system's evolution. However, significant changes can be observed in the middle to upper troposphere; specifically, a dew point depression existed before the onset of heavy rain, which gradually

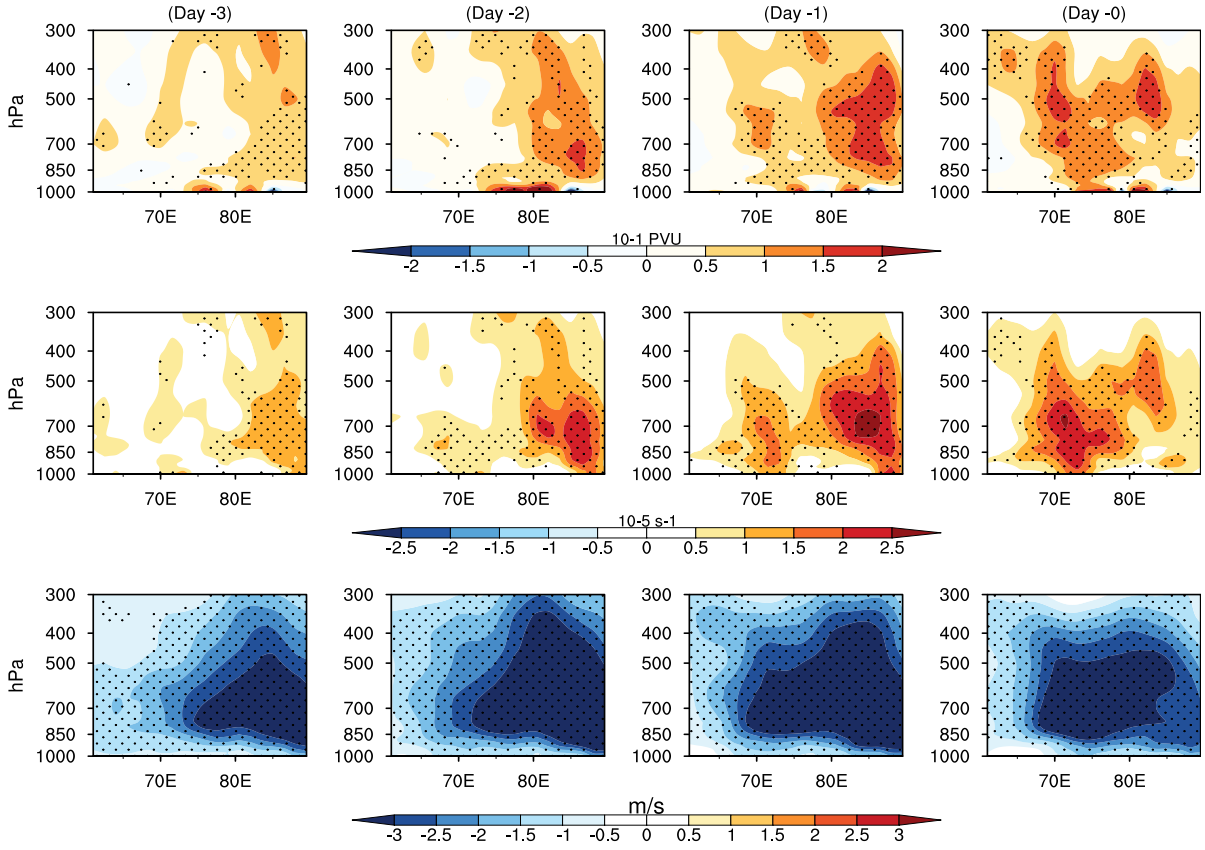

Figure 5.2: Type 2a composites from Day -3 to Day 0. Row 1: Potential vorticity anomaly, Row 2: Relative vorticity anomaly, Row 3: Zonal wind anomaly, Shading denotes regions which are significant at 0.1 significance level under two tailed student-t test. The cross section of vorticity and PV is at 18.5°N and of wind component is at 22°N.

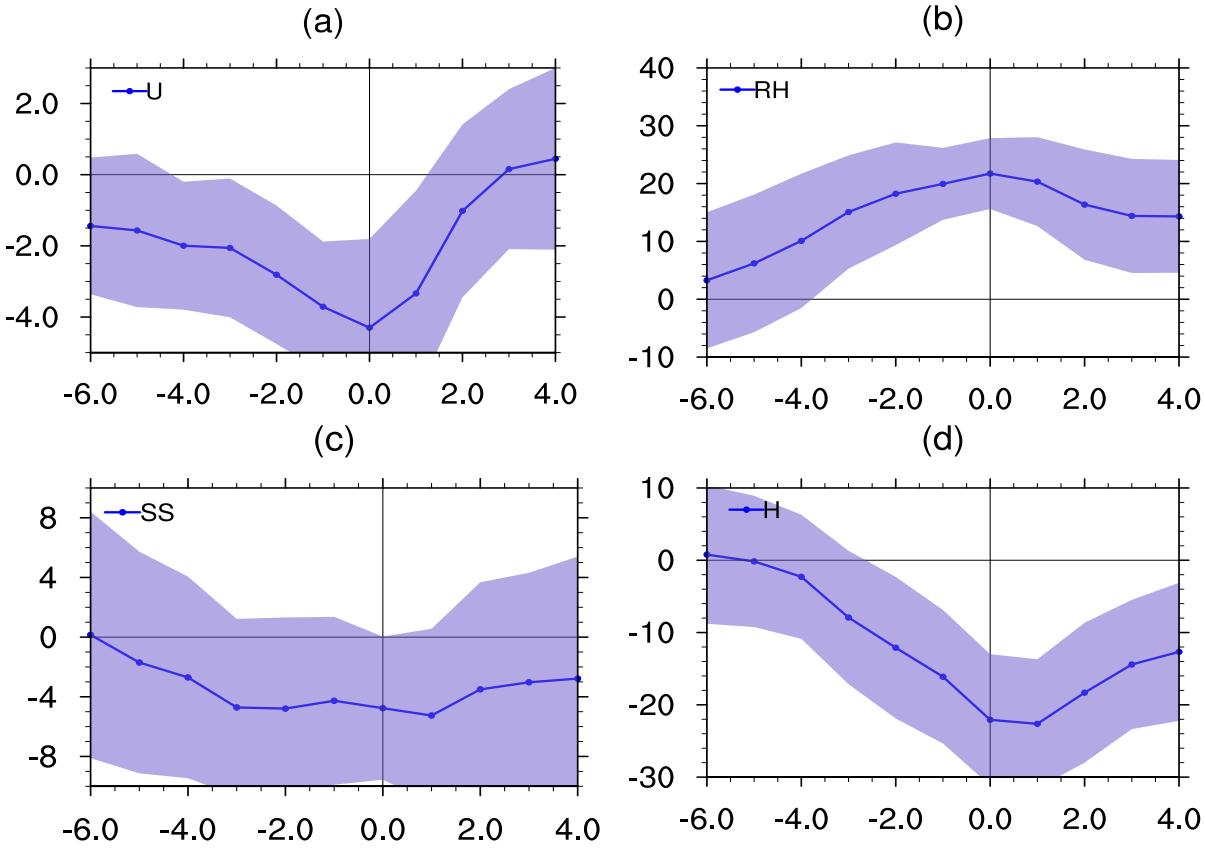

Figure 5.3: Type 2a lag composite time series at 22°N and 72°E. (a) Zonal wind anomaly mean in 600-500 hPa (ms^{-1}); (b) Relative humidity anomaly mean in 600-500 hPa; (c) static stability parameter mean in 700-800 hPa (10^{-5} K/Pa); (c) height anomaly (m) at 500 hPa; shadings are widths of one standard deviation.

reduces, and most of the free troposphere reaches near saturation at Day 0 (i.e., both red and blue curves are closer). Since the atmospheric sounding (red curve; Figure 5.4) remains largely invariant during the system's evolution, the primary factor in reducing the due point depression is likely the anomalous moistening of the middle troposphere, which started around a week ahead of the significant rain event. Hence, anomalous moisture accumulation appears to be the primary controller of precipitation.

The vertical structure of moisture and temperature fields is shown in Figure 5.5. The specific humidity (row 1; Figure 5.5) and relative humidity (row 2; Figure 5.5) suggest gradual deepening of the moist layer in the middle troposphere during the evolution of the system over the Arabian Sea. We also observe slight warming of the upper troposphere and cooling of the lower troposphere, leading to a stabilization effect of the middle to upper troposphere (row 3; Figure 5.5). The composite equivalent potential temperature (θ_e) also shows a significant increase in the middle troposphere (row 4; Figure 5.5). As the warming is small, this change in θ_e is likely again due to the moistening of the free troposphere. In all, moistening of the free troposphere in a favorable vorticity environment is the key for initiation of deep convection and further spin-up of the system by diabatic heating (Murthy and Boos, 2019).

5.2 Moisture budget during Type 2a formation

The analysis so far suggests the critical role of anomalous moistening of the free troposphere in the formation of Type 2a systems. To identify the dominant source of moisture, we perform a moisture budget during the Type 2a formation. The moisture budget is well balanced, and here we only present the dominant terms for brevity. An area average lag time series of various dominant terms of moisture budget and their plan views are shown in the first column and last three columns of Figure 5.6, respectively. Column integrated moisture flux convergence ($-\nabla.[q\mathbf{V}]$; Figure 5.6a) shows a gradual increase of moisture convergence from Day -6 to Day 0, which, however, drops sharply after heavy rain event (from Day 0 to Day 4). Since total moisture convergence (Figure 5.6a) and convergence of climatological moisture by anomalous winds (Figure 5.6e) follow almost the same trend and their magnitude is comparable, it is the climatological moisture (q_c) that couples with anomalous winds to play a dominant role here, i.e., the contribution of $-\nabla\cdot[q_c\mathbf{V}']$ is of most importance.

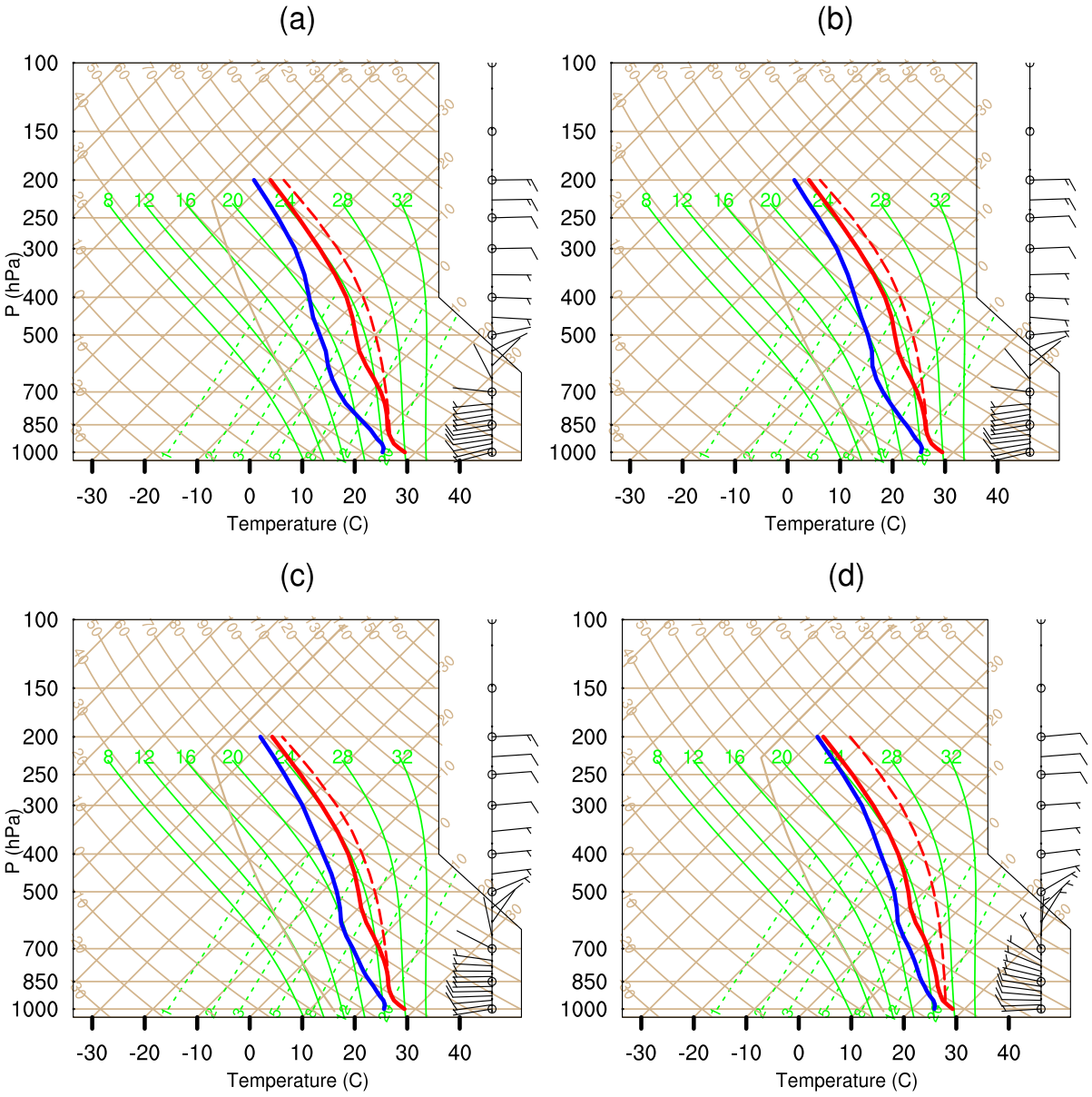

Figure 5.4: Type 2a composite Skew-T, log-P diagram mean over the region 18°N-22°N 68°E-72°E; (a) Day -6; (b) Day -4; (c) Day -2; (d) Day 0. Red lines represent atmospheric sounding, blue lines are dew point temperature, dashed green are constant mixing ratio lines and solid green are saturated adiabats, arrows are winds at different levels.

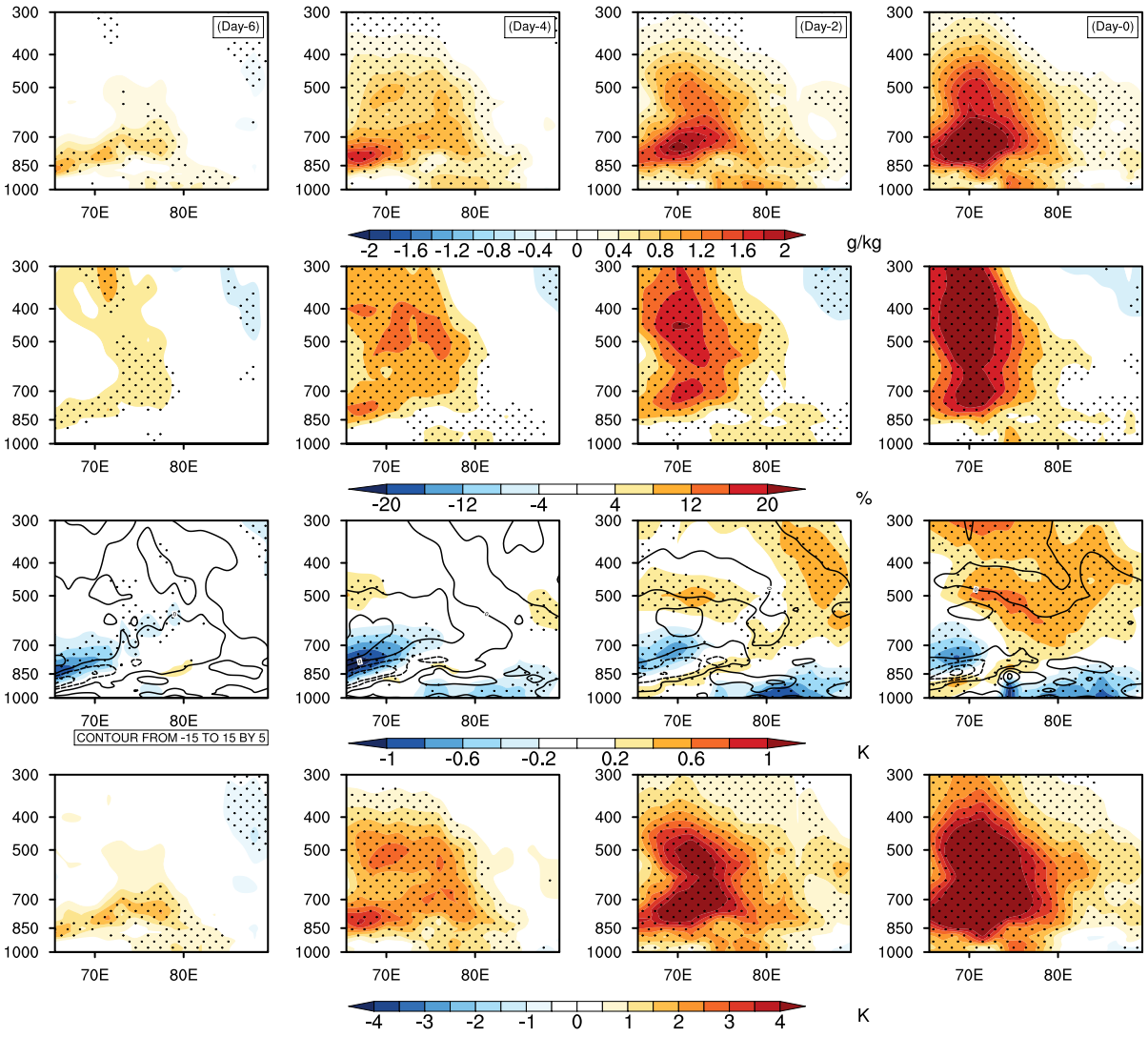

Figure 5.5: Type 2a lag composites from Day -6, Day -4, Day -2 and Day 0 ; Row 1: Specific humidity anomaly. Row 2: Relative Humidity anomaly. Row 3: Temperature and static anomaly (contours); Row 4: Equivalent potential temperature anomaly. Dotted shading denotes the regions which are significant at 0.1 significance under two-tailed student-t test. The cross section is at 22°N.

Further, to understand the relative contribution of advective and convergent fluxes, we partition the $-\nabla\cdot[q_c\mathbf{V}']$ into convergent, $-[q_c\nabla\cdot\mathbf{V}']$ and advective, $-[\mathbf{V}'\cdot\nabla q_c]$ components as per Equation 2.9. The comparison of lag time series of these two suggests that during Day -4 to Day 0, the convergence component dominates (Figure 5.6i), and remains significantly higher than the advective component (Figure 5.6m). However, from Day -6 to Day -4, the advective component remains positive while the convergence component shows a negative tendency. This suggests that at least 4 to 6 days prior to a heavy rain event, the moistening of the north Arabian Sea is dominated by the advective component, not by convergence. This advective component is primarily driven by anomalous easterly winds, which transport moisture down the mean moisture gradient from east to northwest India. This is reflected as the increase of easterly moisture transport from Day -6 to Day 0 over the north Arabian Sea as (arrows of moisture in Figure 5.6). Further, it should be noted that the location of maximum total precipitable water anomaly is around 20°N, 70°E from Day -6 to Day -4 (Figure 5.6b-c), which is closer to that of maximum advective fluxes (Figure 5.6 n-o) as opposed to the convergent component which shows a maximum around 15°N,72°E (Figure 5.6j-k). These results point that both advective and convergence fluxes of moisture appear to be important for the moistening the north east Arabian Sea. As expected from Type 2a formation, another maximum of moisture convergence is situated over the Bay of Bengal, which reflects the presence of a cyclonic system or LPS. As the region of Bay of Bengal moisture convergence and associated circulation moves northward from Day -4 to Day 0, concurrently, the region of moisture convergence over the Arabian Sea also moves northwards. Finally, at Day 0, the region of anomalous moisture convergence reaches south of Gujarat and coincides with the total precipitable water anomaly (Figure 5.6d). In essence, the different terms of moisture budget presented here point to the vital role of anomalous circulation over the Bay of Bengal in controlling the winds, thereby the moisture budgets over the Arabian Sea prior to the formation of Type 2a systems. In particular, the anomalous middle tropospheric easterlies modulated by the Bay of Bengal or East India cyclonic system in the favorable phase of ISO plays an essential role in moisture accumulation over the northeast Arabian Sea and western India.

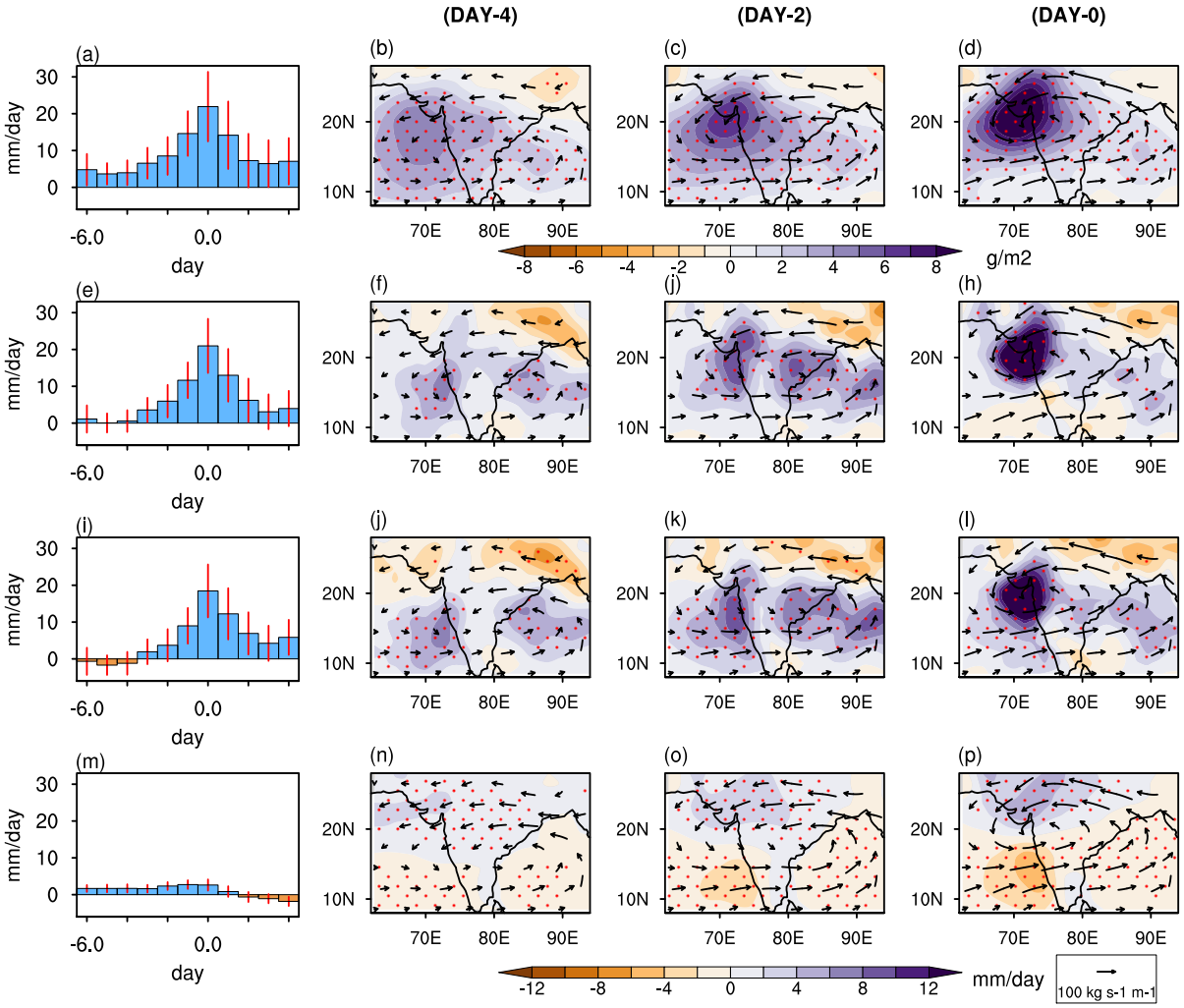

Figure 5.6: Composite moisture budget of Type 2a formation; mean budget term over the region (18°N-22°N 70°E-72°E), are shown in column-1 (a,e,i,m), red bars are the 95 % upper and lower confidence bound derived from student t-test, (a) $-[\nabla \cdot (q\mathbf{V})]$; (e)$-[\nabla \cdot (q_c\mathbf{V}')]$; (i) $-[q_c(\nabla \cdot \mathbf{V}')]$; (m) $-[\mathbf{V}' \cdot \nabla q_c]$; b to d are composite perceptible water anomaly; f to h are $-[\nabla \cdot (q_c\mathbf{V}')]$; j to l are $-[q_c(\nabla \cdot \mathbf{V}')]$; n to p are $-[\mathbf{V}' \cdot \nabla q_c]$ plan view respectively for Days -4, -2 and 0.

5.3 Bogus LPS over the Bay of Bengal

In previous chapters, we observed that during the Type 2a formation, the Bay of Bengal LPS precedes the genesis of MTC over the Arabian Sea. Further, composites from the previous sections show that the Arabian Sea moisture and vorticity fields are modulated by the Bay of Bengal system, and this creates favorable conditions for the genesis of Type 2a Arabian Sea MTCs. Importantly enhanced middle-level zonal shear, moistening of the middle troposphere, and deepening of the middle troposphere trough by a Gill type response through the diabatic heating Bay of Bengal LPS are the essential in creating a favourable environment for the genesis of a cyclonic middle tropospheric system over the Arabian Sea.

To verify our hypotheses regarding the dynamical link between the Bay of Bengal low and the Arabian Sea MTC, we now conduct a set of numerical experiments using the Weather Research and Forecasting Model (WRF). The details of the model, it's configuration, setup and the bogus vortex technique have been described in Chapter 2. In the first set of experiments, twenty-one bogus vortices or monsoon lows are added over different locations of the Bay of Bengal as shown in Figure 5.8. More attention has been given to the bogus LPS ensembles of the region A1 (Figure 5.8) as this is where the first signature of a LPS appears on Day -6 in the composite plan views of Type 2a formation. The rest of the 12 members are added to other locations, A2, A3, and A4 with a slight reduction in $r_m = 200km$ against $r_m = 350km$ in A1 to overcome the difficulties of model blow up due to the effects of the topography of Himalayan regions at higher latitudes during dynamical adjustment. The $v_{max} = 14ms^{-1}$ or 27 kt has been chosen, which is the strength of monsoon depression as defined by IMD. Further, as discussed in the method Chapter 2, the bogus vortices are added over climatology in the model domain shown in Figure 5.7 which includes important component of monsoon such as Somali Jet, the monsoon trough, heat low and the Bay of Bengal.

The 600 hPa geopotential height after 24 hours of simulation for nine members of group A1 is shown in Figure 5.9. All ensemble members show lows in the locations where bogus systems were added (as expected) with a trough extending over the Arabian Sea and western India. Apart from this trough, there is no significant signature of MTC formation over the Arabian Sea. However, the heights at 600 hPa after 63 hours of model integration (Figure 5.10) clearly show MTC formation around 70E and 18N in all the nine ensemble members. After formation, the MTC

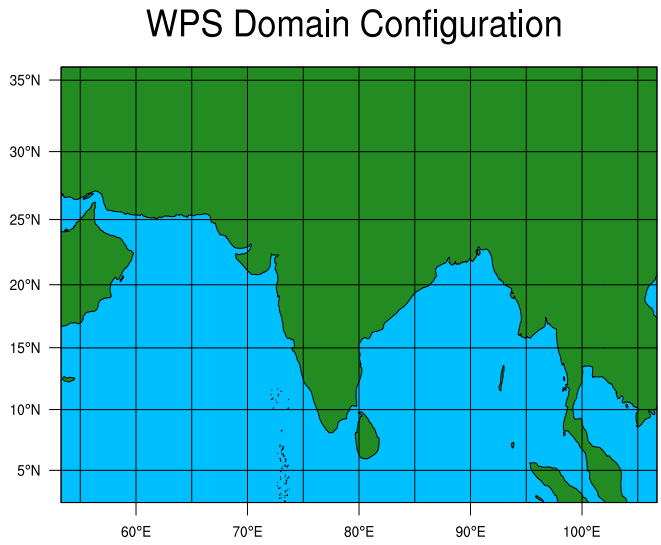

Figure 5.7: Model domain for the numerical simulation of MTCs

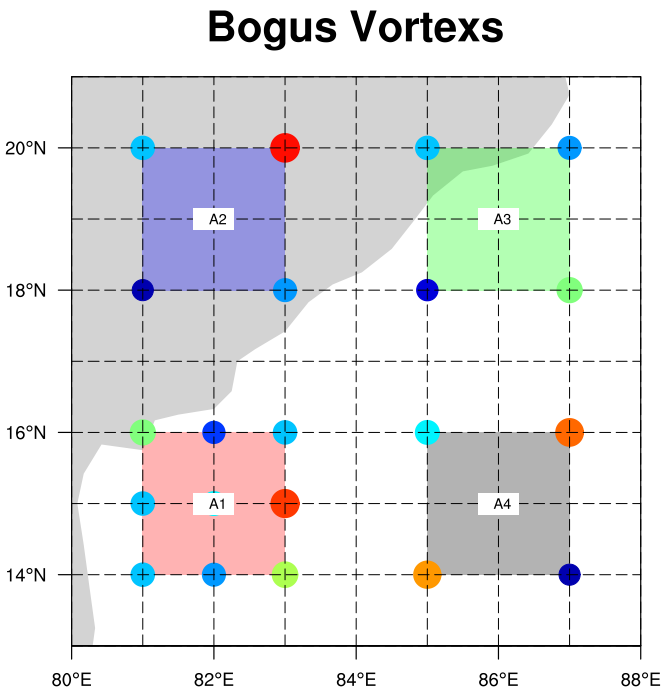

Figure 5.8: Locations of 21 bogus vortices grouped in four sets: A1, A2, A3, A4; group A1 contains nine members; group A2-A4 each contains 4 members.

vortex appears to be joined with Bay of Bengal LPS by a zonal trough, and both the systems encircle each other similar to the observations of Chapter 4, and also consistent with observations of the July 1963 MTC (Miller and Keshavamurty, 1968). Indeed, a close inspection of Figure 5.9 and 5.10 suggests that MTC formation occurred in the middle tropospheric trough induced by the "bogus" Bay of Bengal LPS.

Regarding the other ensemble members, i.e., those where the bogus vortex was added to other regions of the Bay of Bengal. The 600 hPa geopotential surface after 24 hours of model integration of group A2 to A4 is shown in Figure 5.11. During the first 24 hours of simulation, again, similar to group assemble members of A1, we see a westward extending trough up to the Arabian Sea and no closed vortex or MTC formation. However, after 96 hours of model integration, the signature of MTC becomes evident over the Arabian Sea and western India in group A2 (first row; Figure 5.11) and A4 (third row; Figure 5.11). For the members of set A3 (second row; Figure 5.11) we only observe a trough formation, and this does not develop into a closed form vortex or MTC for at least up to 96 hours of model integration. These results strongly suggest that our hypothesis of there being a dynamical link between the Bay of Bengal LPS and the genesis of Type 2a MTCs is correct. Indeed, when a bogus vortex is added to the climatology over the Bay, we clearly see that within 60-100 hours or 2.5 to 4 days, a MTC is triggered over western India or the Arabian Sea.

5.3.1 Vorticity Budget

The production or formation of a cyclonic system immediately leads to the question as to what are the dominant terms in the vorticity budget of the developing MTC. We focus on ensemble members from group A1 as this group was the most efficient in inducing MTC, and locations of added bogus vortices are same as those observed before Type 2a MTC formation. The composite time series of the various terms in vorticity budget mean over MTC region between 500-600 hPa is shown in Figure-5.13. The observed vorticity tendency (Figure-5.13a, green) and the sum of all terms on the right side of the vorticity budget Equation 2.10, (Figure-5.13a ,blue) follow closely, suggesting a well-balanced budget. Further, most of the variability and magnitude of the vorticity tendency is accounted for by the total vortex stretching term (Figure-5.13a, red), which acts as a significant source for mid-level vortex intensification. In contrast, the horizontal advection of vorticity (Figure-5.13a, black) opposes the

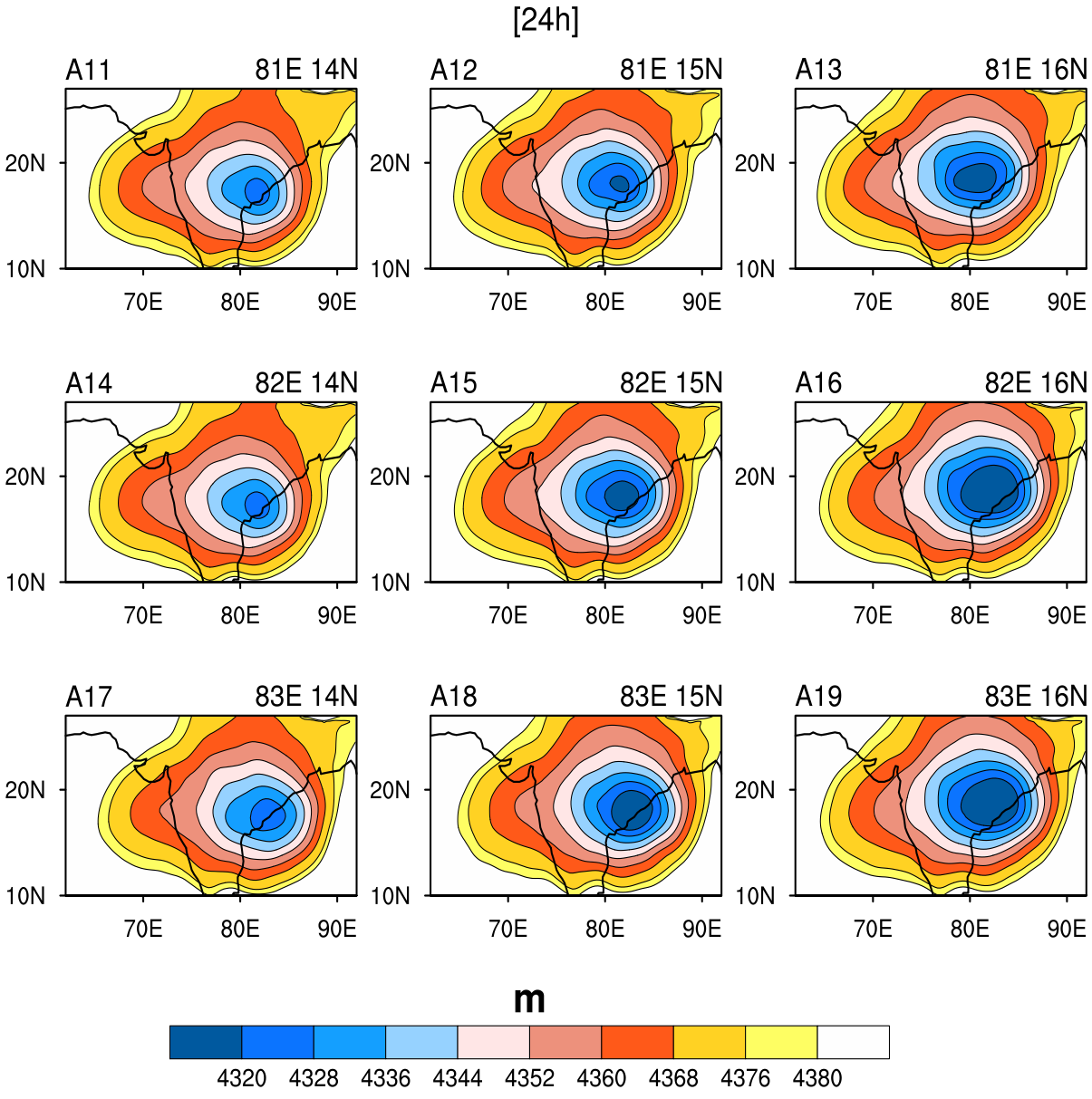

Figure 5.9: Geopotential height at 600 hPa of nine members (A11-A19) of group A1 after 24 hours of simulation.

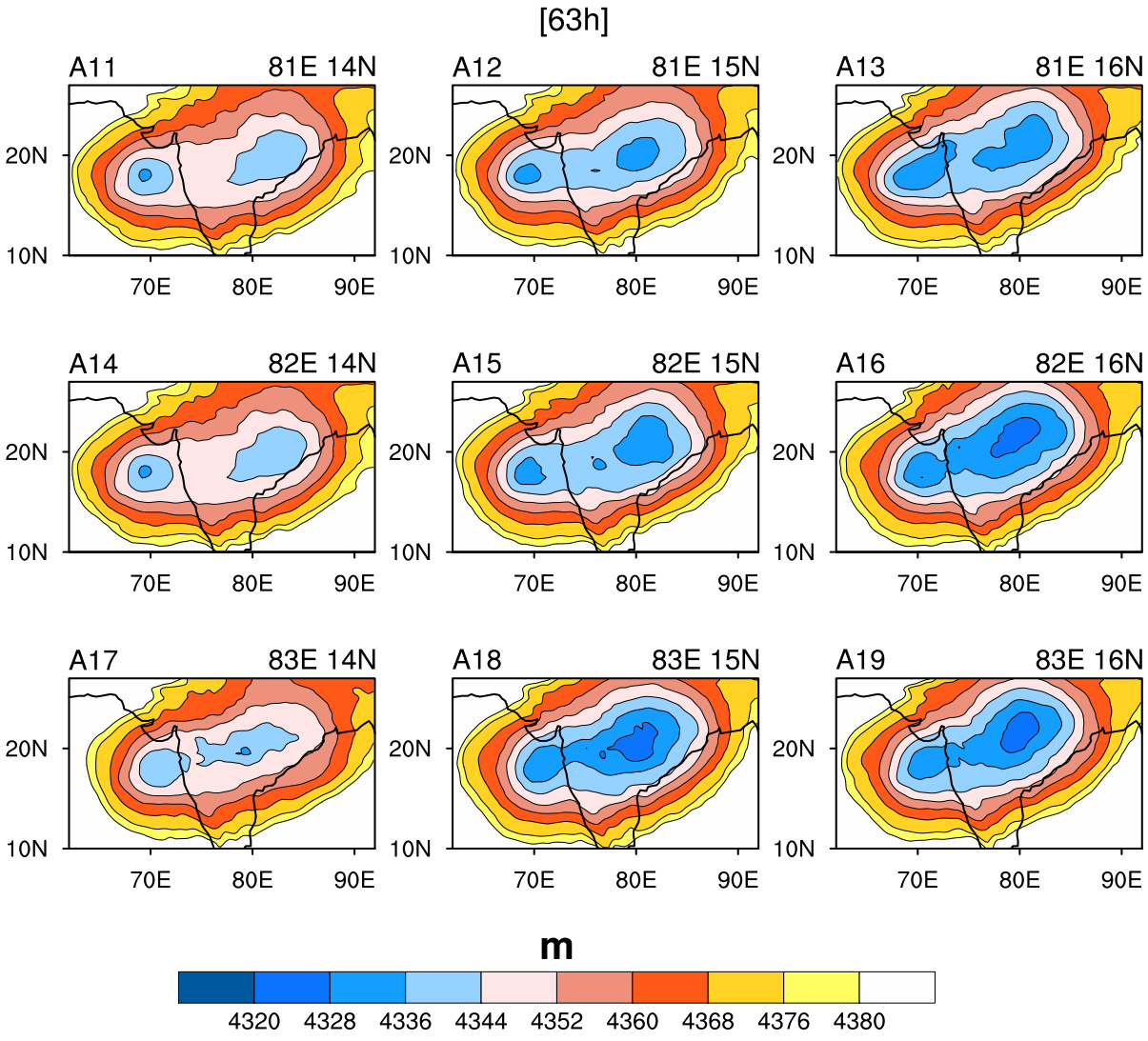

Figure 5.10: Geopotential height at 600 hPa of nine members (A11-A19) of group A1 after 63 hours of simulation.

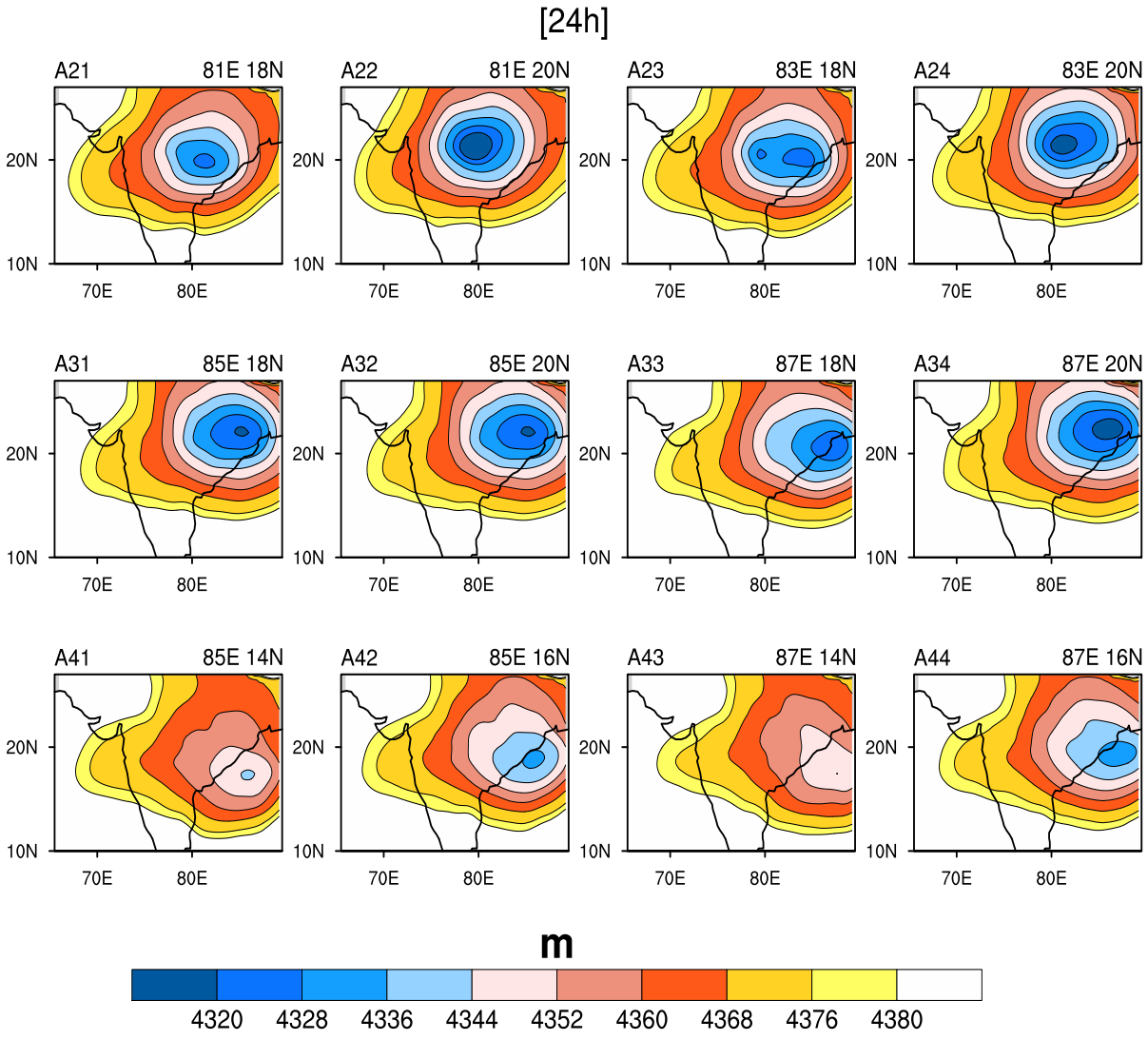

Figure 5.11: Geopotential height at 600 hPa of twelve members of group A2 (row 1) to group A4 (row 3) after 24 hours of simulation, respectively.

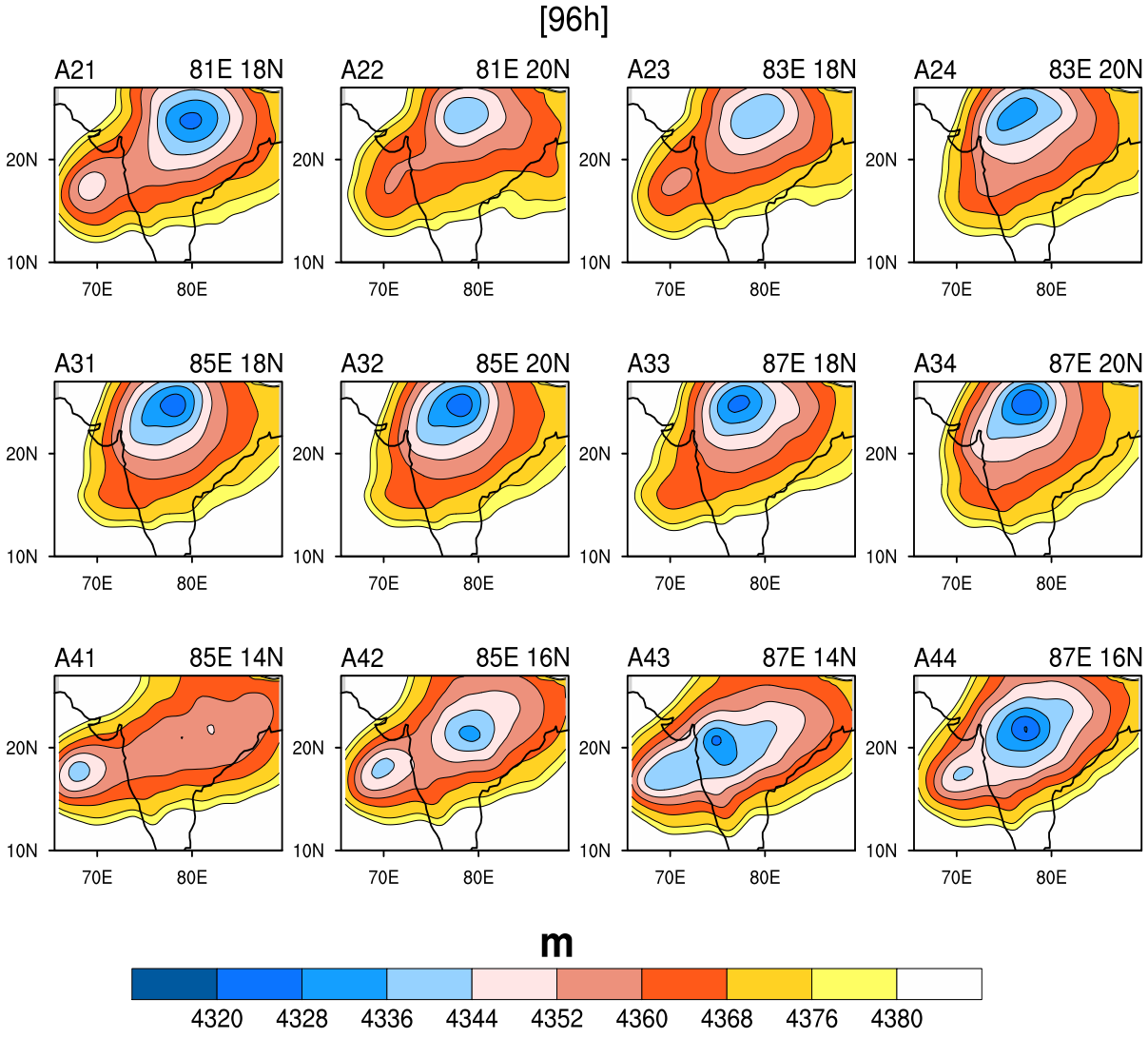

Figure 5.12: Geopotential height at 600 hPa of twelve members of group A2 (row 1) to group A4 (row 3) after 96 hours of simulation, respectively.

vortex stretching and act as a sink of vorticity tendency. Additionally, the β-term (Figure 5.13b, green) also acts as a source of vorticity throughout the formation of MTC; however, it remains relatively small compared to the stretching term and shows relatively larger values during the early phase and decreases afterwards. The vertical advection of vorticity (Figure 5.13b, red) also acts as a source of vorticity; however, it peaks after the maximum intensification, suggesting that it does not contribute significantly during the growth phase of MTC. Also, as it peaks after the intensification of the middle-level maximum, it suggests the shift of MTC vorticity maximum in the lower levels (i.e., the LTC phase, Chapter 3), hence positive vertical advection down the gradient of relative vorticity in the environment of upward velocity. These budgets to a large extent are consistent with the vorticity budget of July 1963 MTC, which also suggested stretching as a major source, followed by vertical advection and β-term, while advection acted as the main sink of vorticity tendency (Carr, 1977). It is important to note that though the vortex stretching term is highest in magnitude, the advection acts opposite. This cancellation occurs in vertically sheared environments wherein the advection tries to tilt the vortex while a large portion of stretching acts to keep it upright (Reasor et al., 2004; Davis and Galarneau, 2009). However, despite this cancellation, the evolution of total vorticity tendency almost follows the vortex stretching, suggesting that vortex stretching not only counters the advection but also contributes to the intensification of the vortex.

A plan view of vorticity budget during initial 24 hours is shown in Figure 5.14; here too, the vorticity tendency, $\frac{\partial \xi}{\partial t}$ (Figure 5.14g), is well matched by the sum of all terms on the right side of vorticity equation (Figure 5.14h) — suggesting an approximate closure of the vorticity budget. Two centers of positive vorticity tendency are observed; a strong one over the Bay of Bengal and East India — related to the intensification of Bogus LPS, and another relatively weak over one the northeast Arabian Sea off the coast of Mumbai linked to the incipient MTC. Consistent with the times series in Figure 5.13h, the Arabian Sea total positive vorticity tendency in plan view (Figure 5.14h) mainly results forms the tilting term (Figure 5.14e), the β-term (Figure 5.14f), and advection of relative vorticity (Figure 5.14c). The β-term (Figure 5.14f) shows broad positive tendencies over the Arabian Sea in the regions of southerly winds in the western sector of the monsoon LPS. The stretching term (Figure 5.14a,b) remains positive over western India; however, it contributes less relative to tilting (Figure 5.14e) and advection of absolute vorticity (Figure 5.14c+f). Notably, vertical advection (Figure 5.14d) does not appear to be a major

vorticity source during the first 24 hours over Arabian Sea. Thus during the initial phase of the genesis of MTC, advection of absolute vorticity and tilting of horizontal vorticity vector by the meridional gradients of vertical motions explains almost the entire geographical distribution of the vorticity tendency.

Moving ahead, a plan view of the vorticity budget during $24 - 48$ hours of model integration is shown in Figure 5.15. The pattern of observed vorticity tendency (Figure 5.15g) and the sum of the right-hand side of the vorticity equation (Figure 5.15h) show similar magnitude and horizontal distribution, again suggesting a small residue. However, in contrast to the budget during the first 24 hours, here, the total vorticity tendency is almost entirely explained by the total stretching term Figure 5.15 (a+b). However, again note that though total tendency following the stretching, the advection act to cancel it and reduce its effectiveness in the intensification. The β-term (Figure 5.15f) again acts like a source; however, its magnitude is much lesser as compared to the stretching term. In contrast to the first 24 hours, here, the advection of relative vorticity by horizontal winds (Figure 5.15c) and tilting term (Figure 5.15e) act to damp the vorticity tendency. The total vorticity tendency (Figure 5.15f, lines) and regions of positive absolute vorticity maximum (Figure 5.15f, colors) almost overlap, suggesting that the vorticity tendency primarily contributes to the intensification, and not much to the motion of the incipient MTC. This is suggestive of a quasi-stationary behavior of MTCs which is consistent with observations (Carr, 1977; Kushwaha et al., 2021). Overall, the vorticity budget suggests that initially the advection of absolute vorticity contributes to the MTC growth; however, during $24 - 48$ hours, the stretching of vorticity dominates the MTC intensification.

Further, as shown in Figures 5.1, 5.2 and the moisture budget in Figure 5.6, the anomalous easterly winds from the Bay of Bengal converge over the Arabian Sea. These middle-level easterlies prevent or reduce dry desert air intrusions from the west and north, reduce the inversion, destabilize the lower troposphere, and increase the middle troposphere moisture content. Figure 5.16 shows evidence of these phenomena in the simulated composite ensemble mean of group A1 MTCs. In particular, Figure 5.16a and b show that prior to the rapid intensification, static stability (Figure 5.16a) and strength of inversion (Figure 5.16b) reduces in the lower troposphere. Following this, relative humidity increases (Figure 5.16c), reaching near saturation just before the maximum intensification.

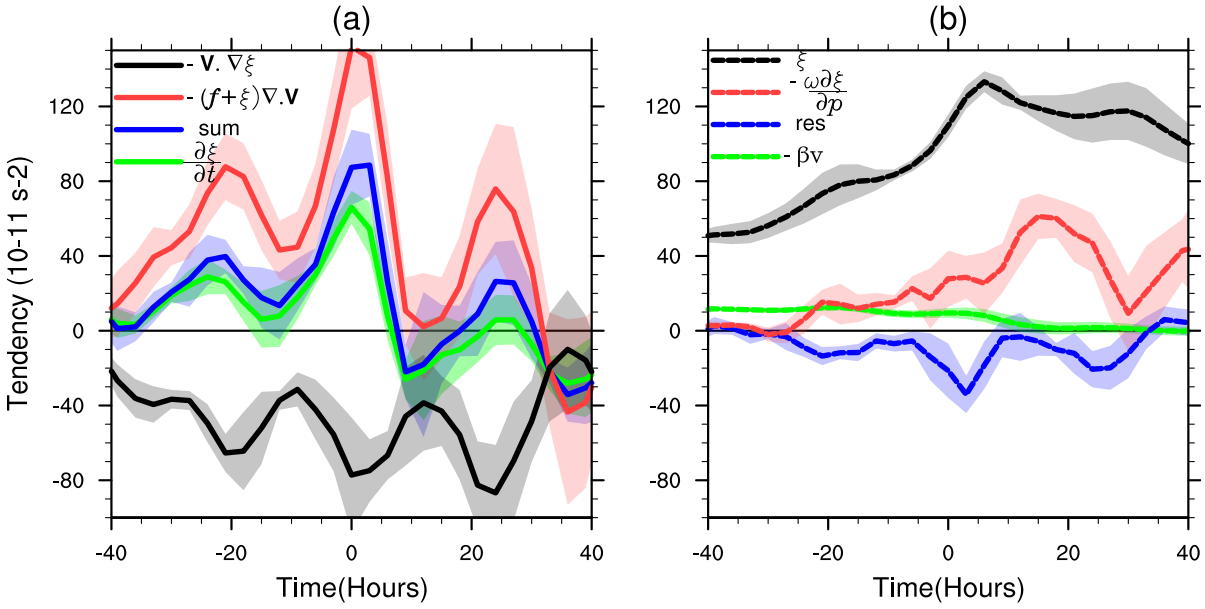

Figure 5.13: Composite time series of various term of Vorticity Budget of group A1, averaged over the MTC region between 500-600 hPa. Zero hour represents the time of maximum intensification rate, $(\frac{\partial \xi}{\partial t})_{max}$, shading represents standard deviation among A1 assemble members.

Similar to the observations (Figure 5.3), both simulated stability and humidity follows trends of the middle troposphere easterly over western India (Figure 5.16d). Moreover, the increase of middle troposphere humidity also suggests the contribution of convection in the vortex stretching. Essentially, consistent with the previous section, Figure 5.16 suggests that the middle troposphere easterlies induced by the Bay of Bengal system eventually alters the thermal profile over the Arabian Sea and western India such that it destabilizes the lower troposphere and allows the moistening of the middle troposphere, and provides the fertile ground for the MTC genesis. These are precisely the features that were observed during the formation of July 1963 MTC (Miller and Keshavamurty, 1968).

5.4 Mechanism Denial Experiment

To further confirm the effect of the Bay of Bengal system on the formation of Arabian Sea MTC, we now consider a real instance of July 2020 MTC as a test case where the Bay of Bengal preceded the formation of Arabian sea MTC (i.e., a Type 2a member). The geopotential height at 600 hPa of four control ensembles initialized on 1 July 00, 06, 12, and 18 UTC 2020 are shown in Figure 5.17 from Row 1 to Row 4, respectively. After 72 hours of

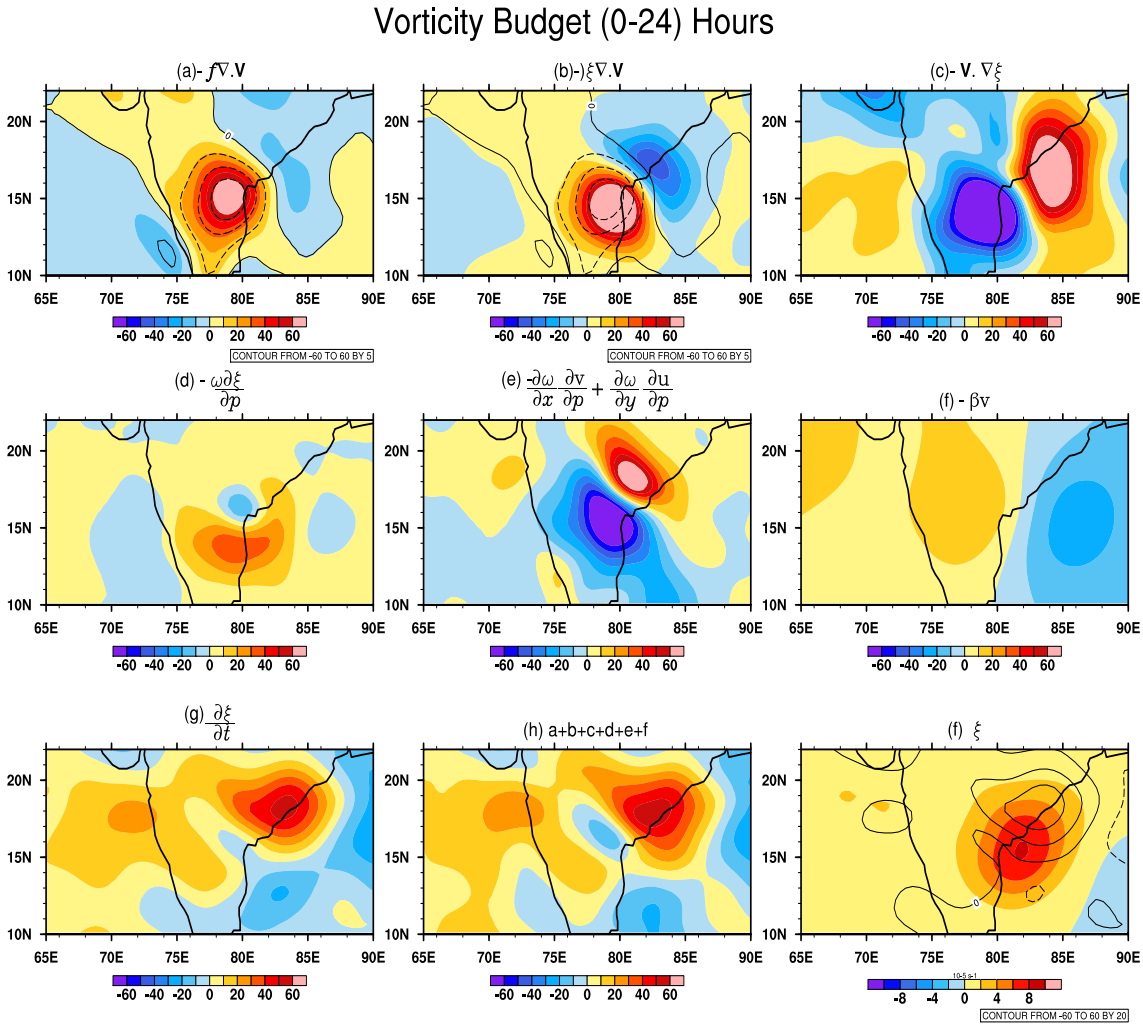

Figure 5.14: Plan view of composite terms in the vorticity budget of group A1, averaged between 500-600 hPa for first 24 hours of simulation; dashed contours represent convergence, and solid contours are divergence in (a) and (b); contours in (f) are $\frac{\partial\xi}{\partial t}$. Symbols have their usual meaning.

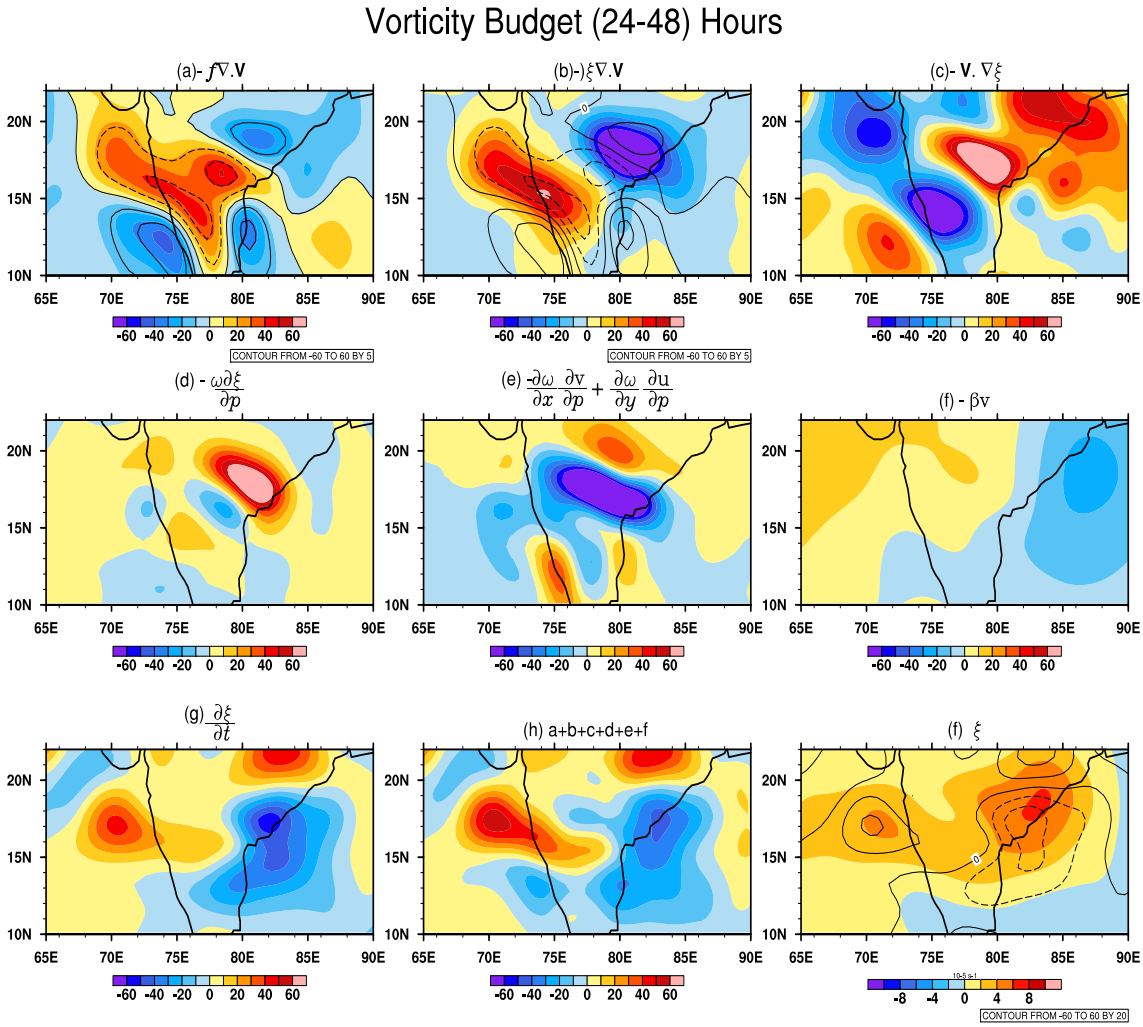

Figure 5.15: Plan view of various terms in the vorticity budget of group A1, averaged between 500-600 hPa for 24-48 hours of simulation; dashed contours represent convergence, and solid contours are divergence in (a) and (b); contours in (f) are $\frac{\partial\xi}{\partial t}$. Symbols have their usual meaning.

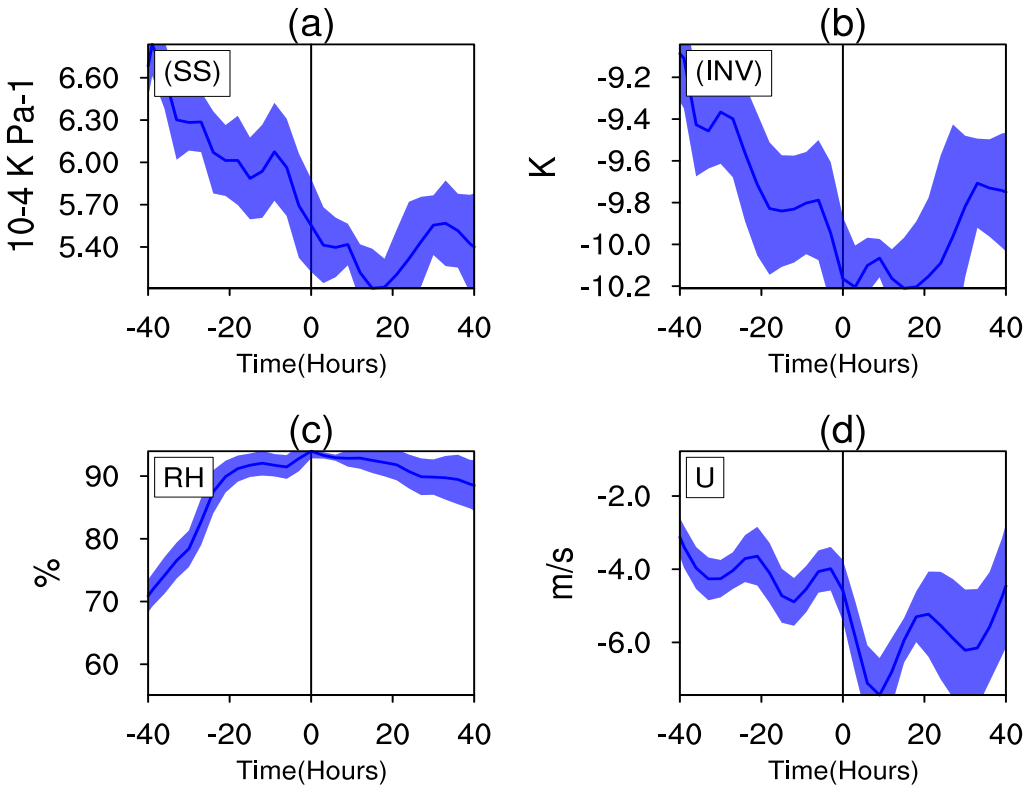

Figure 5.16: Composite moisture fields mean over MTC region; (a) Static stability parameter at 800 hPa; (b) $T_{900} - T_{700}$; (c) mean relative humidity at 500-600 hPa; (d) zonal wind mean at 500-600 hPa.

simulation (Column 1), height anomalies over the Bay of Bengal deepen, and a trough appears over the Arabian Sea and western India. With the intensification of the Bay of Bengal LPS (lowering of height anomalies) the Arabian Sea trough deepens from 72-120 hours (Columns 1 to 3). After 120 hours (Column 3) of simulation, within this middle troposphere trough region, a MTC develops in all the ensemble members. This MTC intensifies and becomes an isolated vortex around 144 hours of simulation (Column 4). Thus, the model replicates the July 2020 Type 2a MTC formation, and this case can be used as a mechanism denial experiment.

Specifically, the mechanism denial experiment is one wherein we look for whether the MTC forms in the absence of the Bay of Bengal system. The suppression of the Bay of Bengal LPS is achieved by cooling and drying the Bay of Bengal, as shown in Figure 5.18. With these altered unfavorable conditions over Bay of Bengal and East India, the simulated geopotential height at 600 hPa of four ensemble members is shown in Figure 5.19. Apart from a slight deepening of height around 96-120 hours (Figure 5.19, Columns 2 to 3) of model integration over the Bay of Bengal and western India, all ensemble members had no significant signature of MTC. This suggests that with the unfavorable conditions over the Bay of Bengal, the local LPS did not intensify, and consequently, the MTC did not form over the Arabian Sea either. These experiments, together with observation of Type 2a composites, suggest that the Bay of Bengal system plays an essential role in the formation of Arabian Sea MTCs. Therefore, the frequent observations in previous work and in Chapter 4 about the coexistence of LPS and MTCs is not just a coincidence; in fact, the Bay of Bengal LPS plays a critical role in the formation and to some extent in the maintenance of Arabian Sea MTCs.

5.5 Conclusions

During the July 1963 Arabian Sea MTC formation, a LPS coexisted throughout over the Bay of Bengal (Miller and Keshavamurty, 1968). Indeed, while analyzing three additional cases of MTCs, Miller and Keshavamurty (1968) noted that the Bay of Bengal vorticity quite frequently precedes the active phase of cyclonic activity over the Arabian Sea. Recently Choudhury et al. (2018) analyzed 20 heavy precipitating MTCs over western India and found the coexistence of LPS over the Bay of Bengal in 90% of the cases. These case studies suggest that the coexistence of LPS over the Bay of Bengal during MTC formation is a frequent phenomenon. Since these

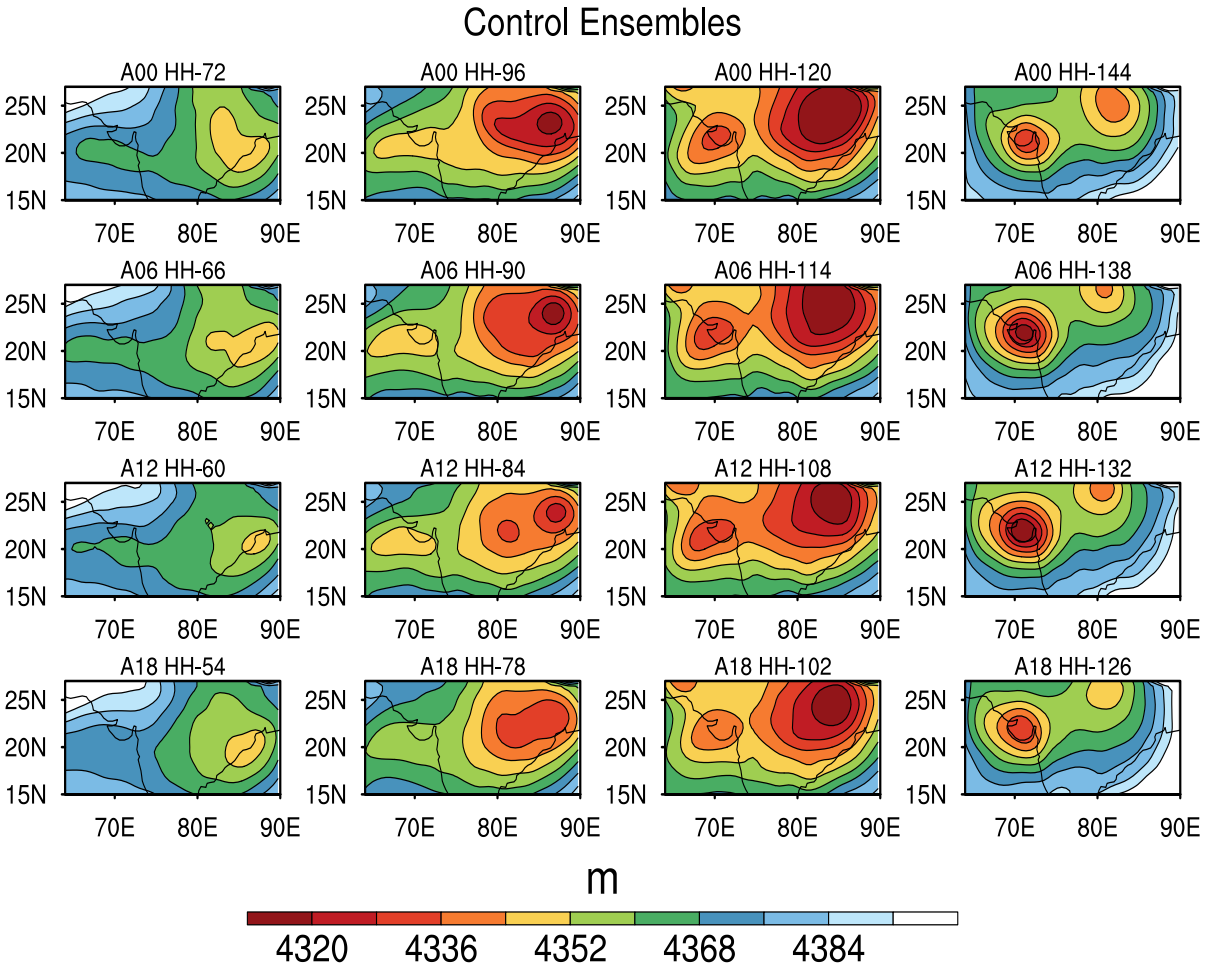

Figure 5.17: Geopotential height at 600 hPa of control ensemble members for the July 2020 MTC. Row 1 to row 4 are simulations initialized on 1 July at 00, 06, 12, and 18 UTC, respectively.

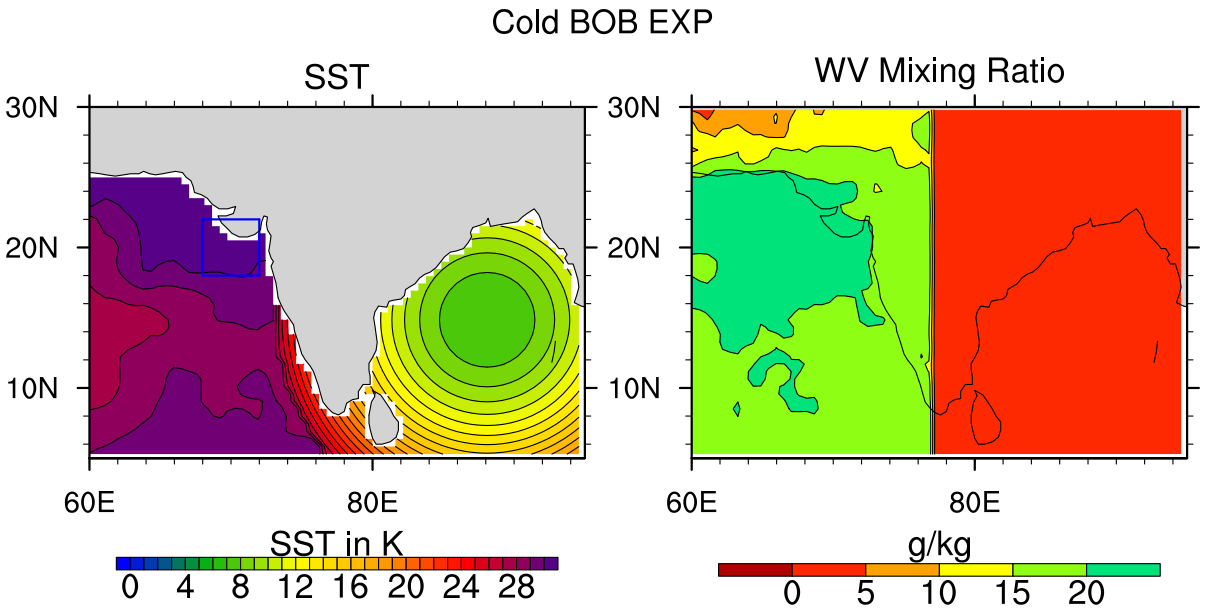

Figure 5.18: Initial conditions (a) cold Gaussian SST blob over Bay of Bengal, (b) Water Vapor (WV) mixing ratio at 1000 hPa — dry east India and BOB.

conclusions were based on a limited number of cases, a detailed classification of MTC in Chapter 4 suggested that almost 83% *in-situ* MTC develop with an LPS over the Bay of Bengal. However, whether this is just a coincidence or whether the Bay Bengal LPS plays a role in Arabian Sea MTC formation was explored in the current chapter using observations and WRF model experiments.

The lag composite dynamical and thermodynamical fields of Type 2a MTCs (those where a Bay of Bengal LPS precedes and then coexists with the MTC) suggested that the Bay of Bengal system induces a westwards extending middle troposphere through a fundamental Gill type response. This altered flow enhances horizontal zonal shear and induces middle troposphere easterlies over the northwest of India. These middle troposphere easterlies prevent dry air mixing in from the desert to the north and west, resulting in depletion of the inversion layer and destabilization of the lower troposphere. These favorable conditions further promote convection and allow the moistening of the middle troposphere over the Arabian Sea. In fact, a moisture budget during Type 2a formation shows that the convergence of climatological moisture due to anomalous winds is the dominant term — induced by the anomalous easterly flow connected with the Bay of Bengal system — in the build up of moisture over western India and the Arabian Sea. Moreover, along with the convergent term, the advective term also contributes significantly to moisture accumulation over the northwest Arabian Sea and western India.

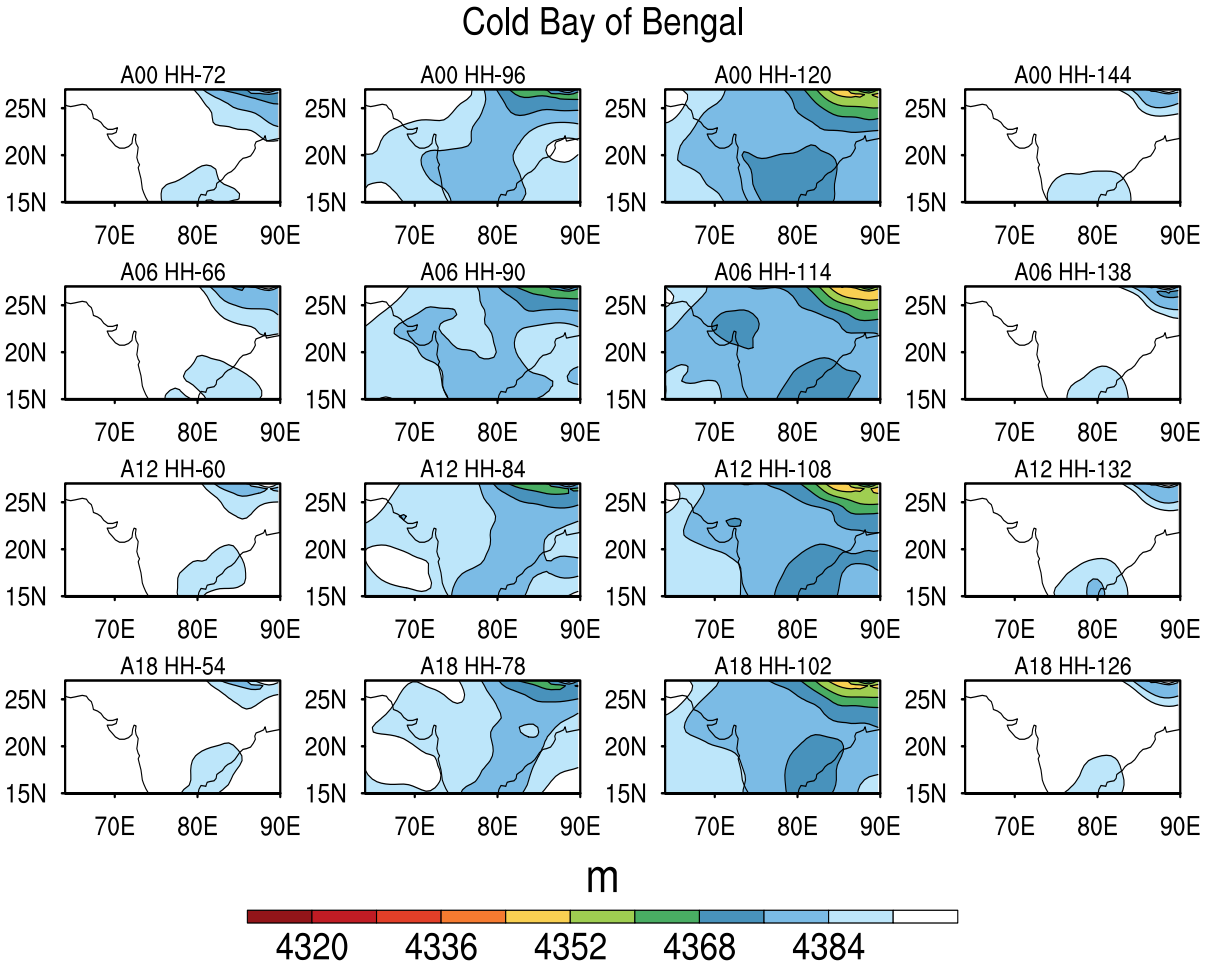

Figure 5.19: Geopotential height at 600 hPa of control ensemble members of cold-dry Bay of Bengal experiment. Row 1 to row 4 are simulations of 00, 06, 12, 18 UTC respectively.

The apparent link between MTC and Bay of Bengal LPS in Type 2a was explored with numerical experiments. Two sets of experiments were performed: first, with added "Bogus Vortex or LPS" over the Bay of Bengal on top of June-July climatology, and in the second, the response of pre-existing MTC is tested by weakening the Bay of Bengal LPS by cooling and drying the Bay of Bengal. With the addition of a Bogus Vortex over the Bay of Bengal, a westward extending trough forms from the Bay of Bengal up to the Arabian Sea; this trough enhances the easterlies north of 20°N and westerlies south of this latitude. This modified flow enhances the horizontal shear and background vorticity. Further, the middle troposphere easterlies prevent dry air intrusion from west and north, reduce the low-level inversion, and destabilize the lower troposphere. Further, most strikingly, almost all ensemble members show the genesis of MTC within the induced middle troposphere trough. In terms of the vorticity budget of the growing MTC, it was found that during the first 24 hours of MTC formation, advection of absolute vorticity and tilting account for the intensification. However, after 24 hours of model integration, vortex stretching dominates. The β- term remains positive throughout, though it contributes mainly in the early phase of intensification. Vertical advection is initially quite weak; but, it does contribute to the vorticity tendency in the middle troposphere in the later stages of MTC development.

A mechanism denial experiment with cooling and drying Bay of Bengal experiment further confirmed the link between LPS and MTC using the July 2020 Type 2a MTC case. The result suggests that in the cold and dry Bay of Bengal case, LPS did not develop and intensify; consequently, the westwards extending trough did not develop, horizontal shear and easterly remained weak, and MTC did not form over the Arabian Sea. Together, this suggests that the coexistence of the Bay of Bengal system during the formation of the Arabian sea MTC may not be just a coincidence, and the genesis and maintenance of Type 2a MTCs could be the direct result of the dynamical influence of the Bay of Bengal LPS.

Chapter 6

Summary and Future Research Directions

Mid-tropospheric cyclones (MTCs) are moist tropical synoptic-scale systems with middle troposphere vorticity maximum and relatively weak signature in the lower troposphere. In this thesis we undertook a systematic examination of these systems; this included a global survey, classification over the Arabian Sea and western India and their mechanisms of genesis. Indeed, apart from their inherent structural differences with more commonly studied monsoon lows, depressions and tropical cyclones, MTCs contribute to the annual precipitation and severe rainfall events over western India and adjoining regions in the tropics during the boreal summer. Thus, it is imperative both from a fundamental viewpoint as well from a practical standpoint to develop a better understanding of these rain bearing systems.

We began our study with an examination of the global tropical occurrence of MTCs. In particular, we carried out analysis over the global tropics $(30°\text{N}-30°\text{S})$ in the boreal summer (June-September) and winter (December-March) for 20 years (2000-2019). Along with MTCs, we also kept track of tropical systems with lower troposphere vorticity maxima, which include monsoon lows, MDs, and TCs (together referred to as lower tropospheric cyclones; LTCs), and the relative fraction of these two types of systems (i.e., MTCs and LTCs) was also analyzed. The main results of this global survey were:

1. The highest density of MTCs is over the North-East Arabian Sea, followed by the Bay of Bengal and the

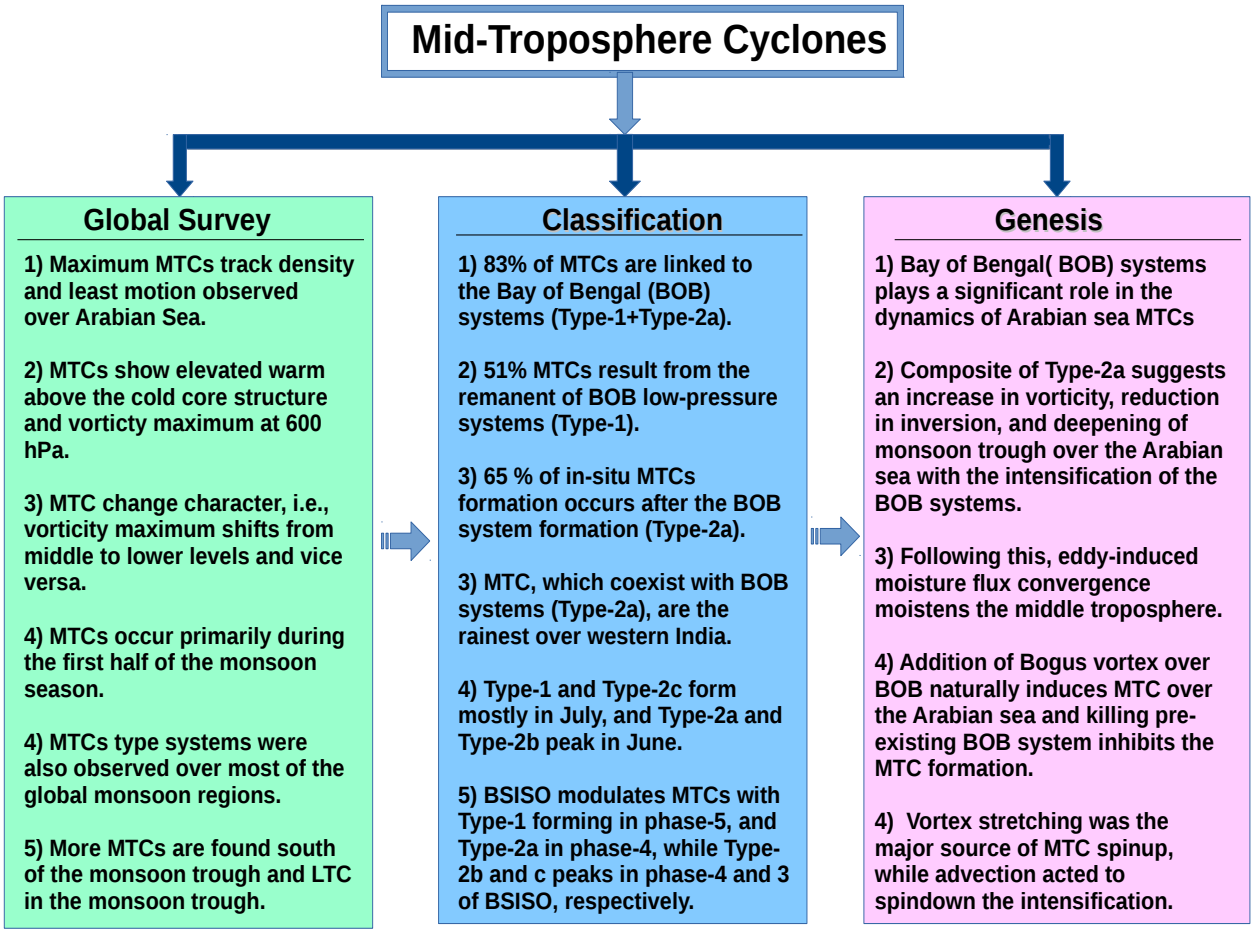

Figure 6.1: Summary of the thesis.

South China Sea. Further, MTCs mainly occur during the early part of the summer monsoon (i.e., June and July).

2. MTCs are part of the life cycle of tropical cyclonic systems. In particular, tracks of systems identified as MTCs change the character and usually exhibit a middle (MTC-phase) and a lower troposphere vorticity maximum (LTC-phase) during different periods of their life cycle.

3. Cross basin motion suggests that MTCs observed in a given region can have a nonlocal or remote genesis.

4. Cyclone motion statistics indicate that MTCs move slowly westward or remain quasi-stationary over the Arabian Sea compared to the Bay of Bengal and the South China Sea.

5. Analysis of the differences of middle and lower troposphere vorticity ($\delta\xi_p$) and mean middle tropospheric vorticity (ξ_m) indicates that the MTC and LTC phases are prevalent south and north of 20°N, respectively.

Cyclone center density over global tropics showed that MTCs form over several monsoonal regions. These include the Arabian Sea, East & West Africa, East Pacific, North Bay of Bengal, and the South China Sea in the boreal summer. During boreal winter North Australia, the South Indian Ocean, South America, and subtropical Africa show significant MTCs activity. Further, near-equatorial regions have more MTCs than LTCs in both hemispheres, while LTCs are more prominent than MTCs away from the equator. In particular, MTCs are dominant equatorward of the monsoon trough and LTCs are prevalent in the vicinity of the monsoon trough itself. Together, the probability density function of differential vorticity versus the height of peak vorticity of cyclonic centers over global tropics is bimodal, with one peak (for MTCs) in the middle and another (for LTCs) in the lower troposphere.

Composites from different global tropical regions show that, apart from their tilt, which is somewhat region-dependent, MTCs are remarkably similar throughout the tropics. In particular, they show high vorticity, potential vorticity, and moisture anomalies in the middle troposphere. Besides, MTCs show a baroclinic structure with warm temperature anomalies over cold anomalies with significant east-west tilt. Though they have maximum intensity in the middle troposphere, in most places, MTCs also show a weak trough-like surface signature to the east of the middle-level center. LTCs, on the other hand, show a maximum vorticity and moisture anomaly in the

lower troposphere with a shallow cold-core below 800 hPa and a relatively warm upright temperature structure. The PV anomalies of MTCs have a single peak in the middle troposphere. In contrast, the potential vorticity profile of LTCs usually shows two peaks, one in the middle troposphere and another in the lower troposphere. Further, LTCs show some regional structural differences, primarily in the low-level cold anomaly, which is almost non-existent in the South Indian Ocean and East Pacific and somewhat deeper in other parts of the tropics.

These findings pose some fundamental questions: for example, why do certain regions show a relative preference for MTCs or LTCs? What decides the transition between LTC and MTC phases? How do the different environmental conditions in these regions affect the dynamics of lower versus mid-tropospheric systems? These are important issues as they may help gain insight into the development of tropical cyclones from mid-level vortices (Raymond et al., 2014a), and why tropical storms and monsoon depressions are more intense over some areas of the globe. Given the remarkable structural similarity of MTCs across the tropics, this also raises the possibility that they might be maintained via similar dynamical mechanisms. In fact, despite high SSTs, near-equatorial regions during summer monsoon months preferentially support MTC activity over LTCs. Interestingly, during monsoon seasons, near-equatorial areas show a strong cross hemisphere flow. This flow is a westerly low-level jet and results in negative vorticity advection (Tomas et al., 1999) in the northern hemisphere. In conjunction with an upper-level easterly flow, these regions are also characterized by a sizeable vertical shear (Wang and Fan, 1999; Aiyyer and Thorncroft, 2006). While top-heavy stratiform diabatic heating may enhance middle troposphere maxima (Choudhury et al., 2018; Russell et al., 2020), negative vorticity advection at low levels with the strong vertical shear could also play a role in localizing cyclonic vorticity in the middle troposphere and supporting MTC profiles.

Classification of MTCs over the Arabian Sea and Western India

Having established that the Arabian Sea and western India are hot spots for MTC activity during the summer monsoon, rain bearing synoptic systems over these regions were analyzed by k-means clustering and cyclone tracking methodologies. Over twenty years of summer monsoon data from modern reanalysis is used to obtain a robust view of the systems responsible for a significant portion of the annual precipitation and extreme rainfall

events in this part of the world. At the outset, a lag correlation analysis of OLR immediately showed a tendency for moist convection to simultaneously occur over the Arabian Sea and western Indian region, and the Bay of Bengal. Further, the nature of the correlation patterns also suggests that large-scale environmental conditions play a role in favoring the formation of rainy systems in this region.

Patterns of the geopotential field over the Arabian Sea and western India extracted by a k-means analysis showed four clusters consisting of middle tropospheric cyclonic circulation anomalies over the northeast Arabian Sea and west India. The height anomalies of the first regime have a northwest orientation and range from the Arabian Sea to the Bay of Bengal. Lagged composites indicate that synoptic systems over the Arabian Sea in this regime develop from the westward movement of monsoon lows over the Bay of Bengal. The second regime shows concomitant cyclonic activity over the Arabian Sea and Bay of Bengal and suggests dynamical interaction between the two circulation patterns. In the third regime, systems form locally in the South Central Arabian Sea and move northwards with a weak transient cyclonic signature in the Bay of Bengal. Further, lagged composites indicate that the Bay of Bengal system intensification precedes or follows the Arabian Sea system genesis in the second and third regimes, respectively. The fourth regime consists of a large-scale cyclonic envelope that gradually moves northwest from the South Bay of Bengal and leads to the formation of a synoptic system in the Arabian Sea.

In more detail, cyclone tracking followed and classified 191 rainy synoptic systems over the northeast Arabian Sea and western India over 22 years. The resulting classification again brought out four categories: the first (Type 1) accounts for 51% of all systems, and these form from the westward (downstream) development of cyclonic lows over the Bay of Bengal. Second, Type 2a accounts for 31% cases and consists of the formation of MTCs over the Arabian Sea with a coexisting Bay of Bengal system that precedes the Arabian Sea system formation. Third, Type 2b (9-10%) formation is again characterized by the coexisting cyclonic circulations over the two basins. However, in this category, the Arabian Sea system precedes a relatively weak and short-lived cyclonic circulation over the Bay of Bengal. Finally, Type 2c accounts for the remaining 7-8% of systems that form locally in the Arabian Sea from a large-scale cyclonic envelope that propagates northwestward from the southern Bay of Bengal. It is noteworthy that no *a priori* constraint was imposed on the tracking procedure, and it too yielded

four categories that qualitatively match the patterns captured by the k-means approach.

We observed that *in-situ* genesis (specifically, Types 2a & 2b) is favored in the early part of the monsoon season (i.e., June). In contrast, downstream development, Type 1 and Type 2c (i.e., *in-situ* Arabian Sea systems triggered from a large-scale cyclonic anomaly of south Bay of Bengal) are most frequently observed in July. Among all categories, Type 2a genesis occurred throughout the monsoon (June-September) and is rainiest, with the highest rain rates in western India that exceeded 60 mm/day. The westward-moving category (Type 1) moves off from western India to the Arabian Sea, but given its track, it accounts for the second rainiest system in this region. Interestingly, Type 2b, where the Arabian Sea system precedes the Bay of Bengal system, motion vectors indicate the possibility of curving into the Indian landmass; thus, though much less frequent than Types 1 & 2a, they too have an influence on rainfall in the western coastal regions of India. Finally, Type 2c systems usually progress northward into the eastern Arabian Sea and at times make landfall over the west coast; however, they contribute the least out of the four categories to rainfall in western India.

This classification of Arabian Sea MTCs allows us to pose critical questions requiring further analysis. For instance, MTCs which coexist with the Bay of Bengal system are the heaviest rain-producing systems; what leads to these characteristics? Further, this category of MTCs shows slow motion or remains quasi-stationary; given the Bay of Bengal coexistence during its life cycle, does the Bay of Bengal system play any role in controlling this behavior? As seen in observations, Type 2a MTCs co-exist with monsoon LPSs, and these encircle and interact with each other; this is similar to the Fujiwhara Effect, which is well known in the context of tropical cyclones and controls the motion of coupled vortices if they are close enough. Therefore it is worth exploring whether the relative motion of a MTC and LPS is similar to that of binary tropical cyclones (Dong and Neumann, 1983). If so then annual frequency of coexisting systems in both basins can have far reaching effects on the rainfall distributions by controlling the motion and duration of rain events.

Genesis of MTCs over the Arabian Sea

During the classical July 1963 MTC formation, an LPS coexisted throughout over Bay of Bengal (Miller and Keshavamurty, 1968). This coexistence was seen on other case studies of Miller and Keshavamurty (1968) and Choudhury et al. (2018). Moreover, our detailed classification of MTCs suggested that almost 83% *in-situ* MTCs develop with an LPS over the Bay of Bengal. Whether this is just a coincidence, or whether the Bay of Bengal LPS plays a role in Arabian Sea MTC formation was an outstanding question which we then explored using observations and numerical model experiments.

From observations, lag composites of Type 2a MTCs — those where the Bay of Bengal LPS precedes the MTC — suggested that the LPS induces a westward extending middle troposphere through a fundamental Gill type response. This enhances horizontal zonal shear and induces the middle troposphere anomalous easterlies over the northwest of India. The middle troposphere anomalous easterlies prevent dry air mixing from the desert to the north and west, resulting in depletion of the inversion layer and destabilization of the lower troposphere. These favorable conditions further promote convection and allows the moistening of the middle troposphere. In fact, a moisture budget during Type 2a formation suggests that the convergence of climatological moisture due to anomalous winds is the dominant term — induced by the anomalous easterly flow connected with the Bay of Bengal system — in the build up of moisture over the Arabian Sea and western India. Though, along with the convergent term, advection also contributes significantly to moisture accumulation over the northwest Arabian Sea and western India.

To establish a clear link between Type 2a MTC formation and Bay of Bengal LPS, we then proceeded to a suite of numerical experiments. Two sets of experiments were performed: first, a "Bogus Vortex or LPS" was added over the Bay of Bengal, and in the second, the response of preexisting MTC is tested by weakening the Bay of Bengal LPS. With the Bogus Vortex over the Bay of Bengal, a westward extending trough forms from the Bay of Bengal up to the Arabian Sea; this trough enhances the easterly north of 20°N and westerly south of it. This modified flow enhances the horizontal shear and background vorticity. Further, the middle troposphere anomalous easterlies prevent the dry air intrusion from west and north, reduces the low-level inversion, and destabilizes the lower troposphere. In fact, after about 2 days of integration, most ensemble members show

the genesis of MTC within the induced middle troposphere trough. A vorticity budget indicates that during the initial 24 hours of genesis, the advection of absolute vorticity plays a role, while during the rapid intensification phase, vortex stretching is dominant. Further, as MTCs form in a vertically sheared monsoon environment, the advection of vorticity act to cancel the vorticity generation by vortex stretching and reduces its effectiveness in MTC intensification. A mechanism denial experiment with cooling and drying Bay of Bengal experiment confirmed the link between LPS and MTC formation. Here, we used the July 2020 Type 2a MTC case which was well simulated in the control numerical run. On drying and cooling the Bay, the LPS did not develop and intensify; consequently, the westwards extending trough did not develop, horizontal shear and easterly remained weak, and MTC did not form over the Arabian Sea. Thus, the composites of Type 2a systems and numerical experiments suggest that the presence of the Bay of Bengal system plays an essential role in the formation of a MTC by enhancing the middle atmospheric moisture and making the region dynamically and thermodynamically unstable, which eventually promotes the MTC formation over the Arabian Sea and western India.

This analysis again points to critical open questions, for instance, it was observed that the vortex stretching plays a dominant role in MTC intensification. What leads to the vortex stretching? Does dynamical uplift play a role, or is it entirely due to the vertical motion induced by diabatic heating (Carr, 1977)? Given the MTC proximity with the western Ghats' topography, this raises the question of whether the topographical barrier and rainfall associated with it plays a significant role in MTC dynamics? Further, the role of heat low in the dynamics of MTCs (Ramage, 1966) remains to be assessed, especially in the early monsoon months. Overall the role of middle troposphere trough, enhanced zonal wind shear and middle troposphere moistening appear to be the dominant dynamical conditions during the formation of MTC. This indicates fertile grounds for barotropic instability in a moist environment. Therefore, it is worth exploring the instability of the mean flow prior to the formation of Type 2a MTCs. Indeed, moist vortex instability (Adames and Ming, 2018a) could be a likely candidate in the genesis of MTCs given that they form in a region of large meridional temperature and moisture gradients. Answering these questions will, to some extent, complete our understanding of the dynamics of MTCs and their contribution to the monsoon variability. The summary of important results of the thesis is presented in Figure **??** for quick reference.

Appendix A

Appendix

Table A.1: Mean, variance, median and probability distributions of δP_ξ of 882 detected systems over $5°$N-$25°$N and $50°$E-$95°E$ (as shown in Figure 2.3) and corresponding number of MTCs and LTCs for various combinations of layer thickness (left portion of the table); the number of MTCs and LTCs are highlighted in bold. The sensitivity of number of MTCs and LTCs for various moisture (Q_m) and relative vorticity (ξ_m) thresholds in in the right portion of the Table.

	LO0	**LO1**	**LO2**	**LO3**
MEAN	0.36	0.41	0.09	0.57
VARIANCE	1.95	0.85	1.17	2.41
MEDIAN	0.38	0.36	0.093	0.55
MTC	**121**	**52**	**66**	**157**
LTC	**246**	**220**	**282**	**238**

Q_m	**MTC**	**LTC**		ξ_m	**MTC**	**LTC**
1.0	145	251		1.0	121	290
2.0	121	246		2.0	120	203
3.0	106	233		3.0	77	126
4.0	98	226		4.0	29	62
5.0	96	223		5.0	6	35
6.0	84	218		6.0	2	21

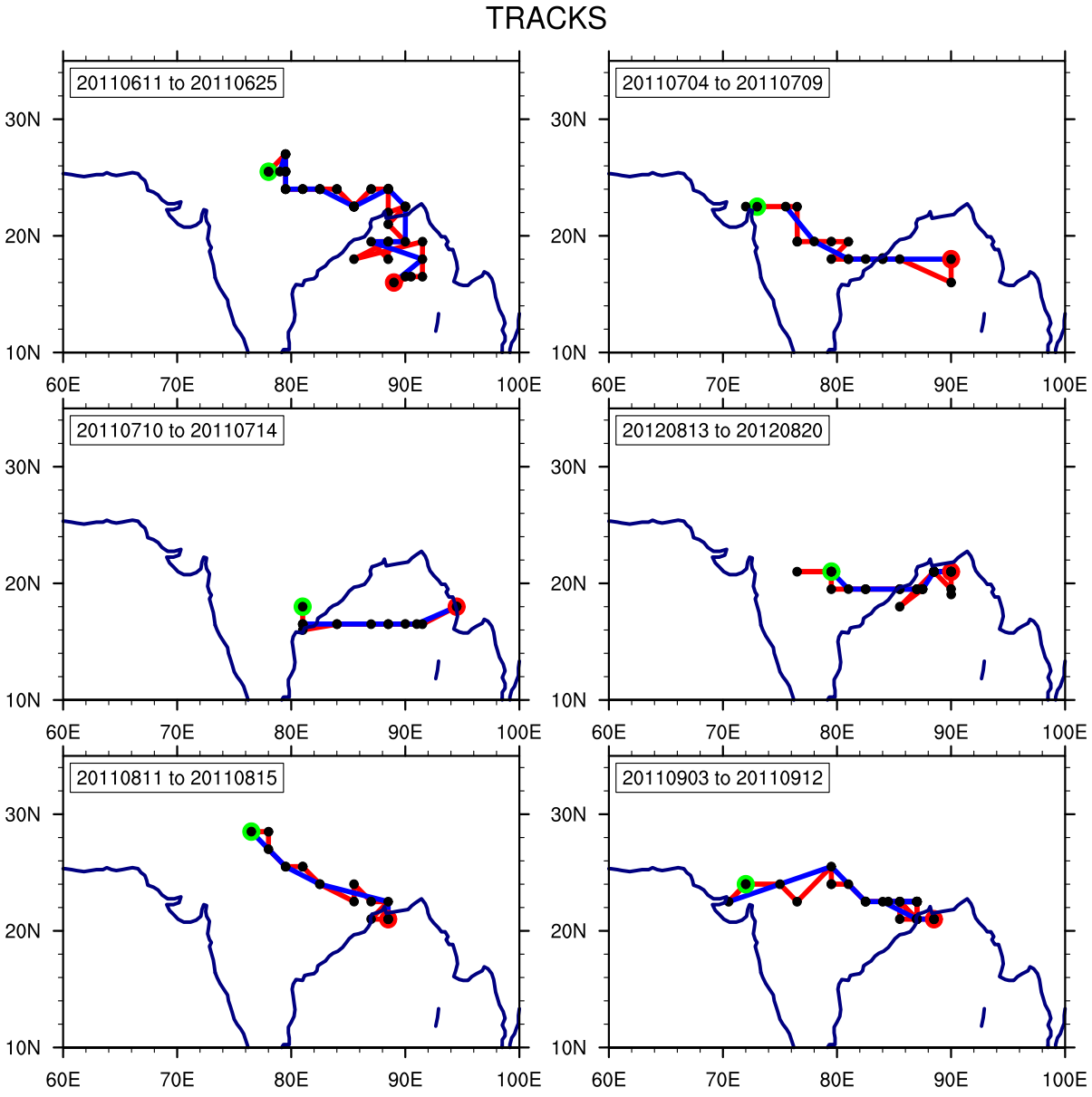

Figure A.1: Cyclone tracks with six. hourly sampling (red) and with 24 hour sampling (blue). Red dots indicate genesis location and green dot denotes lysis; black dots represents the 6 hourly position of cyclone.

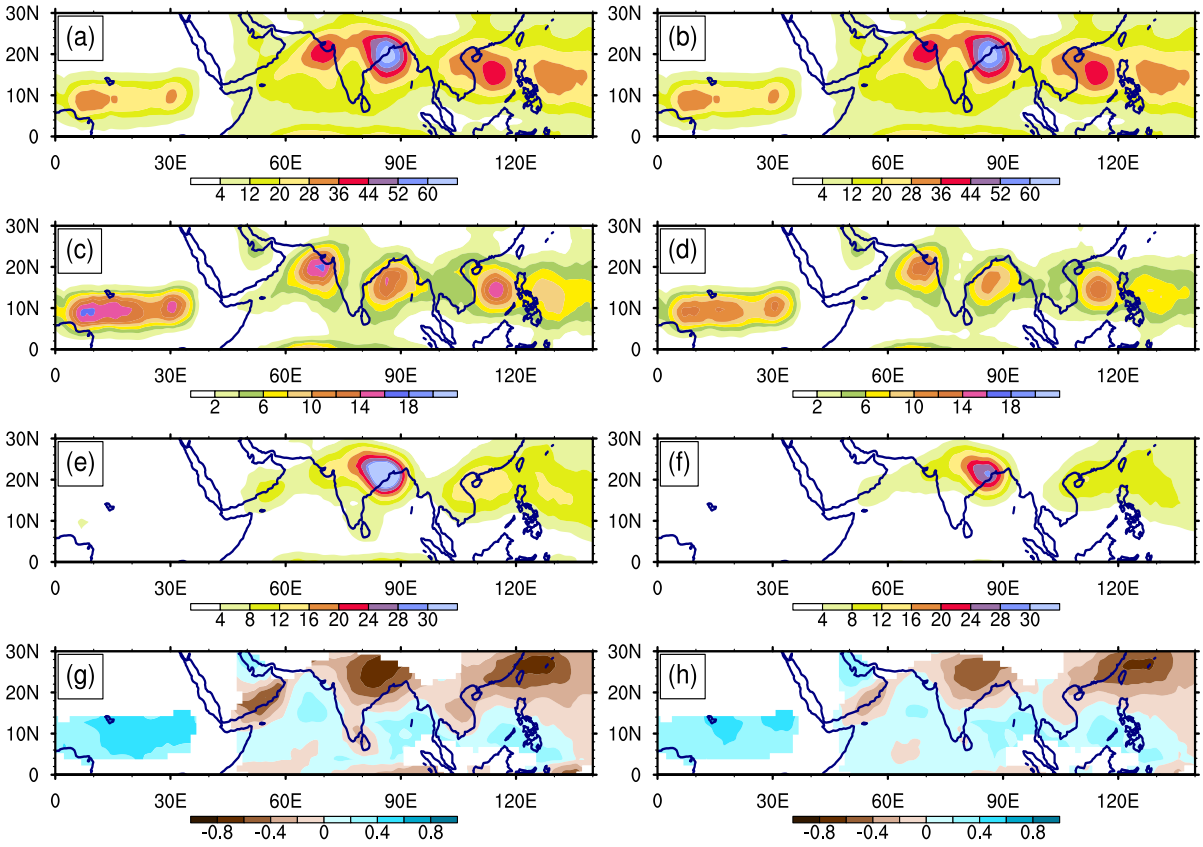

Figure A.2: Overall-center, LTC, MTC center density and MTC to LTC fraction from June to September 2000-2019; left panel (a, c, e, g) without P_ξ constraints; Right panel (b, d, f, h) with all constraints, respectively.

Bibliography

Adames, Á. and Ming, Y. (2018a). Interactions between water vapor and potential vorticity in synoptic-scale monsoonal disturbances: Moisture vortex instability. *Journal of the Atmospheric Sciences*, 75(6):2083–2106.

Adames, A. and Ming, Y. (2018b). Moisture and moist static energy budgets of south asian monsoon low pressure systems in gfdl am4.0. *Journal of the Atmospheric Sciences*, 75:2107–2123.

Adler, R. F., Gu, G., Sapiano, M., Wang, J.-J., and Huffman, G. J. (2017). Global precipitation: means, variations and trends during the satellite era (1979–2014). *Surveys in Geophysics*, 38(4):679–699.

Aiyyer, A. R. and Thorncroft, C. (2006). Climatology of vertical wind shear over the tropical atlantic. *Journal of Climate*, 19(12):2969–2983.

Ames, W. F. (2014). *Numerical methods for partial differential equations*. Academic press.

Annamalai, H. and Slingo, J. (2001). Active/break cycles: diagnosis of the intraseasonal variability of the Asian summer monsoon. *Climate Dynamics*, 18(1):85–102.

Arnason, G. (1958). A convergent method for solving the balance equation. *Journal of Atmospheric Sciences*, 15(2):220–225.

Awan, J. A., Bae, D.-H., and Kim, K.-J. (2015). Identification and trend analysis of homogeneous rainfall zones over the east asia monsoon region. *International Journal of Climatology*, 35(7):1422–1433.

Bengtsson, L., Hodges, K., and Esch, M. (2007). Tropical cyclones in a t159 resolution global climate

model: Comparison with observations and re-analyses. *Tellus A: Dynamic Meteorology and Oceanography*, 59(4):396–416.

Berry, G. J. and Reeder, M. J. (2016). The dynamics of australian monsoon bursts. *Journal of the Atmospheric Sciences*, 73(1):55–69.

Bholowalia, P. and Kumar, A. (2014). Ebk-means: A clustering technique based on elbow method and k-means in wsn. *International Journal of Computer Applications*, 105(9).

Bian, G.-F., Nie, G.-Z., and Qiu, X. (2021). How well is outer tropical cyclone size represented in the era5 reanalysis dataset? *Atmospheric Research*, 249:105339.

Bister, M. and Emanuel, K. A. (1997). The genesis of hurricane guillermo: Texmex analyses and a modeling study. *Monthly weather review*, 125(10):2662–2682.

Boos, W., Hurley, J., and Murthy, V. (2015a). Adiabatic westward drift of indian monsoon depressions. *Quarterly Journal of the Royal Meteorological Society*, 141(689):1035–1048.

Boos, W., Hurley, J., and Murthy, V. (2015b). Adiabatic westward drift of Indian monsoon depressions. *Quarterly Journal of the Royal Meteorological Society*, 141:1035–1048.

Brode, R. W. and Mak, M. (1978). On the mechanism of the monsoonal mid-tropospheric cyclone formation. *Journal of the Atmospheric Sciences*, 35(8):1473–1484.

Burpee, R. (1972). The origin and structure of easterly waves in the lower troposphere of North Africa. *Journal of the Atmospheric Sciences*, 29:77–90.

Carr, F. H. (1977). Mid-tropospheric cyclones of the summer monsoon. *Pure and Applied Geophysics*, 115(5-6):1383–1412.

Charney, J. (1955). The use of the primitive equations of motion in numerical prediction. *Tellus*, 7(1):22–26.

Chaterjee, P. and Goswami, B. (2004). Structure, genesis and scale selection of the tropical quasi-biweekly mode. *Quartely Journal of the Royal Meteorological Society*.

Chen, T.-C. and Weng, S.-P. (1999). Interannual and intraseasonal variations in monsoon depressions and their westward-propagating predecessors. *Monthly weather review*, 127(6):1005–1020.

Chou, C. and Neelin, J. D. (2004). Mechanisms of global warming impacts on regional tropical precipitation. *Journal of climate*, 17(13):2688–2701.

Choudhury, A. D., Krishnan, R., Ramarao, M., Vellore, R., Singh, M., and Mapes, B. (2018). A phenomenological paradigm for midtropospheric cyclogenesis in the indian summer monsoon. *Journal of the Atmospheric Sciences*, 75(9):2931–2954.

Clark, S., Reeder, M., and Jakob, C. (2018). Rainfall regimes over northwestern australia. *Quarterly Journal of the Royal Meteorological Society*, 144(711):458–467.

Das, S. K., Thatte, T., Uma, K., Krishna, U. M., and Saha, S. K. (2021). Characteristics of temperature inversion from radiosonde measurements in the western ghats region. *Atmospheric Research*, 250:105391.

Davis, C. A., Ahijevych, D. A., and Trier, S. B. (2002). Detection and prediction of warm season midtropospheric vortices by the rapid update cycle. *Monthly Weather Review*, 130(1):24–42.

Davis, C. A. and Galarneau, T. J. (2009). The vertical structure of mesoscale convective vortices. *Journal of the Atmospheric Sciences*, 66(3):686–704.

Davis, C. A. and Low-Nam, S. (2001). The ncar-afwa tropical cyclone bogussing scheme. *Air Force Weather Agency (AFWA) Rep*, 12.

Deoras, A., Hunt, K., and Turner, A. (2021). The four varieties of south asian monsoon low-pressure systems and their modulation by tropical intraseasonal variability. *Weather*, 76(6):194–200.

Diaz, M. and Boos, W. R. (2019a). Barotropic growth of monsoon depressions. *Quarterly Journal of the Royal Meteorological Society*, 145(719):824–844.

Diaz, M. and Boos, W. R. (2019b). Monsoon depression amplification by moist barotropic instability in a vertically sheared environment. *Quarterly Journal of the Royal Meteorological Society*, 145(723):2666–2684.

Diaz, M. and Boos, W. R. (2021). Evolution of idealized vortices in monsoon-like shears: Application to monsoon depressions. *Journal of the Atmospheric Sciences*, 78(4):1207–1225.

Ding, A., Wang, T., Zhao, M., Wang, T., and Li, Z. (2004). Simulation of sea-land breezes and a discussion of their implications on the transport of air pollution during a multi-day ozone episode in the pearl river delta of china. *Atmospheric Environment*, 38(39):6737–6750.

Ditchek, S. D., Molinari, J., Corbosiero, K. L., and Fovell, R. G. (2019). An objective climatology of tropical cyclone diurnal pulses in the atlantic basin. *Monthly Weather Review*, 147(2):591–605.

Dong, K. and Neumann, C. J. (1983). On the relative motion of binary tropical cyclones. *Monthly weather review*, 111(5):945–953.

Dwivedi, S., Yesubabu, V., Ratnam, M. V., Dasari, H. P., Langodan, S., Raj, S. A., and Hoteit, I. (2021). Variability of monsoon inversion over the arabian sea and its impact on rainfall. *International Journal of Climatology*, 41:E2979–E2999.

Fletcher, J. K., Parker, D. J., Hunt, K. M., Vishwanathan, G., and Govindankutty, M. (2018). The interaction of indian monsoon depressions with northwesterly midlevel dry intrusions. *Monthly Weather Review*, 146(3):679–693.

Francis, P. and Gadgil, S. (2006). Intense rainfall events over the west coast of india. *Meteorology and Atmospheric Physics*, 94(1-4):27–42.

Frank, W. M. (1977). The structure and energetics of the tropical cyclone i. storm structure. *Monthly Weather Review*, 105(9):1119–1135.

Fredrick, S., Davis, C., Gill, D., and Low-Nam, S. (2009). Bogussing of tropical cyclones in wrf version 3.1. *NCAR Technical Document P*, 1:6.

Gelaro, R., McCarty, W., Suárez, M. J., Todling, R., Molod, A., Takacs, L., Randles, C. A., Darmenov, A., Bosilovich, M. G., Reichle, R., et al. (2017). The modern-era retrospective analysis for research and applications, version 2 (merra-2). *Journal of Climate*, 30(14):5419–5454.

Ghatak, S. and Sukhatme, J. (2022). Southwestward propagating quasi-biweekly oscillations over the south-west indian ocean during boreal winter. *Weather and Climate Dynamics*.

Gill, A. E. (1980). Some simple solutions for heat-induced tropical circulation. *Quarterly Journal of the Royal Meteorological Society*, 106(449):447–462.

Godbole, R. (1977). Composite structure of monsoon depression. *Tellus*, 29:25–40.

Goswami, B. (2005). South Asian summer monsoon. In Lau, W. and Waliser, D., editors, *Intraseasonal Variability in the Atmosphere-Ocean Climate System*, pages 125–173. Praxis.

Goswami, B., Keshavamurty, R., and Satyan, V. (1980). Role of barotropic, baroclinic and combined barotropic-baroclinic instability for the growth of monsoon depressions and mid-tropospheric cyclones. *Proceedings of the Indian Academy of Sciences-Earth and Planetary Sciences*, 89(1):79–97.

Goswami, B. N. (1987). A mechanism for the west-north-west movement of monsoon depressions. *Nature*, 326(6111):376–378.

Grigoriev, S., Gulev, S., and Zolina, O. (2000). Innovative software facilitates cyclone tracking and analysis. *EOS, Transactions American Geophysical Union*, 81(16):170–170.

Gulev, S. K., Zolina, O., and Reva, Y. (2000). Synoptic and subsynoptic variability in the north atlantic as revealed by the ocean weather station data. *Tellus A*, 52(3):323–329.

Hanley, J. and Caballero, R. (2012). Objective identification and tracking of multicentre cyclones in the era-interim reanalysis dataset. *Quarterly Journal of the Royal Meteorological Society*, 138(664):612–625.

Hartigan, J. A. and Wong, M. A. (1979). Ak-means clustering algorithm. *Journal of the Royal Statistical Society: Series C (Applied Statistics)*, 28(1):100–108.

Hawkins, H. F. and Rubsam, D. T. (1968). Hurricane hilda, 1964: Ii. structure and budgets of the hurricane on october 1, 1964. *Monthly Weather Review*, 96(9):617–636.

Hersbach, H., Bell, B., Berrisford, P., Hirahara, S., Horányi, A., Muñoz-Sabater, J., Nicolas, J., Peubey, C., Radu, R., Schepers, D., et al. (2020). The era5 global reanalysis. *Quarterly Journal of the Royal Meteorological Society*, 146(730):1999–2049.

Hodges, K., Cobb, A., and Vidale, P. L. (2017). How well are tropical cyclones represented in reanalysis datasets? *Journal of Climate*, 30(14):5243–5264.

Hodges, K. I., Hoskins, B. J., Boyle, J., and Thorncroft, C. (2003). A comparison of recent reanalysis datasets using objective feature tracking: Storm tracks and tropical easterly waves. *Monthly Weather Review*, 131(9):2012–2037.

Holloway, C. E. and Neelin, J. D. (2009). Moisture vertical structure, column water vapor, and tropical deep convection. *Journal of the atmospheric sciences*, 66(6):1665–1683.

Holton, J. R. (1973). An introduction to dynamic meteorology. *American Journal of Physics*, 41(5):752–754.

Hopsch, S. B., Thorncroft, C. D., and Tyle, K. R. (2010). Analysis of african easterly wave structures and their role in influencing tropical cyclogenesis. *Monthly Weather Review*, 138(4):1399–1419.

Hoskins, B. J. and Rodwell, M. J. (1995). A model of the Asian summer monsoon. Part I: The global scale. *Journal of the Atmospheric Sciences*, 52(9):1329–1340.

Hsieh, J.-S. and Cook, K. H. (2008). On the instability of the african easterly jet and the generation of african waves: Reversals of the potential vorticity gradient. *Journal of the Atmospheric Sciences*, 65(7):2130–2151.

Huffman, G. J., Adler, R. F., Bolvin, D. T., and Nelkin, E. J. (2010). The trmm multi-satellite precipitation analysis (tmpa). In *Satellite rainfall applications for surface hydrology*, pages 3–22. Springer.

Huffman, G. J., Bolvin, D. T., Nelkin, E. J., Wolff, D. B., Adler, R. F., Gu, G., Hong, Y., Bowman, K. P., and Stocker, E. F. (2007). The trmm multisatellite precipitation analysis (tmpa): Quasi-global, multiyear, combined-sensor precipitation estimates at fine scales. *Journal of hydrometeorology*, 8(1):38–55.

Hunt, K., Turner, A., Innes, P., Parker, D., and Levine, R. (2016). On the Structure and Dynamics of Indian Monsoon Depressions. *Monthly Weather Review*, 144:3391–3416.

Hunt, K. M. and Fletcher, J. K. (2019). The relationship between indian monsoon rainfall and low-pressure systems. *Climate Dynamics*, 53(3-4):1859–1871.

Hunt, K. M., Turner, A. G., Stein, T. H., Fletcher, J. K., and Schiemann, R. K. (2021). Modes of coastal precipitation over southwest india and their relationship with intraseasonal variability. *Quarterly Journal of the Royal Meteorological Society*, 147(734):181–201.

Hurley, J. and Boos, W. (2015). A global climatology of monsoon low-pressure systems. *Quarterly Journal of the Royal Meteorological Society*, 141:1049–1064.

Izumo, T., Montégut, C. B., Luo, J.-J., Behera, S. K., Masson, S., and Yamagata, T. (2008). The role of the western arabian sea upwelling in indian monsoon rainfall variability. *Journal of Climate*, 21(21):5603–5623.

Janiga, M. and Thorncroft, C. (2013). Regional differences in the kinematic and thermodynamic structure of African easterly waves. *Quartely Journal of the Royal Meteorological Society*, 139:1598–1614.

Jenkins, M. A. (1995). The cold-core temperature structure in a tropical easterly wave. *Journal of the Atmospheric Sciences*, 52(8):1168–1177.

Jian, G.-J. and Wu, C.-C. (2008). A numerical study of the track deflection of supertyphoon haitang (2005) prior to its landfall in taiwan. *Monthly Weather Review*, 136(2):598–615.

Jiang, N., Qian, W., and Leung, J. C.-H. (2016). The global monsoon division combining the k-means clustering method and low-level cross-equatorial flow. *Climate dynamics*, 47(7):2345–2359.

Karmakar, N., Boos, W. R., and Misra, V. (2021). Influence of intraseasonal variability on the development of monsoon depressions. *Geophysical Research Letters*, 48(2):e2020GL090425.

Karmakar, N. and Misra, V. (2020). Differences in northward propagation of convection over the arabian sea and bay of bengal during boreal summer. *Journal of Geophysical Research: Atmospheres*, 125(3):e2019JD031648.

Kikuchi, K. (2020). Extension of the bimodal intraseasonal oscillation index using jra-55 reanalysis. *Climate Dynamics*, 54(1):919–933.

Kikuchi, K. and Wang, B. (2009). Global perspective of the quasi-biweekly oscillation. *Journal of Climate*, 22(6):1340–1359.

Kikuchi, K. and Wang, B. (2010). Formation of tropical cyclones in the northern indian ocean associated with two types of tropical intraseasonal oscillation modes. *Journal of the Meteorological Society of Japan. Ser. II*, 88(3):475–496.

Kikuchi, K., Wang, B., and Kajikawa, Y. (2012). Bimodal representation of the tropical intraseasonal oscillation. *Climate Dynamics*, 38(9):1989–2000.

Kiladis, G. N., Thorncroft, C. D., and Hall, N. M. (2006). Three-dimensional structure and dynamics of african easterly waves. part i: Observations. *Journal of the atmospheric sciences*, 63(9):2212–2230.

Komaromi, W. A., Majumdar, S. J., and Rappin, E. D. (2011). Diagnosing initial condition sensitivity of typhoon sinlaku (2008) and hurricane ike (2008). *Monthly weather review*, 139(10):3224–3242.

Krishnamurthy, V. and Ajayamohan, R. (2010). Composite structure of monsoon low pressure systems and its relation to indian rainfall. *Journal of Climate*, 23(16):4285–4305.

Krishnamurti, T., Ardanuy, P., Ramanathan, Y., and Pasch, R. (1981). On the onset vortex of the summer monsoon. *Monthly Weather Review*, 109(2):344–363.

Krishnamurti, T. and Bhalme, H. (1976). Oscillations of a monsoon system, Part I: Observational aspects. *Journal of the Atmospheric Sciences*, 33:1937–1954.

Krishnamurti, T. and Hawkins, R. (1970). Mid-tropospheric cyclones of the southwest monsoon. *Journal of Applied Meteorology*, 9(3):442–458.

Krishnamurti, T., Molinari, J., Pan, H.-l., and Wong, V. (1977). Downstream amplification and formation of monsoon disturbances. *Monthly Weather Review*, 105(10):1281–1297.

Krouse, K. D. and Sobel, A. H. (2010). An observational study of multiple tropical cyclone events in the western north pacific. *Tellus A: Dynamic Meteorology and Oceanography*, 62(3):256–265.

Krouse, K. D., Sobel, A. H., and Polvani, L. M. (2008). On the wavelength of the rossby waves radiated by tropical cyclones. *Journal of the atmospheric sciences*, 65(2):644–654.

Kuester, M., Alexander, M., and Ray, E. (2008). A model study of gravity waves over hurricane humberto (2001). *Journal of the Atmospheric Sciences*, 65(10):3231–3246.

Kumar, A., Dudhia, J., Rotunno, R., Niyogi, D., and Mohanty, U. (2008). Analysis of the 26 july 2005 heavy rain event over mumbai, india using the weather research and forecasting (wrf) model. *Quarterly Journal of the Royal Meteorological Society*, 134(636):1897–1910.

Kumar, P. D., Paul, Y. S., Muraleedharan, K., Murty, V., and Preenu, P. (2016). Comparison of long-term variability of sea surface temperature in the arabian sea and bay of bengal. *Regional Studies in Marine Science*, 3:67–75.

Kumar, S. and Bhat, G. (2017). Vertical structure of orographic precipitating clouds observed over south asia during summer monsoon season. *Journal of Earth System Science*, 126(8):1–12.

Kumar, S., Hazra, A., and Goswami, B. (2014). Role of interaction between dynamics, thermodynamics and cloud microphysics on summer monsoon precipitating clouds over the myanmar coast and the western ghats. *Climate dynamics*, 43(3-4):911–924.

Kushwaha, P., Sukhatme, J., and Nanjundiah, R. (2021). A global tropical survey of midtropospheric cyclones. *Monthly Weather Review*, 149(8):2737 – 2753.

Laing, A. G. and Michael Fritsch, J. (1997). The global population of mesoscale convective complexes. *Quarterly Journal of the Royal Meteorological Society*, 123(538):389–405.

Lambert, S. J. (1996). Intense extratropical northern hemisphere winter cyclone events: 1899–1991. *Journal of Geophysical Research: Atmospheres*, 101(D16):21319–21325.

Lee, J.-Y., Wang, B., Wheeler, M. C., Fu, X., Waliser, D. E., and Kang, I.-S. (2013). Real-time multivariate indices for the boreal summer intraseasonal oscillation over the asian summer monsoon region. *Climate Dynamics*, 40(1-2):493–509.

Liebmann, B. and Smith, C. A. (1996). Description of a complete (interpolated) outgoing longwave radiation dataset. *Bulletin of the American Meteorological Society*, 77(6):1275–1277.

Ling, Z., Wang, Y., and Wang, G. (2016). Impact of intraseasonal oscillations on the activity of tropical cyclones in summer over the south china sea. part i: local tropical cyclones. *J. Clim.*, 29(2):855–868.

Low-Nam, S. and Davis, C. (2001). Development of a tropical cyclone bogussing scheme for the mm5 system. In *Preprints, 11th PSU–NCAR Mesoscale Model Users' Workshop, Boulder, CO, PSU–NCAR*, volume 130, page 134.

Ma, Q. and Franzke, C. L. (2021). The role of transient eddies and diabatic heating in the maintenance of european heat waves: a nonlinear quasi-stationary wave perspective. *Climate Dynamics*, 56(9):2983–3002.

Mahto, S. S. and Mishra, V. (2019). Does era-5 outperform other reanalysis products for hydrologic applications in india? *Journal of Geophysical Research: Atmospheres*, 124(16):9423–9441.

Mak, M. (1983). A moist baroclinic model for monsoonal mid-tropospheric cyclogenesis. *Journal of the Atmospheric Sciences*, 40(5):1154–1162.

Mak, M. and Jim Kao, C.-Y. (1982). An instability study of the onset-vortex of the southwest monsoon, 1979. *Tellus*, 34(4):358–368.

Mak, M.-K. (1975). The monsoonal mid-tropospheric cyclogenesis. *Journal of the Atmospheric Sciences*, 32(12):2246–2253.

Manning, D. M. and Hart, R. E. (2007). Evolution of north atlantic era40 tropical cyclone representation. *Geophysical research letters*, 34(5).

Mapes, B. (2011). Heaviest precipitation events, 1998-2007: A near-global survey. In *The Global Monsoon System: Research and Forecast*, pages 15–22. World Scientific.

Masunaga, H. (2014). Free-tropospheric moisture convergence and tropical convective regimes. *Geophysical Research Letters*, 41(23):8611–8618.

Meera, M., Suhas, E., and Sandeep, S. (2019). Downstream and in situ: Two perspectives on the initiation of monsoon low-pressure systems over the bay of bengal. *Geophysical Research Letters*, 46(21):12303–12310.

Mekonnen, A., Thorncroft, C. D., and Aiyyer, A. R. (2006). Analysis of convection and its association with african easterly waves. *Journal of Climate*, 19(20):5405–5421.

Menon, A., Turner, A., Martin, G., and MacLachlan, C. (2018). Modelling the moistening of the free troposphere during the northwestward progression of indian monsoon onset. *Quarterly Journal of the Royal Meteorological Society*, 144(713):1152–1168.

Miller, F. and Keshavamurty, R. (1968). Structure of an Arabian Sea summer monsoon system. *International Indian Ocean Experiment, Metero. Monog.*, 1.

Mohr, K. I. (2004). Interannual, monthly, and regional variability in the wet season diurnal cycle of precipitation in sub-saharan africa. *Journal of climate*, 17(12):2441–2453.

Mooley, D. (1973). Some Aspects of Indian Monsoon Depressions and the Associated Rainfall. *Monthly Weather Review*, 101:271–280.

Muraleedharan, P., Mohankumar, K., and Sivakumar, K. (2013). A study on the characteristics of temperature inversions in active and break phases of indian summer monsoon. *Journal of atmospheric and solar-terrestrial physics*, 93:11–20.

Murthy, V. S. and Boos, W. R. (2019). Understanding the vertical structure of potential vorticity in tropical depressions. *Quarterly Journal of the Royal Meteorological Society*, 145(722):1968–1991.

Nanjundiah, R. S., Srinivasan, J., and Gadgil, S. (1992). Intraseasonal variation of the Indian summer monsoon. *Journal of the Meteorological Society of Japan. Ser. II*, 70(1B):529–550.

Narayanan, M. and Rao, B. (1981). Detection of monsoon inversion by tiros-n satellite. *Nature*, 294(5841):546–548.

Narayanan, M., Rao, B., Shah, S., Prasad, V., and Bhat, G. (2004). Role of atmospheric stability over the arabian sea and the unprecedented failure of monsoon 2002. *Current Science*, pages 938–947.

Nicholson, S. and Grist, J. (2003). The seasonal evolution of the atmospheric circulation over west africa and equatorial africa. *Journal of Climate*, 16:1013–1030.

Nogueira, M. (2020). Inter-comparison of era-5, era-interim and gpcp rainfall over the last 40 years: Process-based analysis of systematic and random differences. *Journal of Hydrology*, 583:124632.

Pattanaik, D. and Rajeevan, M. (2010). Variability of extreme rainfall events over india during southwest monsoon season. *Meteorological Applications: A journal of forecasting, practical applications, training techniques and modelling*, 17(1):88–104.

Pearce, R. and Mohanthy, U. (1984). Onsets of the asian summer monsoon 1979–82. *Journal of Atmospheric Sciences*, 41(9):1620–1639.

Phadtare, J. (2018). Role of eastern ghats orography and cold pool in an extreme rainfall event over chennai on 1 december 2015. *Monthly Weather Review*, 146(4):943–965.

Pope, M., Jakob, C., and Reeder, M. J. (2009). Regimes of the north australian wet season. *Journal of Climate*, 22(24):6699–6715.

Prakash, S., Mahesh, C., and Gairola, R. (2013). Comparison of trmm multi-satellite precipitation analysis (tmpa)-3b43 version 6 and 7 products with rain gauge data from ocean buoys. *Remote sensing letters*, 4(7):677–685.

Praveen, V., Sandeep, S., and Ajayamohan, R. (2015). On the relationship between mean monsoon precipitation and low pressure systems in climate model simulations. *Journal of Climate*, 28(13):5305–5324.

Qian, Y., Hsu, P.-C., and Kazuyoshi, K. (2019). New real-time indices for the quasi-biweekly oscillation over the asian summer monsoon region. *Climate Dynamics*, 53(5):2603–2624.

Rajeevan, M., Bhate, J., and Jaswal, A. K. (2008). Analysis of variability and trends of extreme rainfall events over india using 104 years of gridded daily rainfall data. *Geophysical research letters*, 35(18).

Rajeevan, M., Unnikrishnan, C., Bhate, J., Niranjan Kumar, K., and Sreekala, P. (2012). Northeast monsoon over india: variability and prediction. *Meteorological Applications*, 19(2):226–236.

Ramage, C. (1964). Some preliminary research results from the international meteorological centre. In *Proc. WMO Symposium on Tropical Meteorology, New Zealand*, pages 403–408.

Ramage, C. (1966). The summer atmospheric circulation over the arabian sea. *Journal of the Atmospheric Sciences*, 23(2):144–150.

Ramage, C. S. (1971). Monsoon meteorology. Technical report.

Ray, K., Pandey, P., Pandey, C., Dimri, A., and Kishore, K. (2019). On the recent floods in india. *Current science*, 117(2):204–218.

Raymond, D., Gjorgjievska, S., S, S., and Z, F. (2014a). Tropical cyclogenesis and mid-level vorticity. *Aust. Meteorol. Oceanogr. J.*, 64:11–25.

Raymond, D. and López Carrillo, C. (2011). The vorticity budget of developing typhoon nuri (2008). *Atmospheric Chemistry and Physics*, 11(1):147–163.

Raymond, D., Lopez-Carrillo, C., and Cavazos, L. (1998). Case-studies of developing east pacific easterly waves. *Quarterly Journal of the Royal Meteorological Society*, 124:2005–2034.

Raymond, D. J. (2000). Thermodynamic control of tropical rainfall. *Quarterly Journal of the Royal Meteorological Society*, 126(564):889–898.

Raymond, D. J., Gjorgjievska, S., Sessions, S., and Fuchs, Ž. (2014b). Tropical cyclogenesis and mid-level vorticity. *Australian Meteorological and Oceanographic Journal*, 64(1):11–25.

Raymond, D. J., Sessions, S. L., Sobel, A. H., and Fuchs, Ž. (2009). The mechanics of gross moist stability. *Journal of Advances in Modeling Earth Systems*, 1(3).

Reasor, P. D., Montgomery, M. T., and Grasso, L. D. (2004). A new look at the problem of tropical cyclones in vertical shear flow: Vortex resiliency. *Journal of the Atmospheric Sciences*, 61(1):3–22.

Reed, R. and Recker, E. (1971). Structure and properties of synoptic-scale wave disturbances in the equatorial western pacific. *Journal of the Atmospheric Sciences*, 28:1117–1133.

Reed, R. J., Norquist, D. C., and Recker, E. E. (1977). The structure and properties of african wave disturbances as observed during phase iii of gate. *Monthly Weather Review*, 105(3):317–333.

Rienecker, M. M., Suarez, M., Todling, R., Bacmeister, J., Takacs, L., Liu, H., Gu, W., Sienkiewicz, M., Koster, R., Gelaro, R., et al. (2008). The geos-5 data assimilation system: Documentation of versions 5.0. 1, 5.1. 0, and 5.2. 0.

Rios-Berrios, R. and Torn, R. D. (2017). Climatological analysis of tropical cyclone intensity changes under moderate vertical wind shear. *Monthly Weather Review*, 145(5):1717–1738.

Rodwell, M. J. and Hoskins, B. J. (1996). Monsoons and the dynamics of deserts. *Quarterly Journal of the Royal Meteorological Society*, 122(534):1385–1404.

Rousseeuw, P. J. (1987). Silhouettes: a graphical aid to the interpretation and validation of cluster analysis. *Journal of computational and applied mathematics*, 20:53–65.

Roxy, M. K., Ghosh, S., Pathak, A., Athulya, R., Mujumdar, M., Murtugudde, R., Terray, P., and Rajeevan, M. (2017). A threefold rise in widespread extreme rain events over central india. *Nature communications*, 8(1):1–11.

Russell, J. O. and Aiyyer, A. (2020). The potential vorticity structure and dynamics of african easterly waves. *Journal of the Atmospheric Sciences*, 77(3):871–890.

Russell, J. O., Aiyyer, A., and Dylan White, J. (2020). African easterly wave dynamics in convection-permitting simulations: Rotational stratiform instability as a conceptual model. *Journal of Advances in Modeling Earth Systems*, 12(1):e2019MS001706.

Saikranthi, K., Radhakrishna, B., Narayana Rao, T., and Satheesh, S. K. (2019a). Variability in vertical structure of precipitation with sea surface temperature over the arabian sea and the bay of bengal as inferred by tropical rainfall measuring mission precipitation radar measurements. *Atmospheric Chemistry and Physics*, 19(15):10423–10432.

Saikranthi, K., Radhakrishna, B., Thota, N. R., and Satheesh, S. K. (2019b). Differences in the association of sea surface temperature—precipitating systems over the bay of bengal and the arabian sea during southwest monsoon season. *International Journal of Climatology*, 39(11):4305–4312.

Satopaa, V., Albrecht, J., Irwin, D., and Raghavan, B. (2011). Finding a" kneedle" in a haystack: Detecting knee points in system behavior. In *2011 31st international conference on distributed computing systems workshops*, pages 166–171. IEEE.

Schenkel, B. A. (2016). A climatology of multiple tropical cyclone events. *Journal of Climate*, 29(13):4861–4883.

Schenkel, B. A. (2017). Are multiple tropical cyclone events similar among basins? *Journal of Climate*, 30(15):5805–5813.

Schenkel, B. A., Lin, N., Chavas, D., Oppenheimer, M., and Brammer, A. (2017). Evaluating outer tropical cyclone size in reanalysis datasets using quikscat data. *Journal of Climate*, 30(21):8745–8762.

Seager, R. and Henderson, N. (2013). Diagnostic computation of moisture budgets in the era-interim reanalysis with reference to analysis of cmip-archived atmospheric model data. *Journal of Climate*, 26(20):7876–7901.

Seager, R., Ting, M., Held, I., Kushnir, Y., Lu, J., Vecchi, G., Huang, H.-P., Harnik, N., Leetmaa, A., Lau, N.-C., et al. (2007). Model projections of an imminent transition to a more arid climate in southwestern north america. *Science*, 316(5828):1181–1184.

Seager, R. and Vecchi, G. A. (2010). Greenhouse warming and the 21st century hydroclimate of southwestern north america. *Proceedings of the National Academy of Sciences*, 107(50):21277–21282.

Shapiro, L. (1986). The three-dimensional structure of synoptic-scale disturbances over the tropical atlantic. *Monthly Weather Review*, 114:1876–1891.

Shukla, J. (1978). Cisk-barotropic-baroclinic instability and the growth of monsoon depressions. *Journal of the Atmospheric Sciences*, 35:495–508.

Shyamala, B. and Bhadram, C. (2006). Impact of mesoscale–synoptic scale interactions on the mumbai historical rain event during 26–27 july 2005. *Current Science*, pages 1649–1654.

Sikka, D. and Gadgil, S. (1980). On the maximum cloud zone and the ITCZ over Indian longitudes during the southwest monsoon. *Monthly Weather Review*, 108(11):1840–1853.

Simpson, J., Garstang, M., Zipser, E. J., and Dean, G. A. (1967). A study of a non-deepening tropical disturbance. *Journal of Applied Meteorology*, 6(2):237–254.

Sinclair, M. R. (1994). An objective cyclone climatology for the southern hemisphere. *Monthly Weather Review*, 122(10):2239–2256.

Singh, P., Gnanaseelan, C., and Chowdary, J. (2017). North-east monsoon rainfall extremes over the southern peninsular india and their association with el niño. *Dynamics of Atmospheres and Oceans*, 80:1–11.

Sobel, A. H. and Horinouchi, T. (2000). On the dynamics of easterly waves, monsoon depressions, and tropical depression type disturbances. *Journal of the Meteorological Society of Japan. Ser. II*, 78(2):167–173.

Sørland, S. L. and Sorteberg, A. (2015). The dynamic and thermodynamic structure of monsoon low-pressure systems during extreme rainfall events. *Tellus A: Dynamic Meteorology and Oceanography*, 67(1):27039.

Spengler, T. and Smith, R. K. (2008). The dynamics of heat lows over flat terrain. *Quarterly Journal of the Royal Meteorological Society*, 134(637):2157–2172.

Syakur, M., Khotimah, B., Rochman, E., and Satoto, B. (2018). Integration k-means clustering method and elbow method for identification of the best customer profile cluster. In *IOP Conference Series: Materials Science and Engineering*, volume 336, page 012017. IOP Publishing.

Thiruvengadathan, A. (1972). Synoptic situations associated with spells of strong and weak monsoon over konkan. *Indian Journal of Meteorology and Geophysics*, 23:207–10.

Thorncroft, C. and Hodges, K. (2001). African easterly wave variability and its relationship to atlantic tropical cyclone activity. *Journal of Climate*, 14(6):1166–1179.

Thorncroft, C. and Hoskins, B. (1994). An idealized study of african easterly waves. i: A linear view. *Quarterly Journal of the Royal Meteorological Society*, 120:953–982.

Thorncroft, C. D., Hall, N. M., and Kiladis, G. N. (2008). Three-dimensional structure and dynamics of african easterly waves. part iii: Genesis. *Journal of the Atmospheric Sciences*, 65(11):3596–3607.

Tomas, R. A., Holton, J. R., and Webster, P. J. (1999). The influence of cross-equatorial pressure gradients on the location of near-equatorial convection. *Quarterly Journal of the Royal Meteorological Society*, 125(556):1107–1127.

Trenberth, K. E. (1997). Using atmospheric budgets as a constraint on surface fluxes. *Journal of climate*, 10(11):2796–2809.

Trenberth, K. E. and Guillemot, C. J. (1995). Evaluation of the global atmospheric moisture budget as seen from analyses. *Journal of Climate*, 8(9):2255–2272.

Van Nguyen, H. and Chen, Y.-L. (2011). High-resolution initialization and simulations of typhoon morakot (2009). *Monthly weather review*, 139(5):1463–1491.

Varikoden, H., Revadekar, J., Kuttippurath, J., and Babu, C. (2019). Contrasting trends in southwest monsoon rainfall over the western ghats region of india. *Climate Dynamics*, 52(7):4557–4566.

Vinnarasi, R. and Dhanya, C. (2016). Changing characteristics of extreme wet and dry spells of indian monsoon rainfall. *Journal of Geophysical Research: Atmospheres*, 121(5):2146–2160.

Vishnu, S., Boos, W., Ulrich, P., and O'Brien, T. (2020). Assessing historical variability of south asian monsoon lows and depressions with an optimized tracking algorithm. *Journal of Geophysical Research*, 125:e2020JD032977.

Vuruputur, V., Sukhatme, J., Murtugudde, R., and Roca, R. (2018). *Tropical Extremes: Natural Variability and Trends*. Elsevier.

Wang, B. and Fan, Z. (1999). Choice of south asian summer monsoon indices. *Bulletin of the American Meteorological Society*, 80(4):629–638.

Wang, B. and Xie, X. (1997). A model for the boreal summer intraseasonal oscillation. *Journal of the Atmospheric Sciences*, 54:72–86.

Wang, D., Liang, X., Zhao, Y., and Wang, B. (2008). A comparison of two tropical cyclone bogussing schemes. *Weather and forecasting*, 23(1):194–204.

Wang, X. and Jiang, H. (2019). A 13-year global climatology of tropical cyclone warm-core structures from airs data. *Monthly Weather Review*, 147(3):773–790.

Wernli, H. and Schwierz, C. (2006). Surface cyclones in the era-40 dataset (1958–2001). part i: Novel identification method and global climatology. *Journal of the atmospheric sciences*, 63(10):2486–2507.

Wheeler, M. C. and Hendon, H. H. (2004). An all-season real-time multivariate mjo index: Development of an index for monitoring and prediction. *Monthly weather review*, 132(8):1917–1932.

Widlansky, M. J., Webster, P. J., and Hoyos, C. D. (2011). On the location and orientation of the south pacific convergence zone. *Climate dynamics*, 36(3-4):561–578.

Wilks, D. (2016). "the stippling shows statistically significant grid points": How research results are routinely overstated and overinterpreted, and what to do about it. *Bulletin of the American Meteorological Society*, 97(12):2263–2273.

Wood, K. M. and Ritchie, E. A. (2014). A 40-year climatology of extratropical transition in the eastern north pacific. *Journal of climate*, 27(15):5999–6015.

Xie, S.-P., Xu, H., Saji, N., Wang, Y., and Liu, W. T. (2006). Role of narrow mountains in large-scale organization of asian monsoon convection. *Journal of climate*, 19(14):3420–3429.

Yan, H., Huang, J., He, Y., Liu, Y., Wang, T., and Li, J. (2020). Atmospheric water vapor budget and its long-term trend over the tibetan plateau. *Journal of Geophysical Research: Atmospheres*, 125(23):e2020JD033297.

Yang, M.-J., Zhang, D.-L., and Huang, H.-L. (2008). A modeling study of typhoon nari (2001) at landfall. part i: Topographic effects. *Journal of the atmospheric sciences*, 65(10):3095–3115.

Yeasmin, A., Chand, S., Turville, C., and Sultanova, N. (2021). Detection and verification of tropical cyclones and depressions over the south pacific ocean basin using era-5 reanalysis dataset. *International Journal of Climatology*.

Yihui, D. and Chan, J. C. (2005). The east asian summer monsoon: an overview. *Meteorology and Atmospheric Physics*, 89(1):117–142.

Zhou, C., Zhao, P., and Chen, J. (2019). The interdecadal change of summer water vapor over the tibetan plateau and associated mechanisms. *Journal of Climate*, 32(13):4103–4119.